Hydromechanical coupling in geologic processes

C. E. Neuzil

Abstract Earth's porous crust and the fluids within it are intimately linked through their mechanical effects on each other. This paper presents an overview of such "hydromechanical" coupling and examines current understanding of its role in geologic processes. An outline of the theory of hydromechanics and rheological models for geologic deformation is included to place various analytical approaches in proper context and to provide an introduction to this broad topic for nonspecialists.

Effects of hydromechanical coupling are ubiquitous in geology, and can be local and short-lived or regional and very long-lived. Phenomena such as deposition and erosion, tectonism, seismicity, earth tides, and barometric loading produce strains that tend to alter fluid pressure. Resulting pressure perturbations can be dramatic, and many so-called "anomalous" pressures appear to have been created in this manner. The effects of fluid pressure on crustal mechanics are also profound. Geologic media deform and fail largely in response to effective stress, or total stress minus fluid pressure. As a result, fluid pressures control compaction, decompaction, and other types of deformation, as well as jointing, shear failure, and shear slippage, including events that generate earthquakes. By controlling deformation and failure, fluid pressures also regulate states of stress in the upper crust.

Advances in the last 80 years, including theories of consolidation, transient groundwater flow, and poroelasticity, have been synthesized into a reasonably complete conceptual framework for understanding and describing hydromechanical coupling. Full coupling in two or three dimensions is described using force balance equations for deformation coupled with a mass conservation equation for fluid flow. Fully coupled analyses allow hypothesis testing and conceptual model development. However, rigorous application of full coupling is often difficult because (1) the rheological behavior of geologic media is complex and poorly understood and (2) the architecture, mechanical properties and boundary conditions, and deformation history of most geologic systems are not well known. Much of what is known about hydromechanical processes in geologic systems is derived from simpler analyses that ignore certain aspects of solid-fluid coupling. The simplifications introduce error, but more complete analyses usually are not warranted. Hydromechanical analyses should thus be interpreted judiciously, with an appreciation for their limitations. Innovative approaches to hydromechanical modeling and obtaining critical data may circumvent some current limitations and provide answers to remaining questions about crustal processes and fluid behavior in the crust.

Received: 6 September 2002 / Accepted: 28 October 2002
Published online: 25 January 2003

C. E. Neuzil (✉)
US Geological Survey, 431 National Center,
Reston, VA 20192, USA
e-mail: ceneuzil@usgs.gov
Tel.: +1-703-6485880
Fax: +1-703-6485274

Résumé La croûte poreuse de la Terre et les fluides associés sont intimement liés dans leurs effets mécaniques réciproques. Ce papier présente une analyse d'un tel couplage "hydromécanique" et examine l'état actuel des connaissances de son rôle dans les processus géologiques. La théorie de l'hydromécanique et des modèles rhéologiques pour la déformation géologique est exposée de façon à introduire différentes approches analytiques dans le contexte considéré et à fournir aux non spécialistes une introduction à ce vaste sujet.

Les effets du couplage hydromécanique sont ubiquistes en géologie; ils peuvent être locaux et de courte durée ou régionaux et de longue durée. Des phénomènes tels que le dépôt et l'érosion, la tectonique, la séismicité, les marées terrestres et la pression barométrique produisent des contraintes qui tendent à modifier la pression du fluide. Les perturbations de pression résultantes peuvent être considérables, et de nombreuses pressions dites anormales paraissent avoir été créées de cette façon. Les effets de la pression des fluides sur les mécanismes crustaux sont également profonds. Les milieux géologiques se déforment et faiblissent considérablement en réponse à la contrainte efficace, c'est-à-dire la contrainte totale moins la pression du fluide. Il en résulte que les pressions de fluide contrôlent la compaction, la décompaction et d'autres types de déformations, telles que l'ouverture des fissures, la rupture et le glissement par cisaillement, y compris les évènements qui provoquent des séismes. En contrôlant la déformation et la rupture, les pressions de fluide régulent également les contraintes dans la croûte supérieure.

 DOI 10.1007/s10040-002-0230-8

Les progrès réalisés au cours des 80 dernières années, dont les théories de la consolidation, de l'écoulement souterrain transitoire et de la poro-élasticité, ont été synthétisées dans un ensemble conceptuel cohérent qui permet de comprendre et de décrire le couplage hydromécanique. Le couplage complet en 2 ou 3 dimensions est décrit à partir d'équations du bilan de la déformation associées à une équation de conservation de la masse pour l'écoulement des fluides. Des analyses complètement couplées permettent de tester des hypothèses et de développer des modèles conceptuels. Cependant, l'application rigoureuse du couplage complet est souvent difficile parce que (1) le comportement rhéologique du milieu géologique est complexe et mal connu, et (2) on connaît mal les conditions d'architecture, de propriétés mécaniques et aux limites, ainsi que l'histoire de la déformation de la plupart des systèmes géologiques. L'essentiel de ce que l'on connaît sur les processus hydromécaniques dans les systèmes géologiques provient d'analyses plus simples qui ignorent certains aspects du couplage solide-fluide. Les simplifications introduisent une erreur, mais des analyses plus complètes ne sont habituellement pas justifiées. Les analyses hydromécaniques doivent donc être interprétées de façon judicieuse, avec une appréciation de leurs limites. Des approches innovantes de modélisation hydromécanique et d'obtention de données critiques peuvent contourner quelques limitations courantes et fournir des réponses aux questions en suspens concernant les processus crustaux et le comportement du fluide dans la croûte.

Resumen La corteza porosa de la Tierra y sus fluidos interiores están íntimamente ligados por efectos mecánicos mutuos. Este artículo repasa este acoplamiento "hidromecánico" y examina el conocimiento actual de su papel en los procesos geológicos. Se incluye un bosquejo de la teoría de la hidromecánica y de los modelos reológicos de deformación geológica con el fin de contextualizar los diversos enfoques analíticos y de proporcionar una introducción a este extenso campo para los no especialistas.

Los efectos del acoplamiento hidromecánico son ubicuos en geología; pueden ser locales y breves o regionales y de larga duración. Fenómenos como la deposición y erosión, movimientos tectónicos y sísmicos, mareas terrestres y la carga barométrica producen deformaciones que tienden a alterar las presiones de los fluidos. Las perturbaciones resultantes en la presión pueden ser enormes, y muchas de las denominadas presiones "anómalas" parecen haber sido originadas de esta forma. Los efectos de la presión del fluido en la mecánica de la corteza terrestre son también profundos. Los medios geológicos se deforman y fallan ampliamente en respuesta a la tensión efectiva, equivalente a la tensión total menos la presión del fluido. Como consecuencia, las presiones del fluido controlan la compactación, descompactación y otros tipos de deformación, así como el diaclasado, las cizallas y las cizallas por deslizamiento, incluyendo eventos que generan terremotos. Controlando la deformación y el fallo, las presiones del fluido también regulan los estados tensionales en la corteza superior.

Se ha sintetizado los avances de los últimos 80 años, incluyendo las teorías de consolidación, flujo transitorio de aguas subterráneas y poroelasticidad en un marco conceptual razonablemente completo con el fin de comprender y describir el acoplamiento hidromecánico. Se describe el acoplamiento total en dos o tres dimensiones mediante ecuaciones de balance de fuerzas para la deformación acopladas con una ecuación de conservación de masa para el flujo del fluido. Los análisis completamente acoplados permiten verificar hipótesis y desarrollar modelos conceptuales. Sin embargo, la aplicación rigurosa de un acoplamiento total es a menudo difícil porque (1) el comportamiento reológico de los medios geológicos es complejo y apenas entendido, y (2) la arquitectura, propiedades mecánicas y condiciones de contorno, y la historia de deformación de la mayoría de sistemas geológicos, no son bien conocidas. Mucho de lo que se sabe de los procesos hidromecánicos en sistemas geológicos procede de análisis más sencillos que ignoran ciertos aspectos del acoplamiento sólido-fluido. Las simplificaciones introducen errores, pero habitualmente no se garantiza que haya análisis más completos. Así, los análisis hidromecánicos deberían ser interpretados juiciosamente, siendo conscientes de sus limitaciones. La adopción de enfoques innovadores de modelación hidromecánica y la obtención de datos críticos podrían superar las limitaciones actuales y proporcionar respuestas a las cuestiones no aclaradas sobre los procesos en la corteza terrestre y sobre el comportamiento de los fluidos en su interior.

Keywords Hydromechanics · Poroelasticity · Groundwater hydraulics · Rheology · Deformation

Introduction

Pore fluids control deformation of porous media by bearing loads, and the deformation of porous media affects fluid pressure and flow by altering pore volume (Fig. 1). This two-way interaction is a fundamental aspect of the dynamism that shapes Earth's crust and controls the behavior of water and other fluids in it. There is a growing consensus that many, if not most, geologic processes can be fully understood only by considering the coupling between fluids and deformation. The reciprocal is also true; there are many fluid regimes, particularly those exhibiting anomalous pressures or other transient behavior, that cannot be fully understood except through analysis of porous medium deformation.

Despite its fundamental importance in geology, hydromechanical coupling has received relatively little emphasis from researchers. Although a long history of contributions has provided a reasonably complete understanding of the interaction, many geologists pay scant attention to the pervasive mechanical role played by

 DOI 10.1007/s10040-002-0230-8

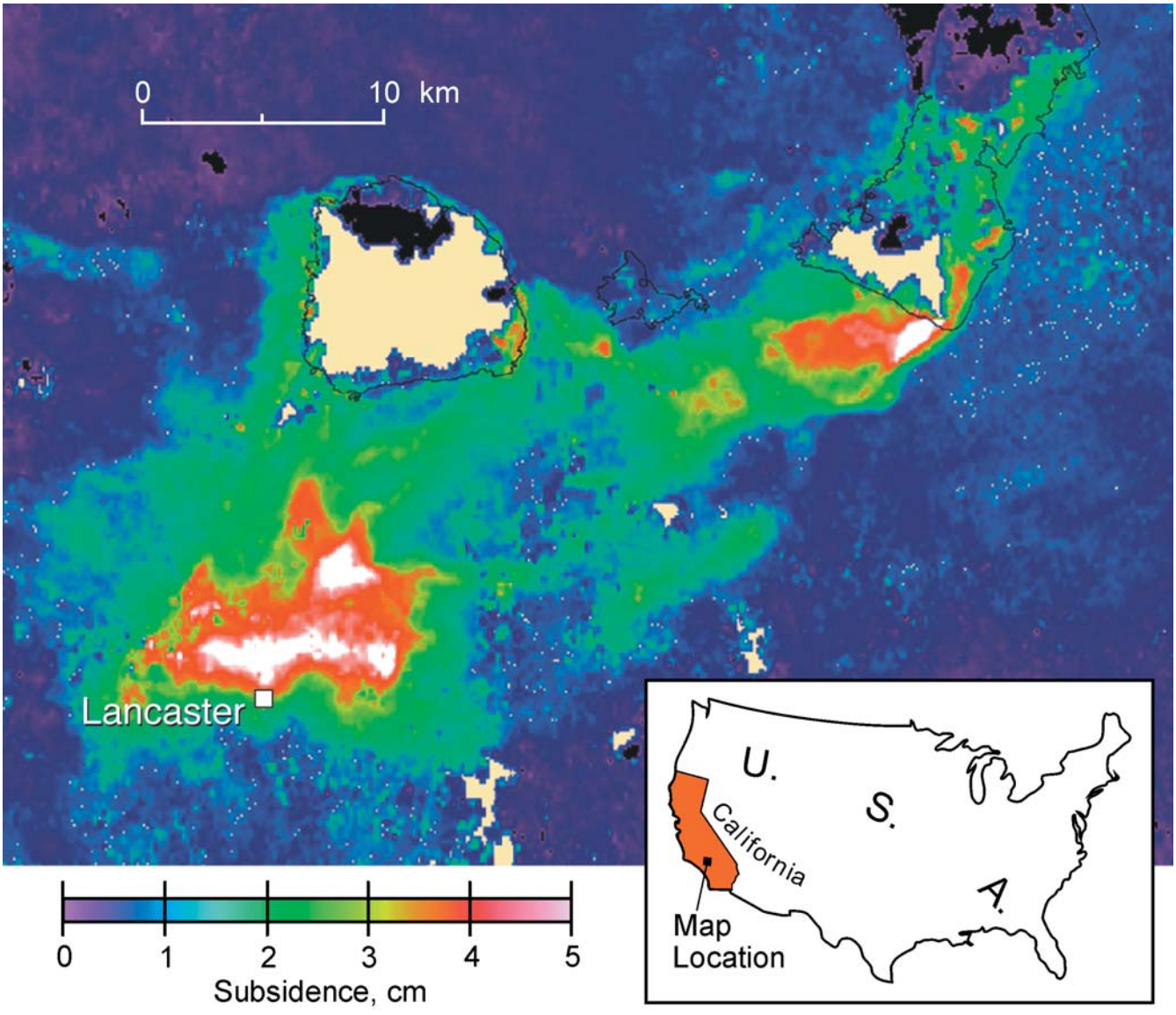

Fig. 1 A portrait of hydromechanical coupling. Agricultural withdrawals of groundwater near Lancaster, California, lowered fluid pressure, shifting some of the overburden load from the fluid to the solid matrix, which then compressed. The resulting subsidence of the ground surface between October 1993 and December 1995 was captured by InSAR (Interferometric Synthetic Aperture Radar) on an orbiting platform, providing a rare chance to "see" the mechanical interplay between fluid pressure and crustal deformation. Dry lake beds, *outlined in black*, are subject to depositional or erosional elevation changes which cannot be characterized interferometrically; these areas are indicated by *solid black* and *tan colors* (Galloway et al. 1999)

fluids, and hydrogeologists do not tend to think of transient fluid flow in terms of the deformation that makes it possible. This has begun to change, but the mechanical interactions that underlie and provide a unifying view of many geologic and hydrogeologic phenomena are still not widely appreciated. These pervasive interactions in the crust and the conceptual framework developed to describe them are the focus of this overview. The topic is a broad one and it will not be possible to treat it in detail. However, the presentation touches upon the various types of interactions to delineate their mechanisms and the commonalities underlying them. It also analyzes the uncertainties inherent in models of hydromechanical coupling in geology to show the need for care when interpreting them. Thus the overview also defines areas where additional research may be desirable.

The presentation is in two main parts. The first briefly develops the conceptual framework now available for analyzing hydromechanical coupling, including a very brief look at its history. Various approaches to describing coupling and the underlying rheological behavior of geologic media are discussed to provide a context for the overview and, for readers unfamiliar with them, an introduction to the concepts of hydromechanics. The second part examines how these approaches have been applied to understand the many manifestations of cou-

 DOI 10.1007/s10040-002-0230-8

pling in the crust, and what has been learned as a result. As the term "hydromechanics" implies, this paper focuses on the aqueous fluids that permeate nearly all of the crust; other fluids, notably magma, are not considered.

Conceptualization of Hydromechanical Coupling in Geologic Systems

Early Concepts

Although mechanical coupling between fluids and porous solids has been recognized for over a century (e.g. Reynolds 1886; King 1892), the first significant conceptual advances in hydromechanics came in the 1920s from attempts to understand two seemingly unrelated phenomena. In Europe, Karl Terzaghi was attempting to analyze consolidation of soil beneath structures and, in the USA, Oscar Meinzer was trying to determine the source of large volumes of water obtained from artesian aquifers. Although they could not know it, both were on the cusp of a revolution in thinking about the connection between pore fluids and geologic deformation.

In attempting to explain time dependence of soil and sediment consolidation after loading, Terzaghi developed two crucial ideas, the notions of effective stress and the diffusion of fluid pressure by flow (Terzaghi 1923). Terzaghi's concept of effective stress, which can be stated as

$$\sigma'_{zz} = \sigma_{zz} - p \tag{1}$$

is deceptively simple; the vertical effective stress, σ'_{zz}, or the portion of the vertical stress tending to compress the porous matrix, is equal to the applied load σ_{zz} less the pore fluid pressure p, which bears part of the load (in this context, these quantities can represent either absolute values or differences). Consolidation could thus be tied directly to the dissipation of excess fluid pressure. Terzaghi was the first to use a diffusion-type equation to describe the dissipation, namely

$$\frac{\kappa}{a}\frac{\partial^2 p'}{\partial z^2} = \frac{\partial p'}{\partial t} \tag{2}$$

Here, κ is "permeability" or hydraulic conductivity, a is a "compaction factor" or storage term, and p' is "hydrostatic overpressure in the pore water" or excess pressure. These ideas comprise Terzaghi's "consolidation theory" and still lie at the core of current understanding of hydromechanical coupling and fluid flow through porous media.

Meinzer (1928) seems to have been the first to recognize that water compressibility alone cannot account for the large amount of water produced from confined aquifers; loss of porosity as the aquifer deforms must also contribute. Meinzer (1928) also published observations of transient pressure increases in aquifers that accompanied transient loading (Fig. 2), further documenting the existence and importance of aquifer deformation. A few years later, C.V. Theis (1935) incorporated the concept of elastic storage into a quantitative model of pressure drawdown near a pumped well. Theis' equation basically represented an independently developed extension of

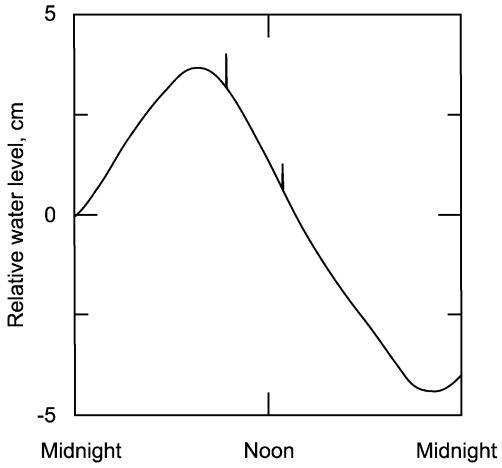

Fig. 2 March 5, 1927 hydrograph of a well near Lodi, California, showing two spikes in water level. The spikes, due to passing trains, are superimposed on a diurnal fluctuation due to pumping. Responses to loading like these were among the earliest observations of the intimate relation between stresses and fluid pressure in geologic media (modified from Meinzer 1928)

Terzaghi's one-dimensional theory of pressure diffusion to two dimensions for flow (but not for deformation). Shortly thereafter, and apparently without knowledge of Theis' work, Rendulic (1936) extended consolidation theory to three dimensions, also considering only vertical deformation. The equations developed by Theis and Rendulic have since evolved into the primary analytical tools used by hydrogeologists to describe transient, or time-varying groundwater flow.

The developments of Terzaghi, Meinzer, and others were important steps in developing a working theory of hydromechanical coupling. However, the conceptual breakthrough that allowed full coupling of three-dimensional deformation with three-dimensional flow would have to wait a few more years. That breakthrough occurred when Belgian-born physicist and classical mechanicist Maurice Biot published his "General Theory of Three Dimensional Consolidation" (Biot 1941), which presented the governing equations for coupled three-dimensional fluid flow and deformation in linear elastic porous media.

Poroelasticity

Biot's development is the basis of what has come to be known as poroelastic theory or simply poroelasticity. Although developed for linear elastic porous media, it laid the foundation for more general descriptions of hydromechanical coupling and truly placed two- and three-dimensional flow and deformation in porous media on a firm theoretical base. Various aspects of poroelasticity were later expanded upon and generalized by Biot, such as incorporating mechanical anisotropy (Biot 1955), viscoelasticity (Biot 1956a), finite deformations (Biot 1972) and nonlinear rheologies (Biot 1973), and elucidating the measurement and meaning of poroelastic

 DOI 10.1007/s10040-002-0230-8

coefficients (Biot and Willis 1957). A number of other workers have also clarified and extended poroelastic theory. Notable contributions in this regard have been made by Geertsma (1966), who used the theory to analyze stresses around boreholes as well as subsidence due to petroleum extraction (and who is credited with coining the term "poroelasticity"), Verruijt (1969), who applied the theory to analyze reverse water-level fluctuations near pumped wells (the Noordbergum effect), Cooley (1975) who showed how Biot's theory relates to standard groundwater equations, and Rice and Cleary (1976), who recast poroelastic relations using familiar physical quantities and developed solutions for certain problems. More recently, van der Kamp and Gale (1983) have developed poroelastic descriptions of earth tide and barometric effects, and Kümpel (1991) has clarified the interpretation of poroelastic parameters. Important syntheses include a concise but clearly presented overview of poroelasticity, including analytical and numerical solution techniques, contributed by Detournay and Cheng (1993) and a comprehensive monograph recently published by Wang (2000).

Although conceptually rigorous, poroelasticity and its more general descendents have seen limited use in geology. Added complexity is, of course, a disincentive, but there are a number of reasons that these tools are rarely applied. Perhaps most important are (1) the inability to describe geologic domains sufficiently well to derive the advantages of applying poroelasticity, and (2) the availability of simpler approaches that yield useful results when judiciously applied. Nevertheless, to understand the limitations of simplified approaches, it is essential to have some familiarity with poroelasticity and its generalizations. In addition, poroelastic and related theories have a crucial role in conceptualization and hypothesis testing in hydromechanics. With this in mind, a very brief outline of poroelasticity and related theories is included here.

This presentation makes use of the thorough treatment by Wang (2000) as well as the work of Rice and Cleary (1976) and van der Kamp and Gale (1983). Readers are referred to these sources as well as Detournay and Cheng (1993) for details. Those unfamiliar with elastic theory and desiring an introductory discussion may find the treatises by Timoshenko and Goodier (1987) and Jaeger and Cook (1969) helpful. Conversely, if an introduction from the point of view of subsurface hydrology or hydrogeology is sought, it should be noted that texts on this topic invariably treat flow as mechanically uncoupled and many fail even to discuss the coupling. Some, such as those by Freeze and Cherry (1979) and Domenico and Schwartz (1998) do briefly discuss deformation of geologic media and its interaction with fluid flow.

Because thermal effects are often important in geology, they have been incorporated in the development presented here. Thus, a more descriptive (but cumbersome) term for the theory outlined might be "thermo-poroelasticity." Although the coupling between fluid pressure and deformation has similarities to that between temperature and deformation, there is a crucial difference. In the latter, the coupling is largely in one direction because deformation has little effect on a temperature regime (except through its effect on fluid flow and advective heat transport) (Zimmerman 2000). Thus, although nonisothermal problems also require an energy transport equation to describe the system's thermal evolution, that aspect will not be addressed. Readers are referred to Noorishad et al. (1984), McTigue (1986), and Rutqvist et al. (2001) for more thorough discussions of the integration of thermoelasticity and poroelasticity and to Boley and Weiner (1960) for a comprehensive presentation of classical thermoelasticity.

This presentation uses the convention followed in rock mechanics that strain is positive for contraction and stress is positive for compression. Symbols for stress and fluid pressure can represent either the absolute values of those quantities or changes in the values of those quantities depending on the context in which they appear. All symbols are defined when first used, but a list of symbols, their definitions, and dimensions is also provided at the end of the paper.

Equations of deformation. As in elasticity, poroelasticity defines strains in the porous matrix in terms of displacements. Specifically, the six components of strain are defined by

$$\varepsilon_{xx} = \frac{\partial u}{\partial x} \qquad \varepsilon_{yy} = \frac{\partial v}{\partial y} \qquad \varepsilon_{zz} = \frac{\partial w}{\partial z}$$
$$\varepsilon_{xy} = \frac{1}{2}\left(\frac{\partial u}{\partial y} + \frac{\partial v}{\partial x}\right)$$
$$\varepsilon_{xz} = \frac{1}{2}\left(\frac{\partial u}{\partial z} + \frac{\partial w}{\partial x}\right) \tag{3}$$
$$\varepsilon_{yz} = \frac{1}{2}\left(\frac{\partial v}{\partial z} + \frac{\partial w}{\partial y}\right)$$

where ε is strain, and u, v, and w are displacements in the x, y, and z coordinate directions. Repeated indices indicate contraction or expansion and mixed indices indicate shear.

Poroelasticity can be used for analyzing dynamic phenomena such as elastic waves in porous solids (Biot 1956b; 1956c). However, the fluid-solid mechanical interactions of interest from a geologic perspective are generally elastostatic, meaning that accelerations can be ignored. Although such systems evolve over time, forces are balanced and that balance is expressed as

$$\frac{\partial \sigma_{xx}}{\partial x} + \frac{\partial \sigma_{yx}}{\partial y} + \frac{\partial \sigma_{zx}}{\partial z} = 0$$
$$\frac{\partial \sigma_{xy}}{\partial x} + \frac{\partial \sigma_{yy}}{\partial y} + \frac{\partial \sigma_{zy}}{\partial z} = 0$$
$$\frac{\partial \sigma_{xz}}{\partial x} + \frac{\partial \sigma_{yz}}{\partial y} + \frac{\partial \sigma_{zz}}{\partial z} = 0 \tag{4}$$

 DOI 10.1007/s10040-002-0230-8

where σ denotes the stresses on the faces of a volume of the porous formation. This representative elementary volume (REV) is small enough for variables such as stress or fluid pressure to have unique, definable values, but large enough to be represented by average values of medium properties. In a manner analogous to that for strain notation, repeated indices indicate normal stresses and mixed indices indicate shear stresses. Equations (4) will be used to describe changes in stress, rather than absolute stress values, allowing gravity to be neglected as a constant body force.

Nur and Byerlee (1971) generalized Terzaghi's effective stress law (1), as

$$\frac{\sigma'_{kk}}{3} = \frac{\sigma_{kk}}{3} - \alpha p \tag{5}$$

where $\sigma_{kk} = \sigma_{xx} + \sigma_{yy} + \sigma_{zz}$ is the change in the sum of normal stresses or volumetric stress, $\sigma'_{kk} = \sigma'_{xx} + \sigma'_{yy} + \sigma'_{zz}$ is the change in the volumetric effective stress, and α=1–K/K_s , where K is the bulk modulus of the porous medium and K_s is the bulk modulus of the solid grains. The change in fluid pressure is denoted by p. Equation (5) accurately describes the behavior of rocks under laboratory conditions. One would anticipate that as porosity approaches zero, K must approach K_s. Equation (5) shows that when this happens, the influence of pore pressure on effective stress vanishes, as would be expected.

Equation (5) implies that volume strain $\varepsilon_{kk} = \varepsilon_{xx} + \varepsilon_{yy} + \varepsilon_{zz}$ is related to effective stress rather than to total stress. Specifically,

$$\varepsilon_{kk} = \frac{1}{K}\left(\frac{\sigma_{kk}}{3} - \alpha p\right) \tag{6}$$

By analogy with linear elastic theory, the poroelastic constitutive equations for strain can then be expressed as

$$\begin{aligned}
\varepsilon_{xx} &= \frac{1}{2G}\left[\sigma_{xx} - \frac{\nu}{1+\nu}\sigma_{kk}\right] - \frac{\alpha}{3K}p - \alpha_T T \\
\varepsilon_{yy} &= \frac{1}{2G}\left[\sigma_{yy} - \frac{\nu}{1+\nu}\sigma_{kk}\right] - \frac{\alpha}{3K}p - \alpha_T T \\
\varepsilon_{zz} &= \frac{1}{2G}\left[\sigma_{zz} - \frac{\nu}{1+\nu}\sigma_{kk}\right] - \frac{\alpha}{3K}p - \alpha_T T \\
\varepsilon_{xy} &= \frac{1}{2G}\sigma_{xy} \qquad \varepsilon_{yz} = \frac{1}{2G}\sigma_{yz} \qquad \varepsilon_{xz} = \frac{1}{2G}\sigma_{xz}
\end{aligned} \tag{7}$$

where G is the shear modulus, ν is the drained Poisson's ratio, α_T is the coefficient of linear thermal expansivity of the porous medium, and is T temperature. In the absence of fluid pressure and temperature effects on deformation, the terms containing p and T in Eq. (7) are zero and the expressions reduce to the standard constitutive relations for an elastic solid. The constitutive relations can also be written with stress as the dependent variable. Adding the first three equations of (7) and solving for σ_{kk} yields

$$\sigma_{kk} = G\frac{2(1+\nu)}{(1-2\nu)}\varepsilon_{kk} + 3\alpha p + G\frac{4(1+\nu)}{(1-2\nu)}\alpha_T T \tag{8}$$

Substituting (8) into (7), one then obtains

$$\begin{aligned}
\sigma_{xx} &= 2G\varepsilon_{xx} + 2G\frac{\nu}{1-2\nu}\varepsilon_{kk} + \alpha p + 2G\frac{1+\nu}{1-2\nu}\alpha_T T \\
\sigma_{yy} &= 2G\varepsilon_{yy} + 2G\frac{\nu}{1-2\nu}\varepsilon_{kk} + \alpha p + 2G\frac{1+\nu}{1-2\nu}\alpha_T T \\
\sigma_{zz} &= 2G\varepsilon_{zz} + 2G\frac{\nu}{1-2\nu}\varepsilon_{kk} + \alpha p + 2G\frac{1+\nu}{1-2\nu}\alpha_T T \\
\sigma_{xy} &= 2G\varepsilon_{xy} \qquad \sigma_{yz} = 2G\varepsilon_{yz} \qquad \sigma_{xz} = 2G\varepsilon_{xz}
\end{aligned} \tag{9a}$$

At this point, it is useful to note that stress and strain, and equations containing them, can be expressed in different ways. For example, using indicial notation, the relation between stress and strain in equations (9a) can be written more compactly as

$$\sigma_{ij} = 2G\varepsilon_{ij} + 2G\frac{\nu}{1-2\nu}\varepsilon_{kk}\delta_{ij} + \alpha p\delta_{ij} + 2G\frac{1+\nu}{1-2\nu}\alpha_T T\delta_{ij} \tag{9b}$$

where δ_{ij}, the Kronecker delta, is zero when $i \neq j$ and one when i=j, and the Einstein summation convention is followed. Stress and strain are second-order tensors and, by bringing the pressure and temperature terms to the left side, Eq. (9b) can be written even more compactly as

$$\sigma''_{ij} = C^e_{ijkl}\,\varepsilon^e_{kl} \tag{9c}$$

where σ''_{ij} and ε^e_{kl} are the thermally compensated effective stress tensor and linear elastic strain tensor, respectively, and C^e_{ijkl} is a fourth-order tensor comprised of the linear elastic coefficients of Eq. (9a). In isothermal systems, σ''_{ij} reverts to the effective stress tensor σ'_{ij}.

The trace of a tensor is the sum of the main diagonal terms, and σ_{kk} and ε_{kk} are occasionally denoted $tr\,(\sigma)$ and $tr\,(\varepsilon)$. Those seeking an introduction to indicial notation and matrix forms of stress-strain relations may wish to consult Lai et al. (1978) or Shames (1964). Indicial notation is widely used because of its compactness, but at the cost of making the relationships difficult to visualize unless one is familiar with the equations. Most equations in this outline will be written out in full for clarity.

Descriptions of deformation in a poroelastic formation can be posed in terms of displacements, stresses, or strains. The governing equations for displacements are obtained by substituting the constitutive equations for stress (9a) into the equations of force equilibrium (4). The strain terms are then written in terms of their component displacements as in (3). The resulting displacement equations are

$$\begin{aligned}
G\nabla^2 u + \frac{G}{1-2\nu}\left[\frac{\partial^2 u}{\partial x^2} + \frac{\partial^2 v}{\partial x\partial y} + \frac{\partial^2 w}{\partial x\partial z}\right] \\
= \alpha\frac{\partial p}{\partial x} + G\frac{2(1+\nu)}{1-2\nu}\alpha_T\frac{\partial T}{\partial x}
\end{aligned}$$

 DOI 10.1007/s10040-002-0230-8

$$G\nabla^2 v + \frac{G}{1-2\nu}\left[\frac{\partial^2 u}{\partial y \partial x} + \frac{\partial^2 v}{\partial y^2} + \frac{\partial^2 w}{\partial y \partial z}\right] = \alpha\frac{\partial p}{\partial y} + G\frac{2(1+\nu)}{1-2\nu}\alpha_T\frac{\partial T}{\partial z}$$

$$G\nabla^2 w + \frac{G}{1-2\nu}\left[\frac{\partial^2 u}{\partial z \partial x} + \frac{\partial^2 v}{\partial z \partial y} + \frac{\partial^2 w}{\partial z^2}\right] = \alpha\frac{\partial p}{\partial z} + G\frac{2(1+\nu)}{1-2\nu}\alpha_T\frac{\partial T}{\partial z} \quad (10)$$

Displacements in poroelastic formations (from which strains and stresses can be computed) are governed by equations (10) and displacement boundary conditions.

If the governing equations are to be cast in terms of strain or stress, an additional step is required. The six components of strain (and by extension, the six distinct components of stress) are uniquely determined by only three components of displacement [u, v, and w in (3)]. Strain and stress components thus are not independent; rather, there are interrelations between them known as compatibility conditions. These conditions can be derived from the definitions of the componenents of strain (3). By further partial differentiation and manipulation of (3), as detailed by Timoshenko and Goodier (1987) or Wang (2000), the following set of compatibility relations can be obtained:

$$\begin{aligned}
2\frac{\partial^2 \varepsilon_{xy}}{\partial x \partial y} &= \frac{\partial^2 \varepsilon_{xx}}{\partial y^2} + \frac{\partial^2 \varepsilon_{yy}}{\partial x^2}\\
2\frac{\partial^2 \varepsilon_{yz}}{\partial y \partial z} &= \frac{\partial^2 \varepsilon_{yy}}{\partial z^2} + \frac{\partial^2 \varepsilon_{zz}}{\partial y^2}\\
2\frac{\partial^2 \varepsilon_{zx}}{\partial z \partial x} &= \frac{\partial^2 \varepsilon_{zz}}{\partial x^2} + \frac{\partial^2 \varepsilon_{xx}}{\partial z^2}\\
\frac{\partial^2 \varepsilon_{xx}}{\partial y \partial z} &= \frac{\partial}{\partial x}\left(-\frac{\partial \varepsilon_{yz}}{\partial x} + \frac{\partial \varepsilon_{xz}}{\partial y} + \frac{\partial \varepsilon_{xy}}{\partial z}\right)\\
\frac{\partial^2 \varepsilon_{yy}}{\partial z \partial x} &= \frac{\partial}{\partial y}\left(\frac{\partial \varepsilon_{yz}}{\partial x} - \frac{\partial \varepsilon_{zx}}{\partial y} + \frac{\partial \varepsilon_{yx}}{\partial z}\right)\\
\frac{\partial^2 \varepsilon_{zz}}{\partial x \partial y} &= \frac{\partial}{\partial z}\left(\frac{\partial \varepsilon_{zy}}{\partial \chi} + \frac{\partial \varepsilon_{zx}}{\partial y} - \frac{\partial \varepsilon_{xy}}{\partial z}\right)
\end{aligned} \quad (11)$$

Substituting the constitutive relations for strains in terms of stresses (7) and the force equilibrium equations (4) into the compatibility relations yields the equations governing deformation written in terms of stress, namely

$$\nabla^2\sigma_{xx} + \frac{1}{1+\nu}\frac{\partial^2\sigma_{kk}}{\partial x^2} - \frac{1-2\nu}{1-\nu}\alpha\left[\frac{1-\nu}{1+\nu}\frac{\partial^2 p}{\partial x^2} + \nabla^2 p\right] - 2G\alpha_T\left[\frac{\partial^2 T}{\partial x^2} + \frac{1+\nu}{1-\nu}\nabla^2 T\right] = 0$$

$$\nabla^2\sigma_{yy} + \frac{1}{1+\nu}\frac{\partial^2\sigma_{kk}}{\partial y^2} - \frac{1-2\nu}{1-\nu}\alpha\left[\frac{1-\nu}{1+\nu}\frac{\partial^2 p}{\partial y^2} + \nabla^2 p\right] - 2G\alpha_T\left[\frac{\partial^2 T}{\partial y^2} + \frac{1+\nu}{1-\nu}\nabla^2 T\right] = 0$$

$$\nabla^2\sigma_{zz} + \frac{1}{1+\nu}\frac{\partial^2\sigma_{kk}}{\partial z^2} - \frac{1-2\nu}{1-\nu}\alpha\left[\frac{1-\nu}{1+\nu}\frac{\partial^2 p}{\partial z^2} + \nabla^2 p\right] - 2G\alpha_T\left[\frac{\partial^2 T}{\partial z^2} + \frac{1+\nu}{1-\nu}\nabla^2 T\right] = 0$$

$$\nabla^2\sigma_{xy} + \frac{1}{1+\nu}\frac{\partial^2\sigma_{kk}}{\partial x \partial y} - \frac{1-2\nu}{1+\nu}\alpha\frac{\partial^2 p}{\partial x \partial y} - 2G\alpha_T\frac{\partial^2 T}{\partial x \partial y} = 0$$

$$\nabla^2\sigma_{yz} + \frac{1}{1+\nu}\frac{\partial^2\sigma_{kk}}{\partial y \partial z} - \frac{1-2\nu}{1+\nu}\alpha\frac{\partial^2 p}{\partial y \partial z} - 2G\alpha_T\frac{\partial^2 T}{\partial y \partial z} = 0$$

$$\nabla^2\sigma_{xz} + \frac{1}{1+\nu}\frac{\partial^2\sigma_{kk}}{\partial x \partial z} - \frac{1-2\nu}{1+\nu}\alpha\frac{\partial^2 p}{\partial x \partial z} - 2G\alpha_T\frac{\partial^2 T}{\partial x \partial z} = 0 \quad (12)$$

Equations (12) are analogous to what are known as the Beltrami-Michell equations of solid elastic theory, but differ from them because of the terms containing p and T that represent the poroelastic and thermoelastic coupling.

By adding the first three equations of (12) and rearranging, one obtains a relatively simple relationship between changes in stress, fluid pressure, and temperature, namely

$$\nabla^2\sigma_{kk} = \frac{2(1-2\nu)}{1-\nu}\alpha\nabla^2 p + 4G\frac{1+\nu}{1-\nu}\alpha_T\nabla^2 T \quad (13)$$

Stresses (and thus deformation) in a poro- and thermoelastic formation are governed by the force equilibrium and compatibility relationships incorporated in equations (12) or (13), subject to appropriate boundary conditions. Equation (13) will be of particular interest regarding a simplifying assumption, discussed later, that is often invoked for analyzing pore fluid flow.

Equations of fluid flow

Although the equations of deformation are based on force equilibrium, the fluid flow equation is based on mass conservation, which can be stated as

$$\frac{\partial}{\partial t}(\rho n) + \nabla\cdot(\rho\boldsymbol{q}) - J = 0 \quad (14)$$

where ρ is fluid density, n is porosity, and $\boldsymbol{q}$ (a vector quantity) is the Darcy, or specific, flux of pore fluid. The first term in (14) describes changes in fluid stored in the REV, and the second term describes the net fluid flux across the REV faces. J is a fluid source or sink, which may be either at discrete locations or distributed in an arbitrary fashion in the domain. Letting $m=\rho n$ denote the mass of the pore fluid per volume of porous formation, changes in this quantity can be denoted as

$$m - m_0 = (\rho - \rho_0)n_0 + \rho_0(n - n_0) \quad (15)$$

 DOI 10.1007/s10040-002-0230-8

Rice and Cleary (1976), among others, have presented the description of porosity changes in terms of compression moduli, and work by Palciauskas and Domenico (1982) has delineated the effects of temperature changes on porosity. Synthesizing their results yields

$$n - n_0 = -\left(\frac{1}{K} - \frac{1}{K_s}\right)\frac{\sigma_{kk}}{3} + \left(\frac{1}{K} - \frac{1}{K_s} - \frac{n}{K_s}\right)p + n_0\,\alpha_{Tp}\,T \tag{16}$$

as a description of porosity changes caused by stress, fluid pressure, and temperature changes. Here, α_{Tp} is the bulk thermal expansivity of the formation pores. Likewise, fluid density changes in response to temperature and pressure changes are given by

$$\rho - \rho_0 = \rho_0 \frac{p}{K_f} - \rho_0\,\alpha_{Tf}\,dT \tag{17}$$

where K_f is the fluid bulk modulus and α_{Tf} is its bulk (or volumetric) thermal expansivity. Substituting (17) and (16) into (15) yields

$$m - m_0 = -\rho_0\left(\frac{1}{K} - \frac{1}{K_s}\right)\frac{\sigma_{kk}}{3} + \rho_0\left[\left(\frac{1}{K} - \frac{1}{K_s}\right) + \left(\frac{n_0}{K_f} - \frac{n_0}{K_s}\right)\right]p - \rho_0\,n_0\left(\alpha_{Tp} - \alpha_{Tf}\right)T \tag{18}$$

Force equilibrium applies to the fluid as well as the porous medium, but is manifested through a constitutive relation between fluid flux and forces driving the flux. For nearly all geologic applications, the appropriate constitutive relation is Darcy's law, which can be expressed as

$$q = -\frac{\boldsymbol{k}}{\mu}(\nabla p + \rho g \nabla z) \tag{19a}$$

where $\boldsymbol{k}$ (a second-order tensor) is the formation permeability, μ is fluid dynamic viscosity, g is gravitational acceleration, and z is elevation above an arbitrary datum. Darcy's law can be written in indicial notation as

$$q_i = -\frac{k_{ij}}{\mu}\left(\frac{\partial p}{\partial x_j} + \rho g \frac{\partial z}{\partial x_j}\right) \tag{19b}$$

but because permeabilty anisotropy is not of primary interest here, it will be more convenient to use Eq. (19a) in what follows. Darcy's law shows that fluid flow is driven by gradients in pressure energy and elevation energy, and substituting Eqs. (19a) and (18) into the statement of fluid mass conservation (14) yields

$$\nabla \cdot \frac{\boldsymbol{k}\rho}{\mu}(\nabla p + \rho g \nabla z) = \rho\left[\left(\frac{1}{K} - \frac{1}{K_s}\right) + \left(\frac{n}{K_f} - \frac{n}{K_s}\right)\right]\frac{\partial p}{\partial t} - \rho\left(\frac{1}{K} - \frac{1}{K_s}\right)\frac{\partial \sigma_t}{\partial t} - n\rho\left(\alpha_{Tf} - \alpha_{Tp}\right)\frac{\partial T}{\partial t} - J \tag{20}$$

The quantity $\sigma_t = \sigma_{kk}/3$ denotes the mean normal or mean total stress.

Here, it is helpful to introduce the three-dimensional specific storage S_{s3}, and three- dimensional loading efficiency β, which are defined as

$$S_{s3} = \rho g\left[\left(\frac{1}{K} - \frac{1}{K_s}\right) + \left(\frac{n}{K_f} - \frac{n}{K_s}\right)\right] \tag{21}$$

and

$$\beta = \frac{\left(\frac{1}{K} - \frac{1}{K_s}\right)}{\left(\frac{1}{K} - \frac{1}{K_s}\right) + \left(\frac{n}{K_f} - \frac{n}{K_s}\right)} \tag{22}$$

β is also known as Skempton's coefficient, honoring Alec Westley Skempton, who first discussed its significance (Skempton 1954). It has a distinct physical interpretation as the ratio of change in fluid pressure to change in mean total stress under undrained conditions, meaning there is no change in fluid mass. For highly compressible media, β approaches unity while in very stiff media it can be close to zero. Substituting these definitions into Eq. (20) gives

$$\nabla \cdot \frac{k\rho g}{\mu}(\nabla p + \rho g \nabla z) = S_{s3}\frac{\partial p}{\partial t} - S_{s3}\,\beta\frac{\partial \sigma_t}{\partial t} - \rho g n \Lambda \frac{\partial T}{\partial t} - gJ \tag{23}$$

as the governing equation for pore fluid flow. The new quantity Λ is a thermal response coefficient for the fluid-porous medium system and is equal to $\alpha_{Tf} - \alpha_{Tp}$. The terms on the right side of Eq. (23) describe effects of fluid storage, stress changes, temperature changes, and fluid sources, respectively. In geologic problems, the fluid source term can represent generation of petroleum or other diagenetic fluids.

An alternative form of Eq. (23) can be written in terms of strain rather than stress. Solving (6) for $\sigma_t = \sigma_{kk}/3$, and substituting the result in (23) gives

$$\nabla \cdot \frac{\boldsymbol{k}\rho g}{\mu}(\nabla p + \rho g \nabla z) = S'_{s3}\frac{\partial p}{\partial t} - \rho g \alpha \frac{\partial \varepsilon_{kk}}{\partial t} - \rho g n \Lambda \frac{\partial T}{\partial t} - gJ \tag{24}$$

where a modified three-dimensional specific storage is defined as

$$S'_{s3} = \rho g\left[\left(\frac{1}{K} - \frac{1}{K_s}\right)(\alpha + 1) + \left(\frac{n}{K_f} - \frac{n}{K_s}\right)\right] \tag{25}$$

Because it can make visualization of flow patterns easier, it is sometimes helpful to formulate the flow equation in terms of hydraulic head rather than fluid pressure. This can be done even when fluid density varies significantly (Garven 1989) by defining relative fluid viscosity and relative fluid density as $\mu_{rel} = \mu_{ref}/\mu$ and $\rho_{rel} = (\rho - \rho_{ref})/\rho_{ref}$ where the subscript *ref* denotes the value at a reference state. Defining hydraulic head with respect to the reference density as $h = p/(\rho_{ref} g) + z$ and hydraulic

 DOI 10.1007/s10040-002-0230-8

conductivity with respect to the reference density and viscosity as ($\boldsymbol{\kappa} = \boldsymbol{k}\rho_{ref}g)/\mu_{ref}$, (23) can be written

$$\nabla \cdot \boldsymbol{\kappa}\, \mu_{rel}\, \rho'(\nabla h + \rho_{rel}\nabla z) = S_{s3}\left(\frac{\partial h}{\partial t} - \frac{\partial z}{\partial t}\right) - \rho'\frac{\alpha}{K}\frac{\partial \sigma_t}{\partial t} - \rho' n\Lambda\frac{\partial T}{\partial t} - \frac{J}{\rho_{ref}} \qquad (26)$$

where $\rho'=\rho/\rho_{ref}$ and it is noted that $\alpha/K = K^{-1} - K_s^{-1}$. The partial derivative of elevation with respect to time ($\partial z/\partial t$) in the storage term is retained because geologic processes can result in significant and spatially varied elevation changes over time. Finally, in systems with isodensity and isoviscosity fluids (that is, where $\rho=\rho_{ref}$ and $\mu=\mu_{ref}$), (26) simplifies to

$$\nabla \cdot \boldsymbol{\kappa}\nabla h = S_{s3}\left(\frac{\partial h}{\partial t} - \frac{\partial z}{\partial t}\right) - \frac{\alpha}{K}\frac{\partial \sigma_t}{\partial t} - n\Lambda\frac{\partial T}{\partial t} - \frac{J}{\rho} \qquad (27)$$

Equations (23), (24), (26), and (27) are versions of the transient flow equations widely used by groundwater hydrologists. They differ by including the time derivatives of mean total stress σ_t or volume strain ε_{kk} and temperature T. The stress or strain term provides the coupling between deformation and flow by representing changes in pore space available to the fluid.

Describing fully coupled fluid flow and deformation in two or three dimensions requires solving (a) either the equations of displacement (10) or equations of strain or stress that incorporate force equilibrium and compatibility such as (12) or (13) and (b) an equation for flow (e.g. 23) in a coupled fashion. Solutions are now generally obtained numerically, and the coupling requires solving the equations sequentially in each time step to obtain the new value of pressure or stress/strain, iterating if necessary. Initial and boundary conditions must be specified for *both* deformation and fluid flow.

Boundary and initial conditions

Boundary conditions for the pore fluid and the porous medium are usually of two kinds (Detournay and Cheng 1993). A Dirichlet-type boundary condition for flow specifies fluid pressure p, hydraulic head h or a related quantity such as excess pressure or head on the boundary; a Dirichlet-type boundary condition for deformation specifies displacement $\boldsymbol{u}=(u, v, w)$. Neumann-type boundary conditions specify a fluid flux normal to the boundary $\boldsymbol{q}_n$, and the traction $\boldsymbol{t}$, or stress vector, acting on the boundary surface. A more rarely used third type of boundary condition, the Fourier type, involves a functional relationship between p or h and $\boldsymbol{q}_n$ in the case of flow, and between $\boldsymbol{u}$ and $\boldsymbol{t}$ in the case of deformation. A domain can (and usually does) have a mix of boundary conditions. In addition, any of these boundary conditions can be made to vary in time. Exclusive use of Neumann-type boundary conditions does not fully define a problem (Detournay and Cheng 1993). In the case of fluid flow, for instance, only the head gradient is constrained and the absolute head values are indeterminate.

Initial conditions for the deformation of the porous medium are required to satisfy the requirement for force equilibrium. The initial conditions for flow, that is, the initial pattern of p or h throughout the domain, often is not an important consideration because it has decreasing influence on system behavior with time. In some situations, however, the initial pressures are of great interest, as when a load increment is instantaneously applied at the beginning of a simulation. In that case, the force equilibrium equations (4) can be solved and the initial fluid pressures computed from the resulting changes in σ_t and the three-dimensional loading efficiency β.

Inelastic Rheologies and Finite Strain

Although poroelasticity offers a rigorous theoretical foundation for analysis, it has important shortcomings for many geologic applications. The most significant are its assumption of infinitesimal linear elastic strains. Although some geologic deformation *is* closely approximated as linear elastic with infinitesimal strains (such as earth tides), much is eminently inelastic, often with large, unrecoverable deformations that are complicated functions of the three-dimensional stress state, temperature, chemical environment, time, and other factors. This is especially, but not solely, true for deformation on geologic time scales that results from a number of nonmechanical as well as mechanical processes. In geologic parlance, much of the inelastic deformation would be referred to as diagenesis.

In addition to controlling hydromechanical coupling, inelastic and finite strain behaviors create what might be called "secondary" couplings. For example, strain hardening alters fluid storage properties and finite strains change permeability, both of which can dramatically affect fluid flow regimes. Although such "secondary" couplings are not a primary concern here, they can be very important (e.g., Bethke and Corbet 1988; Grün et al. 1989; Makurat et al. 1990).

Deformation in crustal processes

To understand the rich variety of hydromechanical processes that occur in nature, one must consider the mechanical behavior of a spectrum of geologic media ranging from soft muds to crystalline rocks. Laboratory tests, observations of engineered or rapidly responding natural systems, and geologic evidence of past deformation indicate that a number of behaviors, including nonlinear elasticity, elastoplasticity, and viscoelasticity occur in geologic media.

Nonlinear elastic, elastoplastic, and viscoelastic behaviors are well illustrated by one-dimensional compaction in sedimentary media. Figure 3a shows a typical relation between uniaxial volumetric strain, represented as changes in void ratio e, and the log of uniaxial stress. The first phase of deformation is nonlinear elastic (which

 DOI 10.1007/s10040-002-0230-8

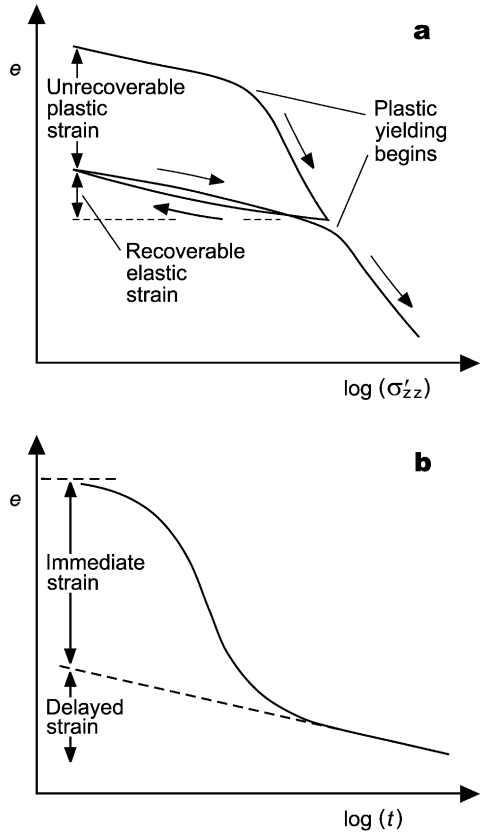

Fig. 3 **a** Plot of volumetric strain ε_{kk} (as void ratio e) versus the log of vertical effective stress σ'_{zz} showing nonlinear elastic and plastic strains typically observed in fine-grained sediments. Deformation data presented in this manner are often called "e-log(p)" plots. **b** Plot of volumetric strain ε_{kk} (again as void ratio e) versus the log of time since applying a load. "Immediate" elastoplastic strain and "delayed" viscous strain, or creep, are depicted as they are typically seen in clayey sediments. The lag in the "immediate" strain reflects the time required to expel pore fluid and reveals the temporal evolution of effective stress

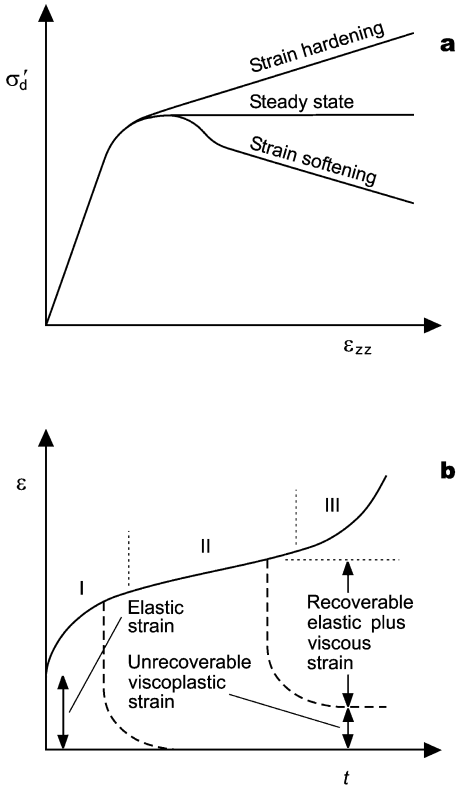

Fig. 4 **a** Plot of axial strain ε_{zz} versus differential stress (maximum principal stress minus minimum principal stress) showing types of plastic yielding observed in rocks. **b** Viscous creep behavior observed in rocks under constant stress (modified from Jaeger and Cook 1969). If the stress is removed in the primary creep region (*I*), all the strain is recovered. If it is removed in the secondary creep region (*II*), there is plastic, or unrecoverable, strain. Tertiary creep (*region III*) progresses rapidly to failure

is linear in this semi-log plot) until the material begins to yield plastically and the slope changes. Once plastic strain has occurred, as Fig. 3a shows, only that portion of the strain which is elastic (often a relatively minor part) can be recovered. Figure 3a also reveals that stress history can be important, with different modes of deformation for stresses greater and less than prior maxima; as a result, the strain state is not a unique function of stress. Viscoelastic behavior in compacting sediments is shown in Fig. 3b, which is a plot of uniaxial volumetric strain (again represented by e) versus the log of time since the application of a load increment. The initial time-dependent response seen in the "immediate strain" in Fig. 3b results from the need to expel fluid; the strain is "immediate" in the sense of its response to *effective* stress. At larger values of time, however, the fluid drainage "catches up," and there is time-dependent strain in response to effective stress; this is the "delayed" or viscous portion of the strain.

Elastoplastic and viscoelastic strains also occur in rocks. Figure 4a shows styles of plastic yielding observed in rocks during constant strain tests. Whether a rock experiences plastic yielding or suffers brittle failure depends on the stress state, temperature, and chemical environment. Plastic deformation can occur as shear as well as volumetric strain, and shear deformation can be important, as shall be seen. Viscoelastic behavior (also called creep or time-dependent deformation in rock mechanics) can also be very important in rocks (Jaeger and Cook 1969). Figure 4b, a plot of strain versus time, shows the viscoelastic behavior typical of rocks, namely initial elastic strain followed by concave down, linear, and concave up strain trends (denoted as regions I, II, and III). Dashed lines show the behavior following removal of stress in different phases; plastic strains that cannot be recovered occur after phase II deformation, showing that rocks exhibit nonlinear elastic, viscoelastic, and elastoplastic behavior.

The actual behavior of geologic media can be and probably often is still more complex than the preceding paragraphs suggest. Not only can geologic media exhibit both elastoplastic and viscoelastic properties as shown in

 DOI 10.1007/s10040-002-0230-8

Fig. 4b, they undoubtedly progress through phases marked by different modes of deformation at different pressures and temperatures (e.g., Schneider et al. 1996). Other styles of deformation are also possible. At high temperatures, for example, rocks begin to behave as Newtonian fluids and then progess to non-Newtonian fluid behavior as pressures increase (Turcotte and Schubert 1982). Geologic media can also exhibit inelastic dilatancy, a volumetric strain during shearing. Rudnicki (1985) suggested that this occurs in rocks when microcracks are opened by locally tensile stresses or widened as asperities slide over opposing asperities. He further proposed that it can be described by $\varepsilon^p_{kk} = \xi\, \varepsilon^p_{shear}$, where ε^p_{kk} is plastic volumetric strain, ε^p_{shear} is plastic shear strain, and ξ is the dilatancy factor, which is negative or positive for shear-induced expansion or contraction. This behavior has been observed in rocks under laboratory conditions (e.g., Brace et al. 1966; Wang 1997) and probably in rocks in situ (Wang 1997). Analogous behavior has been observed in granular media, including clays in laboratory tests (Skempton 1954; Marone et al. 1990) and clayey sediments in situ (Cartwright and Lonergan 1996), about which more will be said in the following section. Even osmotic processes in clay-rich geologic media cause deformations (Barbour and Fredlund 1989) and have been placed in a poroelastic framework by Sherwood (1993). Finally, it must be noted that, in addition to various modes of continuum deformation, there are a number of styles of failure involving fracturing, shear failure, and faulting, of which more will be said later.

Rheology is incorporated in analyses via constitutive relations between stress and strain. Poroelastic theory can be generalized for inelastic rheologies and large strains by analogy with approaches that have been used to generalize linear elastic theory for simple solids. Jaeger and Cook (1969), for example, discuss a number of these generalizations. As already noted, some analytical generalizations were incorporated in poroelastic theory by Biot, including those for viscoelastic and anisotropic media (Biot 1956a) and finite strains (Biot 1972). Other examples include incorporation of elastoplasticity with strain hardening by Smith and Patillo (1983) and inelastic dilatant behavior by Rudnicki (1985) and Wang (1997), among others. Although they complicate the analysis, the incorporation of these behaviors in coupled hydromechanical analyses no longer offers real conceptual difficulties.

The best-studied mode of geologic deformation is undoubtedly burial-related compaction in active sedimentary basin environments. Athy (1930) pioneered quantitative descriptions of porosity-depth trends in sedimentary media, showing porosity decreases approximately as an exponential function of depth. This type of relationship has since been observed in many different environments (e.g., Rieke and Chilingarian 1974; Giles 1997), suggesting that similar processes are at work in each case. The deformation is elastoplastic with the plastic portion dominant because most of the strain is not recoverable. Certain diagenetic processes, however, may also cause viscoelastic-type deformation. Various rheological models for these processes have been proposed, usually invoking viscous and plastic deformation and with a dependence on temperature as well as on stress (e.g., Palciauskas and Domenico 1989; Schneider et al. 1996; Revil 1999). Because development of these models was motivated by depth-related trends, strain has usually been considered to be one-dimensional in them and they have not been applied to hydromechanical coupling in two or three dimensions. See *Uncertain constitutive laws for deformation* for additional discussion of their role in basin analysis.

Inelastic rheologies from a geotechnical perspective

Efforts to generalize poroelastic theory seem to have reached their zenith in geotechnical applications. This undoubtedly reflects the fact that complexities in deformation behavior are often conspicuous in geotechnical problems. Materials typically considered in geotechnical applications tend to have elastoplastic and viscoelastic styles of deformation. Although such behavior has been observed only on short time scales, it is among the best clues to how deformation in sedimentary and other geologic media *might* occur on geologic time scales, and the tools developed to describe it can be helpful in understanding and analyzing long-term geologic deformation. Thus, it is worthwhile to briefly examine some of these approaches. In addition, some geologic problems involving soft sediment deformation may be particularly amenable to geotechnically based approaches (see *Tectonic deformation*).

For this discussion, it will be helpful to use the shorthand of indicial notation to express the relations between stress and strain. Lewis and Schrefler (1987) placed the isothermal poroelastic constitutive relations (Eqs. 9c) in a general context by expressing them as

$$\sigma'_{ij} = C^e_{ijkl}\, \varepsilon^e_{kl} = C^e_{ijkl}\left(\varepsilon_{kl} - \varepsilon^p_{kl} - \varepsilon^v_{kl} - \varepsilon^d_{kl}\right) \tag{28}$$

where ε_{kl}, ε^p_{kl}, ε^v_{kl}, and ε^d_{kl} are the total, plastic, viscous, and diagenetic (Lewis and Schrefler's "autogenous") strain tensors, respectively. Recall that C^e_{ijkl} is a fourth-order tensor comprised of the linear elastic coefficients of (9a) (see Lewis and Schrefler 1987, p. 43). Equation (28) explicitly categorizes deformation processes commonly considered significant in geotechnical applications.

Elastoplastic behavior is especially conspicuous in fine-grained sediments in evolving three-dimensional stress fields and has received a great deal of attention. Mohr-Coulomb and so-called critical state elastoplastic models are widely used for geotechnical problems, and Lewis and Schrefler show that they can be expressed in the same form as (28), specifically

$$\sigma'_{ij} = C^{ep}_{ijkl}\, \varepsilon^{ep}_{kl} \tag{29}$$

where C^{ep}_{ijkl} is a tensor containing the elastoplastic coefficients. Here, it is implicitly assumed that ε^v_{ij} and ε^d_{ij} can be ignored. C^{ep}_{ijkl} has a complex form, but here it is

 DOI 10.1007/s10040-002-0230-8

sufficient to note that poro-elastoplastic descriptions can be implemented with constitutive relations that are similar in form to those describing poroelasticity. The terms in C^{ep}_{ijkl} can be found in Lewis and Schrefler (1987).

A key problem in elastoplasticity is specifying the yield surface, or the boundary between elastic and plastic behavior. This problem is best approached in terms of σ_1, σ_2, and σ_3, which are the largest, intermediate, and least principal stresses, or stresses normal to planes on which shear stresses are zero (see Timoshenko and Goodier 1987 for an introduction to the notion of principal stresses). A simple approach is to treat the yield surface as a Mohr-Coulomb failure envelope, which predicts yielding when the effective principal stresses deviate sufficiently from a hydrostatic state ($\sigma'_1 = \sigma'_2 = \sigma'_3$) (Mohr-Coulomb-style brittle failure in two dimensions is discussed in more detail in *Shearing, faulting, and seismicity*). A more comprehensive approach is provided by critical state theory, which postulates a yield surface dependent not only on effective stresses, but also on the strain state and history. Critical state models are discussed in some detail by Britto and Gunn (1987), for example. Two in particular, the Cam-clay (Roscoe et al. 1963; Schofield and Wroth 1968; named for the University of Cambridge) and modified Cam-clay models (Roscoe and Burland 1968), have seen especially wide use because they successfully incorporate many aspects of three-dimensional clay deformation that are observed in laboratory tests.

In Cam-clay models, the elastic-plastic boundary is considered to be a function of three descriptors of the mechanical state and history of the medium, namely the mean total effective stress σ'_t (here defined in terms of principal effective stresses as $\left[\sigma'_1 + \sigma'_2 + \sigma'_3\right]/3$), differential effective stress σ'_d (defined as $\sigma'_1 - \sigma'_3$), and a measure of volumetric strain state, such as void ratio e. In the modified Cam-clay model the yield surface (Fig. 5a) is ellipsoidal and defined by

$$\frac{\sigma'^2_d}{M^2} + \sigma'_t\left(\sigma'_t - \sigma'_{t\ \max}\right) = 0 \tag{30}$$

where M a constant specific to the porous medium, and $\sigma'_{t\ \max}$ is the maximum value of σ'_t the sediment has experienced. The functional connection of the surface described by (30) with e is provided by $\sigma'_{t\ \max}$ as shall be seen below. The yield surface separates permissible combinations of σ'_t, σ'_d, and e, which lie below the surface, from those that cannot be attained because of plastic yielding.

In visualizing the behavior described by the Cam-clay model, it may help to consider what happens when differential stress σ'_d is zero. The yield surface then reduces to a curve in two-dimensional space defined by e and σ'_t (Fig. 5b). This curve is another form of "e-log(p)" plot, such as the one shown in Fig. 3a, from consolidation testing. Indeed, the model mimics consolidation-rebound behavior with virgin consolidation (consolidation under higher loads than the medium has experienced in the past) described by

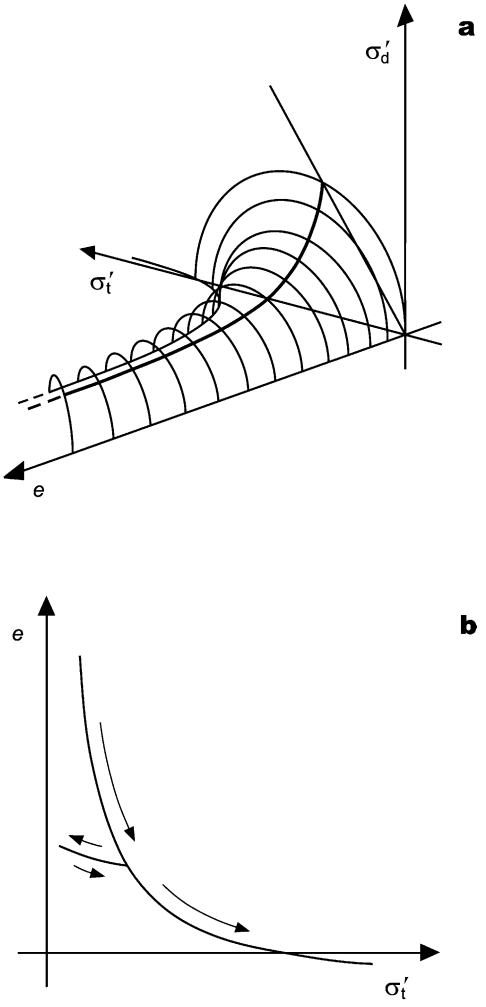

Fig. 5 **a** Plastic yield surface for the Cam-clay deformation model plotted in three-dimensions defined by mean total effective stress σ'_t, differential effective stress σ'_d, and void ratio e. Attainable states of stress and volumetric strain lie below the surface; plastic yielding occurs on the surface, and the "critical state" occurs at the intersection of the surface and the critical state plane (*bold curve*). **b** Yield surface in the $\sigma'_t - e$ plane. Elastic decompaction and recompaction traces (*short arrow segments*) are also shown. These curves become nearly linear, replicating the behavior shown in Fig. 3a, when the σ'_t axis is transformed to $\log \sigma'_t$

$$e = e_0 - \lambda_{cc}\ \ln\left(\sigma'_t\right),\ \sigma'_t = \sigma'_{t\ \max} \tag{31}$$

and decompaction and recompaction given by

$$e = e_{\sigma\ \max} + \kappa_{cc}\ \ln\left(\sigma'_{t\ \max} - \sigma'_t\right),\ \sigma'_t < \sigma'_{t\ \max} \tag{32}$$

Here, $e_{\sigma\ \max}$ is the void ratio corresponding to $\sigma'_{t\ \max}$, e_0 is a reference void ratio, and $-\lambda_{cc}$ and $-\kappa_{cc}$ are the slopes of the relations in $e - \log\left(\sigma'_t\right)$ space. Equation (31) describes the main consolidation trend in Fig. 5b, and Eq. (32) describes the short decompaction-recompaction segment in Fig. 5b. It can now be seen that the third, vertical (σ'_d) dimension of Fig. 5a allows the differences in this behavior under various differential effective stresses to be accounted for. Note that the yield surface displays strain

 DOI 10.1007/s10040-002-0230-8

hardening; it expands, allowing the medium to sustain greater σ'_t and σ'_d as compression reduces e (Fig. 5a).

The remaining component of Cam-clay models is the critical state line, defined as the intersection of the plane

$$\sigma'_d = M\sigma'_t \tag{33}$$

with the yield surface. The resulting curve in three dimensions (Fig. 5a) defines the "critical state," where plastic shearing proceeds indefinitely without volume strain or changes in stress. Elsewhere on the yield surface, plastic shearing involves either volumetric expansion or contraction as conditions approach the critical state. This merely reflects the tendency of loose or undercompacted sediments to compact and of compacted sediments to dilate during shear. It is analogous to the volumetric strain observed in rocks undergoing shear that was described in the previous section.

This very brief outline glosses over many aspects of the Cam-clay model, such as describing the direction of plastic strains, details of which can be found in the treatments of Britto and Gunn (1987), Lewis and Schrefler (1987), and others. Of interest here, however, is the notion that deformation is controlled not only by the total effective stress, but also by *differential effective stress and by deformation state and history*. Geologic deformation in some settings is probably similar.

Although Cam-clay and related rheological models provide rather good descriptions of the elastoplastic behavior of soft sediments (Lewis and Schrefler 1987), they have the significant limitation of ignoring viscous components of deformation. This could be an important limitation for geologic problems because viscous deformation is sometimes observed in laboratory experiments on media such as shale (e.g., Neuzil 1993) and may also be analogous to certain forms of diagenetically caused deformation, such as pressure solution.

A number of models have been developed for viscous strain, or creep, in rocks (Jaeger and Cook 1969) and sediment (Šuklje 1969). A relatively simple viscoelastic model proposed by Gibson and Lo (1961) for soft-sediment consolidation can be visualized as a Hookean (elastic) spring in series with a Kelvin body composed of a second spring in parallel with a dashpot (Fig. 6). Upon application of an effective stress change, the first Hookean spring responds immediately. The Kelvin body, however, responds over time as the dashpot compresses and transfers the effective stress to the second Hookean spring. Lewis and Schrefler (1987) show how Gibson and Lo-type viscous deformation can be incorporated into a fully coupled hydromechanical model. If diagenetic strains are either ignored or subsumed within the viscous term, the resulting constitutive relation has the form

$$\sigma'_{ij} = C^{e}_{ijkl}\,\varepsilon^{e}_{kl} + C^{c1}_{ijkl}\,\varepsilon^{c1}_{kl} + C^{c2}_{ijkl}\,\dot{\varepsilon}^{c2}_{kl} \tag{34}$$

where C^{c1}_{ijkl} and C^{c2}_{ijkl} are tensors containing the stress-strain coefficients for the Kelvin body spring and dashpot, ε^{c1}_{kl} is the strain tensor for the spring, and $\dot{\varepsilon}^{c2}_{kl}$ is the rate of strain tensor for the dashpot. The term $C^{e}_{ijkl}\,\varepsilon^{e}_{kl}$ represents the elastic response of the independent Hookean spring in Fig. 6. This formulation thus does not consider plastic deformation.

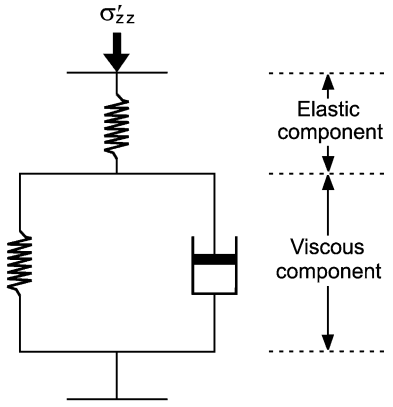

Fig. 6 Gibson and Lo (1961) phenomenological model for viscous creep deformation in sediments and soils (modified from Šuklje 1969)

The need for a more general rheology was recognized by Borja (1984) and Borja and Kavazanjian (1985), who incorporated viscous creep into the modified Cam-clay elastoplastic framework. Borja (1984) showed that the constitutive relation for this "visco-elastoplasticity" model can be written in a rate form as

$$\dot{\sigma}'_{ij} = C^{vep}_{ijkl}\,\dot{\varepsilon}^{vep}_{kl} - \dot{\sigma}'^{r}_{ij} \tag{35}$$

where C^{vep}_{ijkl} is the tensor containing the visco-elastoplastic coefficients, $\dot{\sigma}'_{ij}$ is the rate of change of the effective stress tensor, $\dot{\varepsilon}^{vep}_{kl}$ is the visco-elastoplastic strain rate tensor, and $\dot{\sigma}'^{r}_{ij}$ is the effective stress relaxation rate. The latter describes the viscous relaxation of stress under conditions of no strain. Borja (1984) showed how this constitutive relation can be incorporated into coupled two-dimensional numerical analyses.

Inherent Uncertainties in Descriptions of Hydromechanical Behavior of Geologic Systems

As the preceding section shows, numerous generalizations have been developed for linear poroelastic theory, with many arising from geotechnical research. However, it has often proven quite difficult to apply these generalizations in analysis of geologic processes. An important reason is profound uncertainty about when and where various rheological models apply.

Uncertain constitutive laws for deformation

Geologic deformation often occurs on time scales that are orders of magnitude longer than can be observed, and geologic deformation rates are correspondingly small. Geologic strain rates of 10^{-14} s^{-1} or less are common, but it is difficult to directly observe strain rates smaller than about 10^{-5} or 10^{-6} s^{-1} (Tullis and Tullis 1986). In some instances processes of interest can be accelerated. Plastic

 DOI 10.1007/s10040-002-0230-8

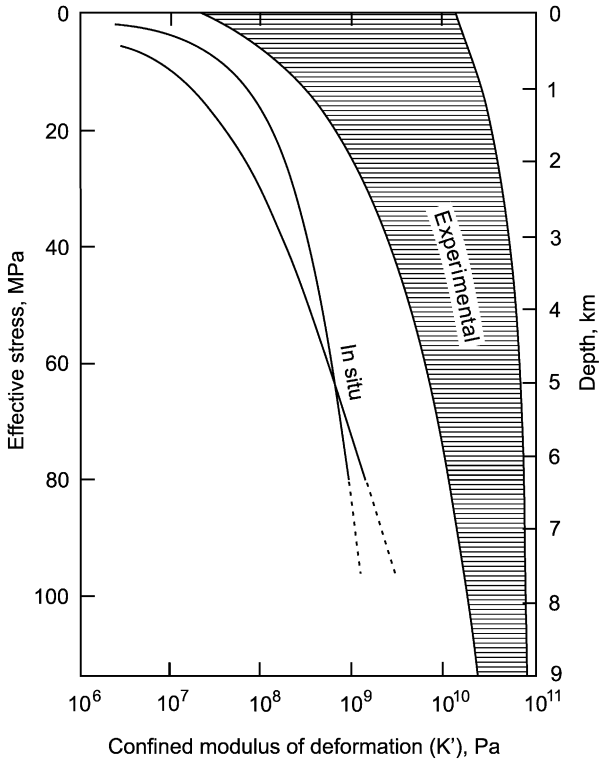

Fig. 7 Plot comparing laterally confined moduli of deformation (K') of sedimentary media determined experimentally and from representative porosity-depth trends (adapted from Neuzil 1986). The in situ curves were calculated by assuming that vertical effective stress σ'_{zz} increases at 1.3×10^4 Pa m^{-1}. The difference between in situ and experimental moduli, as much as three orders of magnitude at low effective stresses, reflects the mechanical and nonmechanical deformation mechanisms that occur in situ on geologic time scales but not under laboratory conditions and on short time scales. A full description of hydromechanical coupling would require incorporating these in situ effects in a process-based fashion

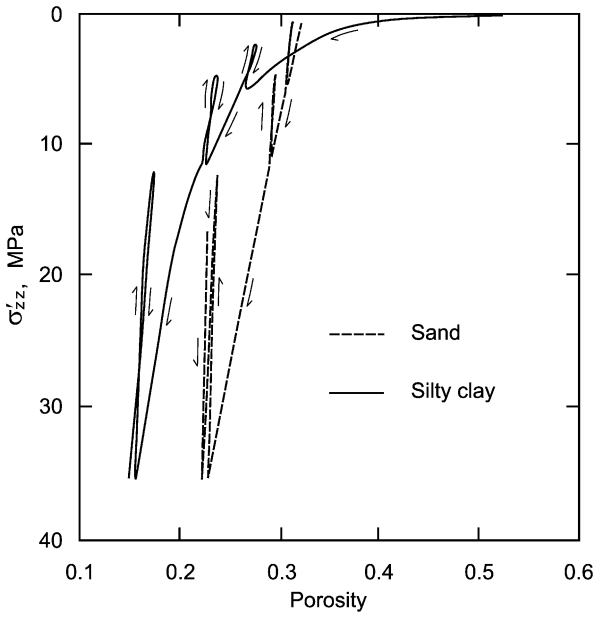

Fig. 8 Plot of porosity versus uniaxial effective stress for sand and silty clay undergoing laterally confined compaction under laboratory conditions. Cycles of loading and unloading are indicated by *arrows*. These laboratory data are notable for the high stresses attained; the maximum effective stress of 35 MPa corresponds (in a normally pressured fluid regime) to a depth of about 2.7 km (adapted from Karig and Hou 1992)

strain in rocks, for example, can be accelerated by increasing the temperature. In general, however, one is limited to studying "snapshots" of various stages in the evolution of geologic systems. The appropriate constitutive laws must then be inferred by somehow integrating the information in these snapshots. This can be a very uncertain undertaking.

The difficulties are well illustrated by the problem of sediment compaction in basins. Sediment compaction is comparatively well-constrained in the sense that it is laterally confined (and thus largely one-dimensional) and the history of the stress changes that have driven deformation (predominantly increasing overburden load) can often be determined. It nevertheless shares many of the complexities of other deformation styles, such as those due to tectonism, making it is a useful model for discussion. Consider Fig. 7, which shows the modulus for laterally confined deformation (K') of sedimentary media with depth as determined by deformation tests *and* by observed loss of porosity with depth in situ. Note that this comparison is not between laboratory and in situ experimental values, which show some differences; rather, it is between experimentally determined moduli in general and long-term apparent moduli in natural processes. One can see that long-term in situ compaction moduli computed from porosity loss are as much as three orders of magnitude smaller than experimental values.

Further evidence of the differences between experimental and in situ compaction processes is provided by Fig. 8, a plot of porosity loss trends for sand and silty clay obtained under laboratory conditions. Note that although the silty clay displays the familiar exponential porosity decrease with stress (or its equivalent, depth), the decrease in sand porosity is linear. This is unlike in situ porosity-depth trends observed in sands and sandstones, almost all of which also display an exponential form (Giles 1997, Fig. 10.31).

The difference between experimental and geologic compaction revealed by Figs. 7 and 8 clearly results from deformation processes that occur over long periods of time in situ but not over short periods of time under experimental conditions. Some of the difference is undoubtedly due to mechanical or physicochemical processes and can, at least in principle, be related to effective stress and temperature. To understand these processes, researchers have considered phenomena occurring at grain-to-grain contacts.

Pressure solution may be an important component of geologic deformation in many cases. High grain-to-grain stresses cause minerals to dissolve in the thin films of water present between grains (Turcotte and Schubert

 DOI 10.1007/s10040-002-0230-8

1982, p. 335). The dissolved mass then diffuses to the pores where it precipitates. Loss of porosity results from both collapse of the porous structure and infilling of the pores. Theoretical considerations indicate that this process may mimic viscoelastic creep. A simple analysis by Turcotte and Schubert (1982, p. 335), for example, suggests that the porosity loss is proportional to effective stress and gradually slows as contact areas between grains grow. Presumably, however, temperature also plays an important role, and this spurred analyses by Angevine and Turcotte (1983) and Palciauskas and Domenico (1989) that included temperature effects. It appears likely that temperature effects lead to qualitative differences in deformation styles at different depths. Connolly and Podladchikov (2000), for example, distinguish a "pseudoelastic" deformation regime in shallow sediments that becomes increasingly viscous with increasing depth and temperature. Similarly, Schneider et al. (1996) have proposed that a nonlinear elastic-type deformation prevails at shallow depths, whereas a temperature-dependent viscous deformation becomes important at greater depths. Though based on different conceptual models, many approaches (e.g., Palciauskas and Domenico 1989; Schneider et al. 1996; Connolly and Podladchikov 2000) can explain observed porosity profiles, highlighting the nonuniqueness of this problem.

Part of the difference in moduli evident in Fig. 7 must be due to processes that are purely chemical and perhaps even biochemical, and is thus dependent upon factors other than effective stress and temperature. Chemically driven deformation can occur when fluids transport reactive solutes, dissolving enough of the solid matrix to cause the pore structure to partially collapse. The dissolved mass may then be precipitated elsewhere, reducing porosity without deformation of the porous skeleton. Analysis of these processes is becoming feasible with simulators such as CIRF (Potdevin et al. 1992) and RATEQ (Curtis 2002) that can simulate transport of multiple chemical species with reactions, and HBGC123D (Gwo et al. 2001) that can also simulate biologically mediated reactions. What has been learned to date is primarily that these processes are highly complex. Some exhibit self-organizing behavior that is believed to have led to the development of so-called pressure seals, or thin zones of sediment with low porosity and permeability (Ortoleva et al. 1995). Biological mediation of solution and precipitation in the subsurface has been systematically studied only relatively recently. Microbially enhanced solubility (McMahon et al. 1992; Bennett et al. 2000) can increase porosity, or reduce it by inducing collapse of the pore structure. Unlike other processes, however, it is limited to environments cool enough for microbes to survive, or approximately the upper 4 km of the crust.

Despite the numerous difficulties, it would be inaccurate to leave the impression that long- term geologic deformation is completely intractable. There is evidence, for example, that a relatively simple elastoplastic model can describe sediment compaction and the resulting three-dimensional stress state over geologic time scales (Karig and Hou 1992). Broadly speaking, however, it remains difficult to definitively test conceptual models of geologic deformation.

Uncertain boundary and initial conditions

Analysis of a geologic domain or process requires that it be placed in its geologic context, meaning that the influence exerted by its surroundings must be properly described. This is accomplished by specifying appropriate boundary and initial conditions for both flow and deformation. Boundary and initial conditions are inherently problematic for the same reason that descriptions of the deformation processes themselves are uncertain: researchers cannot observe geologic systems evolving and instead must infer their histories. In some cases, boundary or initial conditions themselves are the object of investigation.

When included in the problem domain, the land surface is usually the least problematic boundary. Mechanically, it is nearly always represented as a free surface with traction $\boldsymbol{t}$ of zero. Hydraulically, it is usually adequate to represent it with pressure p=0 or, equivalently, head $h=l_s$, where l_s is the elevation of the land surface. This condition is based on the observation that the water table (by definition where p=0) often lies close to the ground surface, mimicking surface topography. Occasionally, fluid flux $\boldsymbol{q}_n$ is specified at the land surface if the rate of recharge or discharge of water is known, but experience has shown that even modest errors in the flux can cause large errors in computed fluid pressures.

Most problems arise when specifying conditions along side and bottom boundaries, and this is especially true for mechanical behavior. Presumed symmetry boundaries can be represented as having zero normal displacement, but otherwise the choices are usually difficult. Although qualitative stress or displacement histories can often be inferred from geologic evidence such as total deformation or style of fracturing, quantitative estimates of the stress or displacement history are another matter. Present-day near-surface strain rates can be measured (e.g., Simila 1998; Ward 1998), and past strain rates can be broadly constrained (e.g., Pfiffner and Ramsay 1982; Jayko 1996) but specific displacement histories are largely speculative. A simple expedient is to assume either constant stress or rates of displacement, but this can obscure aspects of system behavior that may be of interest. Clearly, both stresses and strain rates wax and wane in response to large-scale crustal processes. Occasionally, a system can be considered to have a mechanically stable setting, in which case regional lateral stresses can be represented by fixed stresses or zero displacement at large distances (Wang 2000).

Hydraulic conditions along side and bottom boundaries also present problems. Fixed (often hydrostatic) pressures or heads are sometimes appropriate for side boundaries, but no-flow or zero permeability boundaries are perhaps the most widely used hydraulic boundary

 DOI 10.1007/s10040-002-0230-8

condition. They are used to represent symmetry boundaries, interfaces with formations presumed to have relatively low permeability, or geologic features such as faults (e.g., Bethke 1989; Ge and Garven 1992). Hydraulic boundary conditions can be "finessed" by analyzing a domain larger than the region of interest. With increasing distance, hydraulic boundary conditions have decreasing influence. The use of rather arbitrary hydraulic boundary conditions is sometimes justified for this reason (e.g., Corbet and Bethke 1992; Gordon and Flemings 1999). This is not necessarily true of mechanical boundary conditions which can cause deformation, and accompanying fluid pressure changes, throughout a domain. The pervasive influence of the mechanical boundary conditions is important to keep in mind.

Initial conditions for both deformation and flow pose relatively few problems because their influence diminishes with time. Arbitrary initial conditions can be used if a sufficiently long period of time is simulated. Initial conditions can be of great importance in certain situations, however, such as those involving the response of a system to an instantaneous mechanical perturbation. To analyze these phenomena, fluid pressure changes that result from the perturbation can be pre-calculated and superimposed on the existing fluid flow regime (such as an equilibrated flow system) to obtain the initial condition for flow. Constant stress or zero displacement boundary conditions can then be applied to analyze how the flow system evolves following the perturbation. This approach has been used to study the response of flow systems to tectonic shortening (see *Tectonic deformation*) and to seismic strains (see *Creep and seismic slip along faults*).

Pragmatism in Analysis: Widely Used Simplifications

Endemic uncertainty about geologic environments and their histories has forced researchers to resort to a variety of analytical tricks to approximate hydromechanical coupling effects. These approaches can yield edifying and useful results, but the limitations they introduce are frequently overlooked or forgotten. To objectively evaluate such analyses, it is imperative that their limitations be understood and taken into account. Some popular approaches and their limitations are outlined below.

The assumption of purely vertical strain

Lateral gradients in fluid pressure and pressure changes tend to be small compared to vertical gradients. It is thus often assumed that the resulting deformations can be approximated as purely vertical. This allows a particularly helpful simplification of hydromechanical coupling by preselecting the mechanical boundary conditions and simplifying the analysis, as shown below. This approach is widely used and sometimes abused.

Consider the constitutive equations for strain presented earlier as Eqs. (7). If the ground surface is a free surface, and if there are no overburden changes (that is, no deposition or erosion), the vertical stress change, σ_{zz}, is zero. In addition, if strain is purely vertical, ε_{xx} and ε_{yy} are zero. Under these conditions, the first two equations of (7) can be rearranged to show that

$$\sigma_{xx} = \sigma_{yy} = \frac{3\nu}{1+\nu}\sigma_{kk} + \frac{1-2\nu}{1+\nu}\alpha p + 2G\alpha_T T \tag{36}$$

With σ_{zz} equal to zero, $\sigma_{kk} = \sigma_{xx} + \sigma_{yy}$ and, by doing this sum and rearranging, it is found that

$$\sigma_{kk} = \frac{2(1-2\nu)}{1-\nu}\alpha p + 4G\frac{1+\nu}{1-\nu}\alpha_T T \tag{37}$$

This shows that changes in mean normal stress are linearly related to changes in fluid pressure and temperature. Applying the ∇^2 operator to Eq. (37) yields

$$\nabla^2\sigma_{kk} = \frac{2(1-2\nu)}{1-\nu}\alpha\nabla^2 p + 4G\frac{1+\nu}{1-\nu}\alpha_T\nabla^2 T \tag{38}$$

which is identical to Eq. (13), the equation representing force equilibrium and compatibility that was presented in *Equations of deformation*. Thus, Eq. (13) and the deformation constraints it represents are automatically satisfied under these conditions.

A practical result of this circumstance is that transient fluid flow is fully described by the flow equation alone, a situation Wang (2000) describes as "uncoupling" of stress and fluid pressure. The pressure diffusion equation under these conditions is obtained by substituting Eq. (37) into (23). This yields

$$\nabla\cdot\frac{\boldsymbol{k}\rho g}{\mu}(\nabla p + \rho g\nabla z) = S_s\frac{\partial p}{\partial t} - \rho g n\Lambda'\frac{\partial T}{\partial t} - gJ \tag{39}$$

where

$$S_s = S_{s3}(1-\lambda\beta) = \rho g\left[\left(\frac{1}{K}-\frac{1}{K_s}\right)(1-\lambda) + \left(\frac{n}{K_f}-\frac{n}{K_s}\right)\right] \tag{40}$$

The new quantity S_s is the one-dimensional specific storage (van der Kamp and Gale 1983) and $\Lambda' = \alpha_{Tf} + (\lambda/n)\hat{\alpha}_T - \alpha_{Tp}$ is the modified thermal response coefficient. $\hat{\alpha}_T$ is the formation bulk thermal expansivity and $\lambda = 2\alpha\ (1-2\nu)/3(1-\nu)$. In the absence of fluid sources and temperature changes, and with isodensity and isoviscosity fluid, Eq. (39) simplifies to

$$\nabla\cdot\boldsymbol{\kappa}\nabla h = S_s\left(\frac{\partial h}{\partial t} - \frac{\partial z}{\partial t}\right) \tag{41}$$

Finally, by noting that $K' = [3(1-\nu)/(1+\nu)]K$, and by assuming that κ is a scalar constant, that there are no significant elevation changes with time, and that solid grains are incompressible ($K_s = \infty$), Eq. (41) reduces to

$$D_h\nabla^2 h = \frac{\partial h}{\partial t} \tag{42}$$

D_h is the hydraulic diffusivity, in this case equal to κ/S_s with

 DOI 10.1007/s10040-002-0230-8

$$S_s = \rho g\left(\frac{1}{K'} - \frac{n}{K_f}\right) \tag{43}$$

(van der Kamp and Gale 1983). D_h mediates the "diffusion" of hydraulic head (or, equivalently, pressure) in a transient flow system.

Equations (39), (41), and (42) and similar forms of the transient-flow equation are widely used to analyze time-varying flow of groundwater and other fluids in the subsurface. As the preceding analysis makes clear, the assumptions of purely vertical strain and constant vertical stress are implicit in the use of these descriptions of transient flow, although they are rarely mentioned. Strictly speaking, the wide use of these equations to describe two- and three-dimensional flow regimes represents an inconsistency, because two- and three-dimensional transient flow necessarily produces horizontal strains. However, as discussed in more detail in *Hydrodynamic disequilibria*, the resulting errors are often small.

Mechanical and hydraulic behavior can also be "partially coupled" under certain conditions. Compaction and decompaction due to deposition and erosion often involve load changes that are relatively homogeneous areally, especially when viewed on geologic time scales. In the case of a changing but areally homogeneous load, the lateral strains ε_{xx} and ε_{yy} are again zero, but changes in vertical stress σ_{zz} are not. Adding σ_{zz} to $\sigma_{xx}+\sigma_{yy}$ from Eq. (36) to obtain σ_{kk}, and then rearranging yields

$$\sigma_{kk} = \frac{2(1-2\nu)}{1-\nu}\alpha p + \frac{3(1+\nu)}{3(1-\nu)-2\alpha\beta(1-2\nu)}(1-\lambda\beta)\sigma_{zz} + 4G\frac{1+\nu}{1-\nu}\alpha_T T \tag{44}$$

(Neuzil 1993). Comparing this relation with Eq. (37), it is seen that an additional term containing σ_{zz} is now present. If overburden changes are homogeneous and laterally extensive, the change in vertical stress σ_{zz} should also be spatially homogeneous. Because of this, $\nabla^2\sigma_{zz}=0$ and applying the ∇^2 operator to Eq. (44) again yields an equation identical to (13); here, too, force equilibrium and compatibility are automatically satisfied, uncoupling the flow and deformation equations. Substituting Eq. (44) into (23) and simplifying, the resulting flow equation is

$$\nabla\cdot\frac{\boldsymbol{k}\rho g}{\mu}(\nabla p + \rho g\nabla z) = S_s\frac{\partial p}{\partial t} - S_s\zeta\frac{\partial\sigma_{zz}}{\partial t} - \rho g n\Lambda'\frac{\partial T}{\partial t} - gJ \tag{45}$$

where $\zeta=[\beta(1+\nu)]/[3(1-\nu)-2\alpha\beta(1-2\nu)]$ is a one-dimensional loading efficiency. Although Eq. (45) alone provides a complete description of transient flow, the flow is definitely affected by stress changes. To account for this, the change in overburden load with time, $\partial\sigma_{zz}/\partial t$, must be specified. Finite vertical deformation can also be accounted for by tracking the effective stress and specifying a porosity-effective stress relationship. This partially coupled approach is widely used to analyze fluid flow and compactional strain in active basins (see *Sediment compaction*).

Porosity and stress gradients as indicators of long-term strain or effective deformation moduli.

Some analysts have adopted a pragmatic approach to the complexities attending sediment deformation by using porosity loss as a surrogate for specifying long-term in situ sediment deformation properties. The in situ K' values shown in Fig. 7 were obtained in this manner. In this approach, porosity gradients are used together with sediment packet trajectories through the domain to determine either rates of volumetric strain or effective moduli for deformation that apply on geologic time scales. If strain rates are determined, this information effectively supplants mechanistic descriptions of deformation. A similar approach is to specify trajectories along stress gradients.

Porosity and stress gradients have been used to determine volumetric strain rates in accretionary complexes, an application discussed in *Tectonic deformation*. The most common application of porosity and stress gradients, however, is in analyzing compaction in active sedimentary basins. Using a porosity-depth relation (ideally from the basin of interest) and the rate of change of effective stress with depth (usually calculated by assuming hydrostatic fluid pressures), one can calculate the *effective* confined modulus K'_{eff} as a function of effective stress. The result can then be used to describe the coupling between sediment loading, compaction, and fluid pressure. As usually implemented, this approach implicitly assumes purely vertical strain during compaction and results in a non-linear poroelastoplastic-style of deformation. In such a system, lateral stresses σ_{xx} and σ_{yy} are unique functions of vertical stress σ_{zz}. Because of this, the poroelastic constitutive Eqs. (7) can be manipulated to yield an expression for vertical strain in terms of fluid pressure and vertical stress alone; it is found that

$$\varepsilon_{zz} = \frac{1}{K'}\sigma_{zz} - \frac{\alpha}{K'}p \tag{46}$$

If it is further assumed that the solid grains are incompressible, positive vertical strain ε_{zz} is equal to porosity loss and α=1. Taking the derivative of Eq. (46) with respect to elevation z then yields

$$\frac{dn}{dz} = -\frac{1}{K'}\frac{d\sigma'_{zz}}{dz} \tag{47}$$

To simplify the analysis, porosity-depth or porosity-effective stress behavior is usually approximated by fitting to it a modified Athy (1930) relationship of the form

$$n = (n_s - n_{ir})\ \exp\left(-\gamma\sigma'_{zz}\right) + n_{ir} \tag{48}$$

where n_s is porosity at the sediment surface, n_{ir} is a supposed "irreducible" porosity at great depth and γ is a fitting coefficient. Equation (48) provides a good fit to many porosity-effective stress profiles. Taking the derivative of (48) with respect to z and then eliminating dn/dz and $d\sigma'_{zz}/dz$ between the resulting equation and (47) gives

 DOI 10.1007/s10040-002-0230-8

$$\frac{1}{K'_{eff}} = \gamma(n_s - n_{ir})\ \exp\left(-\gamma\sigma'_{zz}\right) \tag{49}$$

as an expression for the effective confined deformation modulus as a function of effective stress.

When using Eq. (49), all processes causing porosity loss are included in the analysis in a de facto manner. This approach has intuitive appeal and is used in compaction algorithms in various basin flow simulators, including Basin2 (Bethke et al. 1999), BASIN3D2P (Tokunaga 1996), DYME-TOUGH2 (McPherson and Bredehoeft 2001), and RIFT2D (M. Person et al., Indiana University, in preparation, 2002).

Although tying deformation properties to porosity profiles appears to solve many problems, it is not the proverbial "free lunch" one might wish for. Important assumptions that can conceal significant uncertainties are implicit in its use. For example, some lateral strain can be expected in compacting basins (Luo et al. 1998), and is subsumed arbitrarily within the computed values of K'_{eff}. More fundamentally, however, the approach is based on the dubious premise that the porosity-effective stress relation seen in a thick sedimentary sequence at a moment in time is a surrogate for porosity changes in a single packet of sediment as it is advected along the effective stress gradient over a long period of time. In effect, it is assumed that

$$\frac{Dn}{Dt} = \frac{D\sigma'_{zz}}{Dt}\frac{dn}{d\sigma'_{zz}} \tag{50}$$

where the left-hand term represents deformation as porosity loss in a packet of sediment over time; it is equated to changes in effective stress in the same sediment packet over time and, in the last term, to changes in porosity with effective stress as determined from the porosity-depth curve. Implicit in the last term of Eq. (50) is the assumption that porosity loss is a unique function of vertical effective stress. As previously noted, however, this is unlikely to be the case. Instead, porosity loss usually depends on mechanical, physicochemical, chemical, and biochemical processes that themselves depend on time, temperature, chemical environment, and other factors.

One can imagine solving this difficulty by devising a generalization of the porosity gradient technique that recognizes porosity loss is *not* a unique function of effective stress. In fact, such an approach has been proposed by Schneider et al. (1996). Their formulation considers compactional strain to be the sum of stress effects that create an Athy-type porosity gradient *and* time-dependent viscous effects. Expressed in terms of the effective confined modulus, their conceptual model yields an extended form of Eq. (49):

$$\frac{1}{K'_{eff}} = \gamma_1(n_s - n_{ir})\ \exp\left(-\gamma_1\ \sigma'_{zz}\right) + \gamma_2(n_s - n_{ir})\ \exp\left(-\gamma_2\ \sigma'_{zz}\right) + \frac{\omega}{\dot{\sigma}'_{zz}}\sigma'_{zz} \tag{51}$$

Here, $\dot{\sigma}'_{zz}$ is the time derivative of effective vertical stress, γ_1 and γ_2 are Athy-type fitting coefficients, and ω is a viscous coefficient that includes a temperature-dependent sediment viscosity. The exponential terms (there are two to better fit observed profiles) describe stress-driven strains, and the last term represents the viscous strains. This formulation is conceptually satisfying because it defines a distinct viscous component of compaction, but familiar difficulties remain. Although Schneider et al. (1996) suggest that γ_1 and γ_2 can be determined with laboratory testing, it is not clear that this is always, or even usually, a viable approach. As already seen, laboratory compaction of fine-grained (clay-rich) sediment generally follows an Athy-type pattern, but compaction of somewhat coarser (sand-rich) sediment may not (Fig. 8). In addition, obtaining an appropriate value for ω is likely to be difficult, although some generic estimates may provide guidelines. Finally, even if values for the parameters can be estimated, it is impossible to test the estimates by comparing predicted behavior with actual geologic deformation.

How limiting are these problems? The answer, of course, depends on the questions one is trying to answer. An optimistic observation is that many porosity-depth curves typically display similar types of more-or-less regular forms, suggesting that Eqs. (49) or (51) can be reasonable approximations. Analyses that use them may capture the gross interaction between deformation and fluid flow even if the processes responsible for it are not correctly represented.

Approximating deformation over short time steps as poroelastic

Sufficiently large stress changes invariably result in nonlinear and plastic strains (if not brittle failure). An approach that has proved useful for mimicking this behavior is to assume that linear poroelasticity applies only to the small deformations occurring in each time step in a numerical simulation while permitting properties to change between time steps. This approach is implicit in the notion of effective deformation moduli discussed in the previous section and is readily implemented in numerical simulators. Deformation moduli are recalculated in each time step, allowing for strain stiffening, and finite strain can also be included by adjusting the dimensions of cells or elements accordingly. Plastic strain can be incorporated by allowing the deformation modulus to assume a larger value when stress begins to decrease. A variant of this technique is used in the Cam-clay model [see Eqs. (31) and (32)].

Assuming poroelastic behavior over each time step while allowing properties to vary between time steps is a relatively simple and heuristically satisfying way to approximate nonlinear and plastic behavior in an analysis. However, it implies a rather specific behavior of the system and no careful analyses have been done to compare this approach with more rigorous methods of analysis or with the behavior of real geologic systems. In

 DOI 10.1007/s10040-002-0230-8

view of this, possible limitations of the technique should be kept in mind.

Manifestations of Flow and Deformation Coupling in Geologic Systems

This part of the paper presents a selective survey of the many ways hydromechanical coupling is manifested in the Earth's crust. In addition to providing an overview, an attempt has been made to illustrate the common mechanisms that underlie different phenomena, and to highlight particularly conspicuous gaps in current understanding of them. The presentation is divided into (1) the effects of deformation on fluid regimes (*Effects of Deformation, Fracturing, and Faulting on Flow*) and (2) the effects of fluids on deformation (*Effects of Fluid Pressure on Crustal Mechanics*). This distinction is necessarily arbitrary because there is always coupling in both directions. However, the two categories do provide a structured way to consider the numerous phenomena that arise from coupling. In some instances the effects of deformation on the pore fluids are the most important, obvious, or interesting aspects of the coupling; in other cases the reverse is true. Such is the rationale for the arrangement used.

An additional goal of this section is to showcase less widely recognized applications of hydromechanical coupling. Fluid pressure regimes, for example, contain information about geologic processes such as rates, timing, and patterns of deformation. Specifically, it can be shown that significant fluid pressure anomalies are generated and maintained when

$$\dot{\varepsilon}_{kk} > \frac{\kappa}{l} \tag{52}$$

(Neuzil 1995), where $\dot{\varepsilon}_{kk}$ is volumetric strain rate, κ is domain hydraulic conductivity, and l is the distance from the center of the domain to the nearest boundaries. In certain settings, the presence of anomalous pressures can reveal strain occurring at rates that are as small as 10^{-15} to 10^{-17} s^{-1} (Neuzil 1995) and that would otherwise be undetectable. Likewise, the mechanical state of rocks can provide clues to the history of fluid regimes, such as when jointing in rocks points to the existence of superhydrostatic fluid pressures at some time in the past.

Effects of Deformation, Fracturing, and Faulting on Flow

Hydrodynamic disequilibria

Pore fluid flow in the crust tends to be stable and adjusted to the geologic setting, unless fluid sources, changes in boundary conditions, or some other sufficiently vigorous perturbation affects it. Once perturbed to disequilibrium, a flow regime will tend to return to equilibrium unless the disturbance is ongoing. This process occurs as transient fluid flow, undoubtedly the most pervasive aspect of hydromechanical coupling in everyday human experience. Transient flow is a result of deformation and fluid compression or expansion in response to fluid pressure changes. This allows fluid to be stored or released as pressures change, and this fluid uptake and release generally must be undone by flow before equilibrium can be regained.

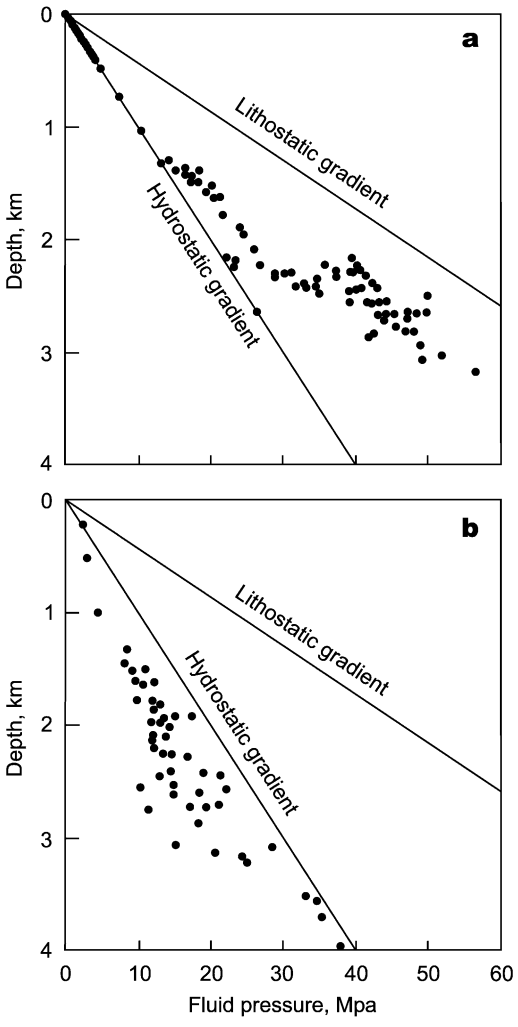

Fig. 9 Typical occurrences of anomalous pressure. **a** Over-, or superhydrostatic pressures in the Biharkeresztes region of the Pannonian Basin, Hungary (modified from Tóth and Almási 2001); **b** under- or subhydrostatic pressures in the Anadarko Basin, Oklahoma, USA (modified from Fertl 1976). Each plot superposes data from a number of different boreholes

The disequilibrium and transient flow that occur when fluids are extracted from the subsurface have been studied for several decades by groundwater hydrologists and petroleum reservoir engineers. From a geologic perspective, disequilibrium is of interest because it occurs in nature and is an important aspect of most of the phenomena discussed in the sections that follow. Natural disequilibria are called anomalous pressures (Fig. 9); found in a variety of geologic environments, anomalous pressures are generally considered to be either (1) evolving slowly toward equilibrium by transient flow or

 DOI 10.1007/s10040-002-0230-8

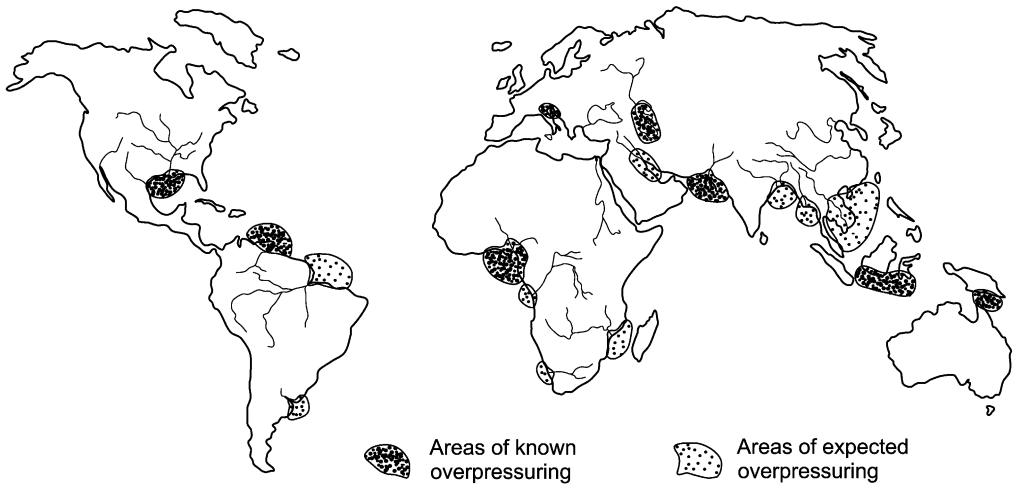

Fig. 10 Known and expected occurrences of overpressures caused by compactional strain (modified from Domenico and Schwartz 1998)

(2) evidence of ongoing geologic perturbation (Bredehoeft et al. 1994; Neuzil 1995).

Whether anthropic or naturally occurring, flow disequilibria are typically analyzed using the flow equation uncoupled from the deformation equation (e.g. 42). As seen in the section *The assumption of purely vertical strain*, this amounts to assuming that horizontal strains are zero. The viability of this approach is situation-dependent. A sense of the problem can be gleaned from analyses of fluid extraction, which almost exclusively use an uncoupled approach; examples include compilations of flow equation solutions for different boundary and initial conditions by Muskat (1937), Kruseman and de Ridder (1970), Lohman (1979), and Batu (1998). Fluid extraction causes lateral strains that are largest near the producing well and the presumption of purely vertical strain clearly introduces error. Occasionally, the shortcomings are apparent, as when the lateral strains in a pumped aquifer cause short-lived fluid pressure increases (the so-called Noordbergum effect; see Verruijt 1969) or even fault slippage (Segall 1989) in a confining layer. In a majority of analyses, however, the assumption of one-dimensional strain has been found to provide quite useful results. Gambolati (1974) was able to show that this should be expected in many cases. He also delineated the conditions, namely fluid extraction from reservoir units that are relatively thick and shallow, that lead to the greatest error.

Although directly applicable only to fluid extraction problems, Gambolati's results may have promoted acceptance of uncoupled approaches for other fluid flow problems, such as the evolution of anomalous pressures. For better or worse, uncoupled and partially coupled fluid flow equations have been and continue to be the dominant approach used in hydrogeology.

Sediment compaction

Most of the anomalous overpressures encountered during drilling exploration worldwide are almost certainly due primarily to compactional strain. This deformation process is most pronounced beneath deltas of large river systems and other areas of vigorous sedimentary deposition (Fig. 10). Overpressures are generated when compactional strain is too rapid for fluid outflow to accomodate it. In geotechnical terms, the behavior of these systems is somewhere between "drained" and "undrained".

Despite the pitfalls discussed earlier (see *The assumption of purely vertical strain*), treating compaction as purely vertical strain frequently appears to be the most viable approach. Although lateral strain is probably the rule rather than the exception during compaction (e. g., Luo et al. 1998), its magnitude and history are invariably so poorly understood that it makes more sense to incorporate it implicitly via a porosity-depth relation (see *Porosity and stress gradients as indicators of long-term strain or effective deformation moduli*) than to attempt to include it explicitly. In many instances, deposition is so areally extensive that compactional strain may in fact be very close to purely vertical. In any event, it is worth keeping in mind that errors of uncertain magnitude are introduced by this approach.

As shown earlier, the assumption of no lateral strain with nonzero σ_{zz} to represent the depositional loading leads to partial coupling (see *The assumption of purely vertical strain*). Force equilibrium and compatibility conditions are automatically met and the flow equation alone is sufficient to describe flow and to compute the compactional strains throughout the system. The flow equation under these circumstances was developed earlier as Eq. (45) and is

$$\nabla \cdot \frac{\boldsymbol{k}\rho g}{\mu}(\nabla p + \rho g \nabla z) = S_s \frac{\partial p}{\partial t} - S_s \zeta \frac{\partial \sigma_{zz}}{\partial t} - \rho g n \Lambda' \frac{\partial T}{\partial t} - gJ \tag{53}$$

 DOI 10.1007/s10040-002-0230-8

The partial coupling is manifested through the time derivative of σ_{zz}, or rate of change of vertical stress, which must be specified independently to represent the rate of loading. The thermal term is often retained in compaction studies because deposition displaces sediments downward through the geothermal profile, causing the temperature of a packet of sediment to increase with time. In some cases, the source term is also retained because fluid sources from processes such as smectite dehydration or petroleum generation are thought to be important.

A complicating feature of active depositional systems (and the erosional systems discussed below) is that the domain size changes with time. This is a result of the addition or removal of sediment, which can move the upper domain boundary significantly, and of compactional and decompactional strains, which have a comparatively small effect on domain size. Early studies ignored the latter in order to simplify analysis. Further simplifications that were invoked included considering isodensity fluid and sediment, a constant, linear geothermal gradient, and constant permeability. Changes in vertical stress could then be related to the changes in land-surface elevation through $\partial\sigma_{zz}/\partial t=[(1-n)\rho_s+n\rho]g(\partial l_s/\partial t)$ and an excess hydraulic head, or head above land surface could be defined as $h'=p/(\rho g)-(l_s-z)$. Substituting these definitions into (53) yields

$$\kappa\frac{\partial^2 h'}{\partial z^2}=S_s\frac{\partial h'}{\partial t}-\left[\frac{\zeta[(1-n)\rho_s+n\rho]-\rho}{\rho}+\frac{nG_T}{S_s}\Lambda'\right]\frac{\partial l_s}{\partial t} \tag{54}$$

where G_T is the geothermal gradient (Neuzil 1993). Although the term in brackets looks complex, it is a constant for the assumptions noted. In the case of constant $\partial l_s/\partial t$ (and thus an upper boundary moving upward at a constant rate), an analytical solution of Eq. (54) was obtained by the pioneering geotechnical researcher R.E. Gibson (Gibson 1958). Bredehoeft and Hanshaw (1968) were the first to apply Gibson's solution to the geologic problem of sedimentation in an active basin and other researchers (e.g. Domenico and Palciauskas 1979) followed suit. The most significant contribution of these studies was to demonstrate that compaction strain is quite capable of generating strong fluid overpressures. This was one of the earliest instances of recognition of the importance of hydromechanical coupling in geologic processes.

Although these analyses provided enlightening results, many researchers considered the assumptions embodied in them to be worrisome. Domenico and Palciauskas (1979) examined the error associated with assuming infinitesimal strain by considering equations for conservation of both fluid and solid mass. For most applications, they concluded that it was not necessary to account for finite deformation. Others, including Keith and Rimstidt (1985), Bethke and Corbet (1988), and Grün et al. (1989), examined the shortcomings that arise from ignoring "secondary" coupling, or the effects of finite, plastic deformation on system properties κ and S_s. Significant nonlinearities are introduced by the changes in permeability and deformation moduli as sediments compact, and Bethke and Corbet and Grün et al., among others, have shown that predicted behaviors with and without the nonlinearities are quite different.

Numerical solution techniques have allowed many restrictive assumptions to be relaxed and two- and three-dimensional domains to be studied using Eq. (53) or equivalent descriptions. A representative example is a study of the Gulf of Mexico Basin by Bethke (1989). His simulation of the development of fluid overpressures by compactional strain and thermal effects in the Gulf of Mexico Basin through the last 31 Ma is shown in Fig. 11. Although this analysis constrained the strain to be purely vertical, the deposition rate was varied in space and time, finite strains were accounted for by deformation of the computational grid, and effective deformation moduli were determined by the observed loss of porosity with depth (although the terminology and method of implementation differed from that presented here). Thus, the compactional rheology was determined by fitting Eq. (48) to representative porosity profiles for sand- and clay-rich Gulf Coast sediments. Bethke (1989) also included thermal effects and clay dehydration but concluded, like other workers who have conducted similar analyses (e.g. Shi and Wang 1986; Harrison and Summa 1991; Luo and Vasseur 1995; Wilson et al. 1999; Dugan and Flemings 2000), that compactional strain is by far the dominant pressuring process in most active basins.

More recent analyses of active basin environments (e.g., Harrison and Summa 1991; Luo and Vasseur 1995; Wilson et al. 1999; Gordon and Flemings 1999; Bekele et al 2000; Bitzer et al. 2000; Swenson and Person 2000), have perpetuated the use of partial coupling of the flow and deformation by assuming purely vertical strain. Indeed, all geologic basin flow simulators known to the author, including Basin2 (Bethke et al. 1999), BASIN3D2P (Tokunaga 1996), BASIN (Bitzer 1997), DYME-TOUGH2 (McPherson and Bredehoeft 2001), RIFT2D (M. Person et al., Indiana University, in preparation, 2002), and an unreleased simulator by Luo and Vasseur (1996) use partial coupling and solve only Eq. (53) or an equivalent flow equation. The error that results from this simplification has received little study and would, in any event, be difficult to assess. In one pertinent study, Schiffman et al. (1969) analyzed a semi-infinite domain loaded over part of its surface, a situation analogous to spatially varied sedimentary loading. What was considered significant differences were found in the behavior predicted by partially coupled and fully coupled analyses, ranging from the longevity of overpressures to the existence of the so-called Mandel-Cryer effect. The latter is an additional increase in overpressures after the load is applied and, like the Noordbergum effect mentioned in the preceding section, is caused by lateral strains. The importance of these differences, however, is certainly relative; the resulting errors are probably modest

 DOI 10.1007/s10040-002-0230-8

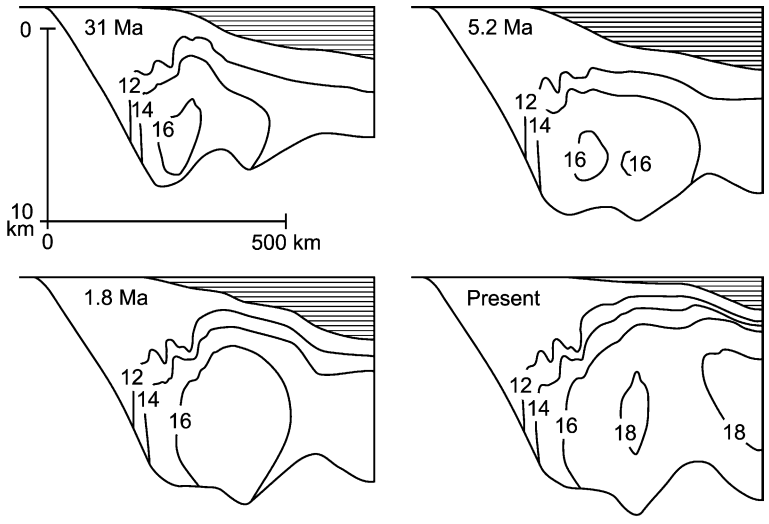

Fig. 11 Generation of fluid overpressures by compaction of sediments in the Gulf of Mexico Basin. Contours represent the pressure gradient referenced to the surface and are in units of MPa km^{-1}. A hydrostatic pressure gradient is approximately 10 MPa km^{-1}. The simulation assumed strictly vertical deformation, which partially uncoupled the flow equation from the force equilibrium equations for solid deformation. Lateral deformation and diagenetic effects were included in a de facto manner by tying deformation to a porosity-depth profile (adapted from Bethke 1989)

when considered in the context of other uncertainties in the analyses.

It is, of course, feasible to apply more sophisticated hydromechanical models to sediment compaction. This presumably could be done using existing hydromechanical simulators such as CRISP (Gunn and Britto 1981; Britto and Gunn 1987), SPIN 2D (Borja 1984), Plascon (Lewis and Schrefler 1987), CESAR (Humbert 1988), BIOT2 (Hsieh 1994), and ABAQUS (Hibbitt, Karlsson, and Sorenson, Inc. 1998), although most would require at least some modification. For example, Luo et al. (1998) analyzed sedimentation and compaction using CESAR, a fully coupled hydromechanical simulator that permits incorporating a Cam-clay rheology (see *Inelastic rheologies from a geotechnical perspective*). The self-described result of the effort was a limited success because continuous sedimentation, a phenomenon the simulator was not designed to handle, created computational difficulties. Such problems aside, however, the more fundamental difficulties of describing the rheology and mechanical boundary conditions of compacting sediments remain. Specifically, the rheology would have to account for diagenesis as well as compaction. As for mechanical boundary conditions, if one takes the Gulf of Mexico Basin (Fig. 11) as an example, its asymmetry makes choosing them quite difficult. Limitations such as these make it questionable whether fully coupled hydromechanical analyses will yield truer or more useful representations of sediment compaction and fluid flow in basins than partially coupled analyses.

Erosional decompaction

The gradual erosion occurring in most terrestrial environments results in a lessening of vertical stress and resulting strains that increase porosity and can decrease fluid pressure, sometimes leading to underpressures. However, despite erosional unburdening being nearly ubiquitous above sea level, decompactional underpressures are rather rare. This probably reflects the fact that compaction in sediments is predominantly unrecoverable plastic strain (see *Deformation in crustal processes* and *Inelastic rheologies from a geotechnical perspective*; also Figs. 3a, 5b, and 8) and rates of porosity increase are correspondingly small. That said, there appear to be a few geologic settings, distinguished by relatively deformable, low permeability formations and vigorous erosion, where decompactional strain has generated significant underpressures.

Like compaction, decompaction has been analyzed by partially decoupling the flow equation, amounting to a de facto assumption of negligible horizontal strains. Unlike compaction, however, porosity profiles or other evidence of past deformation are not very helpful for estimating relevant deformation moduli or choosing how to represent the rheology. This presents some difficulties that have been approached in different ways. Decompactional strains are relatively small, making the use of linear elasticity a possibility. For example Neuzil (1993) applied a linear elastic model to shale decompaction after determining that viscous deformations could be subsumed within the elastic moduli; decompaction moduli were estimated based on the shale's decompaction behavior in laboratory tests. In other words, the deformation was represented as a linear relationship fitted to the elastic component of strain shown in Fig. 3a. Another approach used in some analyses is similar to that utilized in Cam-clay models [see Eqs. (31) and (32)]. It recognizes the mild nonlinearity often observed in decompaction tests, and utilizes a porosity-effective stress relation analogous to Eq. (48), namely

 DOI 10.1007/s10040-002-0230-8

$$n = (n_{\min} - n_{ir})\ \exp\left[-\gamma_d\left(\sigma'_{zz} - \sigma'_{zz\,(\max)}\right)\right] + n_{ir} \qquad (55)$$

where $\sigma'_{zz\,(\max)}$ is the maximum vertical effective stress the formation has experienced, $n_{\min}$ is the corresponding porosity, and γ_d is an Athy-type coefficient for decompaction. Laboratory data are helpful for estimating the coefficients in Eq. (55). This strategy is especially useful in combination with Eq. (48) when analyzing both deposition and erosion in the same domain. Corbet and Bethke (1992), among others, have tried this approach using a range of generic laboratory-determined decompaction moduli in their analysis of underpressures in southern Alberta, Canada. When realistic coefficient values are used in Eq. (55), it probably differs very little from assuming a linear elastic rheology. In addition, judging by the results of fully coupled analyses discussed below, the errors attributable to partial coupling are probably small.

In some ways, defining constitutive laws for decompactional strain is a more tractable problem than for other types of deformation, including compaction. In addition to relatively small strains, temperatures are decreasing rather than increasing, and much of the troublesome nonmechanical diagenesis has ceased. Apparently as a result of this, attempts have been made to apply relatively rigorous hydromechanical analyses to decompaction, including full hydromechanical coupling in two dimensions. Picarelli and Urciuoli (1993), for example, analyzed an eroding terrain in the southern Apennines, Italy, using the two-dimensional coupled flow and deformation simulator CRISP (Gunn and Britto 1981; Britto and Gunn 1987). Guided by laboratory studies of the formation in question, they adopted an elastoplastic rheology (in this case the Cam-clay model; see *Inelastic rheologies from a geotechnical perspective*) to simulate the effects of valley erosion (Fig. 12). In order to examine the role of mechanical boundary conditions, Picarelli and Urciuoli tried two conceptual models: one specified zero displacement along side and bottom boundaries and the other allowed displacements parallel to the bottom and right boundaries. The results from both were nearly the same, suggesting that for a problem of this type at least, the choice of mechanical boundary conditions is not very significant. Coupled two-dimensional simulations of valley erosion were also reported by Vinard et al. (1993) and Vinard (1998) as part of an analysis of erosion at Wellenberg, Switzerland, using the simulator ABAQUS (Hibbitt, Karlsson, and Sorenson, Inc. 1998). The formation being analyzed had a relatively low porosity and large K. The analysis was notable because both Cam-clay and linear elastic rheologies were tried. Although the two rheologies did not yield significantly different results, this was a rare (and perhaps unique) application of a clay-based rheological model to a relatively lithified formation. This analysis provides another instance in which different mechanical boundary conditions had relatively little effect on the calculated fluid underpressures.

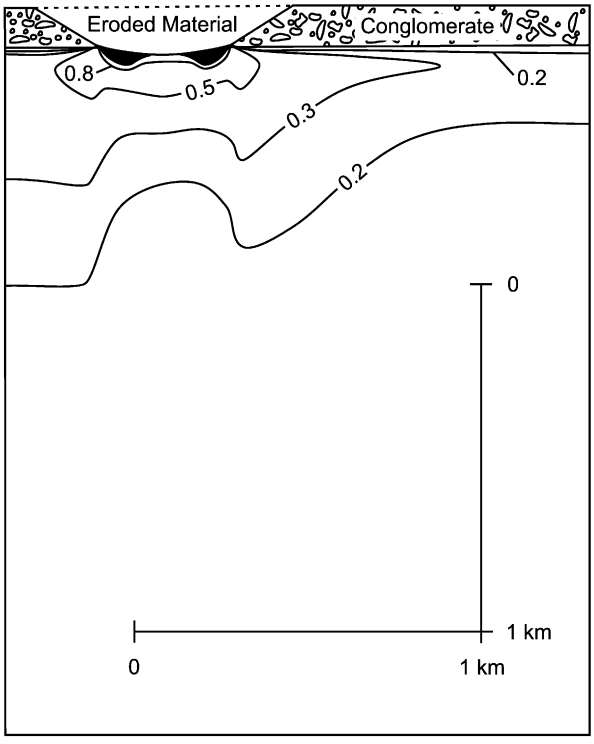

Fig. 12 Fluid pressure decreases caused by valley erosion and resulting dilational strain in an elastoplastic clay. In these simulation results adapted from Picarelli and Urciuoli (1993), the contours represent pressure decrease as a fraction of the hydrostatic pressure, with zones in *black* indicating suction (a decrease exceeding hydrostatic pressure). In this fully coupled two-dimensional simulation, the left boundary was constrained to have no displacements, the right and bottom boundaries allowed displacement along, but not normal to the boundary, and the top boundary was a free surface. Hydraulic boundary conditions were no flow at bottom and sides and $p = 0$ at the land surface

Tectonic Deformation

The possibility of a causal link between tectonism and anomalous pore fluid pressures has been recognized for some time. More than four decades ago, Hubbert and Rubey (1959) noted that tectonically active regions, including the Andean foothills in Argentina, the Himalayan foothills in Pakistan, and oil fields in Iran, Trinidad, and Burma tend to host fluid overpressures, and suggested that tectonic squeezing was responsible. Berry (1973) later suggested that fluid overpressures in the Coastal Ranges and Great Valley of California result from east–west tectonic compression between the Coastal Ranges and the Sierra Nevada to the east. Similar observations continue to be made. Tóth and Almási (2001) have suggested a tectonic origin for high fluid pressures in the Pannonian Basin of Hungary, a result of squeezing between the Bohemian Massif, the Moesian Platform, and the Adriatic microplate. A related speculation that excited interest was made by Oliver (1986), who argued that certain ore deposits were probably emplaced by fluids expelled during orogenic deformation, a phenomenon termed the "squeegee" effect.

 DOI 10.1007/s10040-002-0230-8

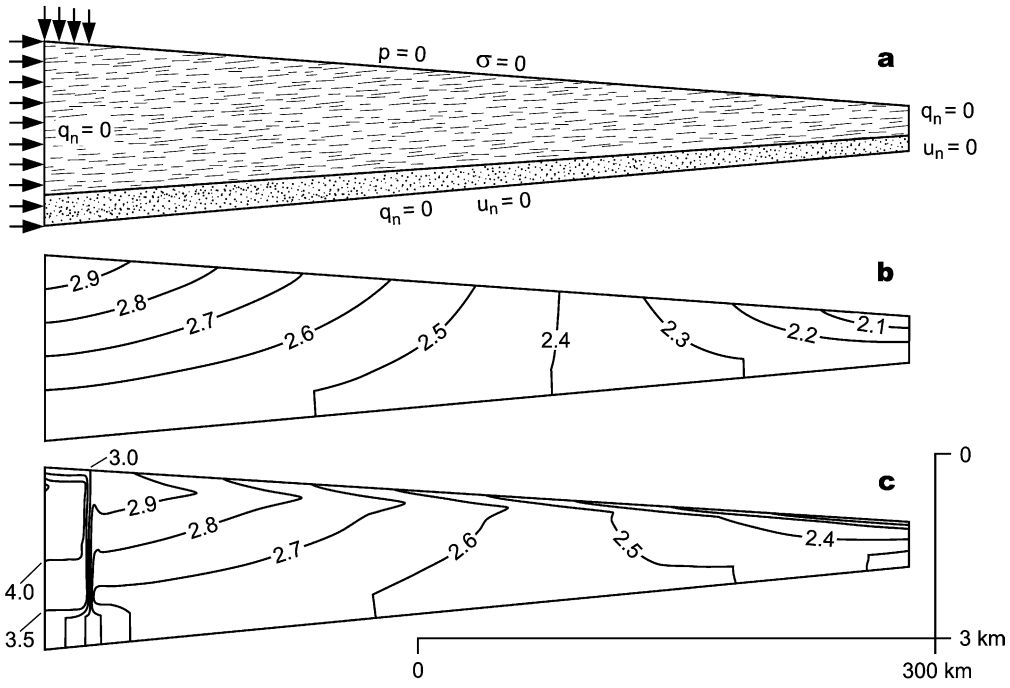

Fig. 13 Effects of tectonism on the fluid flow regime in a generic foreland basin as simulated by Ge and Garven (1989, 1992) (figure modified from the same source). The two-dimensional simulation used fully coupled poroelastic equations. **a** Simulation domain, featuring a confining layer above a more permeable aquifer, and mechanical and hydraulic boundary conditions. **b** Equilibrated hydraulic heads before applying stresses. **c** Hydraulic heads after applying stress changes indicated in **a** by *arrows*

Quantitative considerations support a link as well. Comparison of inferred and measured geologic strain rates with estimates of those needed to perturb fluid pressures indicates that tectonism can, and probably often does, generate significant fluid overpressures (Neuzil 1995). However, more specific analyses face a number of difficulties. Beside the uncertainty concerning specific strain or stress histories in two or three dimensions (see *Uncertain boundary and initial conditions*), tectonism produces large, inelastic strains that are not well described by simple rheologies or, in some cases, by any continuum deformation models. Fracturing and faulting are common, and have their own complicating effects on mechanical properties and permeability. However, if one considers a snapshot in time (geologically speaking), strains will be relatively small and poroelasticity or other continuum rheologies may offer a useful analytical approach, as already noted in *Approximating deformation over short time steps as poroelastic*. Because of inherent uncertainties such analyses are useful primarily for testing the feasibility of conceptual models rather than accurately describing the behavior of specific systems. As shall be seen, however, certain tectonic environments are particularly amenable to analysis, and reasonably detailed pictures of their hydromechanical behavior are emerging.

Ge and Garven (1989, 1992) were among the first to apply poroelastic theory to tectonic deformation to examine its effect on fluid pressure and flow, choosing to examine lateral compression and thrust faulting in a foreland basin-type environment. They simulated flow and deformation in these elongate basins using a vertical, two-dimensional slice normal to the structural trend. Flow was described with

$$\kappa \nabla^2 h = S_{s3} \frac{\partial h}{\partial t} - \frac{1}{K} \frac{\partial \sigma_t}{\partial t} \tag{56}$$

This equation is equivalent to Eq. (27) if one assumes incompressible grains, a constant scalar hydraulic conductivity, no fluid sources or thermal effects, and no elevation changes of the formation. Equation (56) was coupled with displacement equations, namely

$$G \nabla^2 u + \frac{G}{1-2\nu}\left[\frac{\partial^2 u}{\partial x^2} + \frac{\partial^2 v}{\partial x \partial y}\right] = \frac{\partial p}{\partial x}$$
$$G \nabla^2 v + \frac{G}{1-2\nu}\left[\frac{\partial^2 u}{\partial y \partial x} + \frac{\partial^2 v}{\partial y^2}\right] = \frac{\partial p}{\partial y} \tag{57}$$

These equations are two-dimensional versions of Eqs. (10) for incompressible grains and isothermal conditions. For implementation in a finite-element numerical simulator, Ge and Garven used integral forms of Eq. (57). Coupling was accomplished by iterating between the flow and displacement equations.

One of Ge's and Garven's goals was to test Oliver's (1986) "squeegee" hypothesis. This boils down to the following question: can lateral compression and overthrusting generate enough fluid flow to transport significant quantities of heat and mass? The wedge-shaped domain used in the analysis is shown in Fig. 13a with the deformation and flow boundary conditions as indicated. A horizontal stress increase was instantaneously applied to the left boundary and a vertical stress increase was instantaneously applied to an adjoining portion of the upper boundary (Fig. 13a) to mimic lateral compression plus overloading by a thick thrust sheet. Instantaneous application of the stress changes represented a significant simplification designed to maximize fluid transport. Other simplifications included constant values of compressibil-

 DOI 10.1007/s10040-002-0230-8

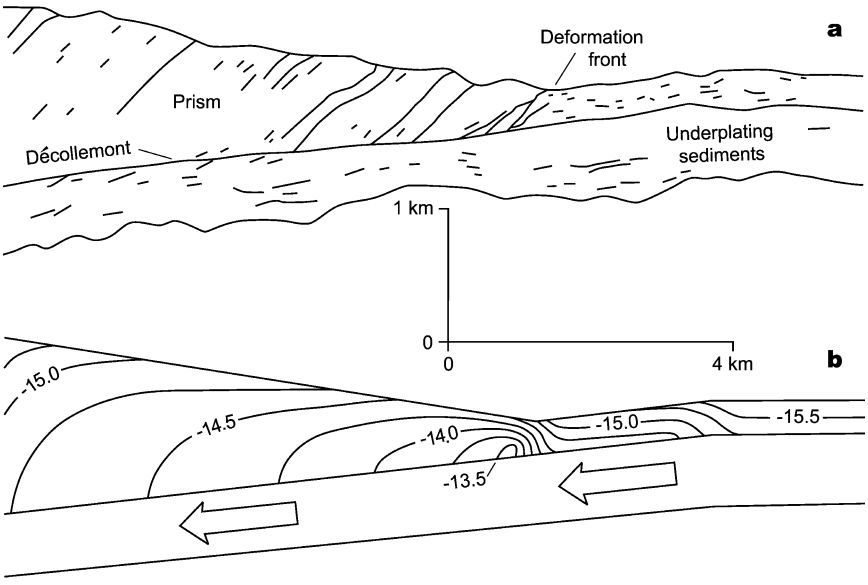

Fig. 14 Cross sections of the Barbados accretionary complex. **a** Structure adapted from Vrolijk et al. (1991). When viewed from a frame of reference tied to the continental plate, the oceanic basement and underplating sediments move downward and to the left (landward) while the deformation front moves to the right (oceanward) as the complex thickens behind it. **b** Volumetric strain rate in the prism and environs as adapted from Screaton et al. (1990); contours are values of $\log_{10}(-\nabla\cdot\mathbf{v}_s)$, which represents the loss of pore volume per unit volume of sediment per second ($\mathbf{v}_s$ is sediment velocity)

ity, permeability, and other system material properties as well as impermeable side and bottom boundaries.

The loading produced rather dramatic changes in the fluid flow regime as indicated by the changes in the pattern of hydraulic head (Fig. 13b, c). Ge and Garven (1992) obtained similar results in a simulation based on the Arkoma Basin, central USA. The perturbations, however, dissipated rather quickly (within 5×10^3 simulation years) because rather high permeabilities were specified. Although the stresses resulted in significant changes to the flow regime, both the generic and Arkoma Basin simulations did not allow the anticipated transport of heat or mass, casting doubt on the "squeegee" effect and its role in mass transport.

Although they implied that tectonism cannot generate significant mass transport by fluids, Ge's and Garven's results reinforced the notion of a significant role for tectonism in pressure generation. This important result supports the idea that anomalous fluid pressures can be useful indicators of ongoing but slow tectonic processes. Careful mapping and analysis of pressure anomalies could reveal patterns of crustal dynamism that are otherwise too subtle to be detected. Further clarification of this idea comes from a study of tectonic shortening in the Sacramento Valley of California. Berry's (1973) hypothesis of a tectonic origin for overpressures in the Sacramento Valley motivated McPherson and Garven (1999) to mount a careful analysis of the system using poroelastic theory. Using a modified version of the simulator developed by Ge and Garven (1989, 1992, 1994), they simulated measured shortening rates across the basin of a few mm per year and found that they generated overpressures similar to those observed.

As already noted, analyses such as that of McPherson and Garven (1999) should be viewed as a "snapshot" of tectonic deformation. Over sufficiently long time scales tectonic strains often involve inelastic deformation or faulting. McPherson and Garven (1999) explicitly recognized the importance of faulting in their study when they stated (p. 458) that "...rapid and finite fault slip may release stress...we are essentially simulating those periods of time between finite fault slip events." By implication, the resulting volumetric strains and associated fluid pressure increases may be cyclical and the only persistent effect on pressure may be loading by overriding thrust sheets. This is implicit in the analyses by Ge and Garven (1989, 1992) in which loading by overriding thrust sheets turned out to be the most important mechanism for generating overpressures. A more complete analysis of these phenomena would thus require incorporating fault mechanics.

Many of the difficulties associated with tectonic deformation and its effect on fluids can be bypassed when porosity or stress gradients are known and the trajectories of the porous medium along them can be predicted (see *Porosity and stress gradients as indicators of long-term strain or effective deformation moduli*). This is possible in at least one tectonic environment: accretionary complexes. Accretionary complexes occur where oceanic crustal plates dive beneath continental plates, having much of their sediment scraped off in the process. The scraped off sediment accumulates in voluminous, deforming prisms that are kilometers thick and tens of kilometers across. Sediments have high porosity before accretion, much of which is later lost, and various lines of evidence indicate that high fluid pressures are produced in the process.

The predictability of accretionary prisms stems from the fact that their shape is thought to remain relatively constant as the deformation front migrates oceanward (Fig. 14a). By adopting a frame of reference pinned to the deformation front, accretionary complexes can be analyzed as quasi-steady systems with a continuous and temporally unvarying flux of sediment and pore water through them. As such, by specifying (a) either the state of stress or the porosity throughout the complex and (b)

 DOI 10.1007/s10040-002-0230-8

the paths of sediment advection through the complex, the rates of stress change or deformation for any sediment packet can be established.

Karig (1985) apparently deserves credit as the first to consider deformation in accretionary complexes from a frame of reference tied to the moving deformation front. Shi and Wang (1988) recognized the advantage of this approach for analyzing the hydromechanics of the complexes, and used it to examine fluid pressures and flow in the Barbados accretionary complex. They described two-dimensional fluid flow using

$$\frac{1}{\rho}\nabla\cdot\frac{\boldsymbol{k}\rho}{\mu}\nabla(p+\rho gz)=\left(\frac{1}{K_{eff}}+\frac{n}{K_f}\right)\frac{Dp}{Dt}-\frac{1}{K_{eff}}\frac{D\sigma_t}{Dt}-n\,\alpha_{Tf}\frac{DT}{Dt}-\frac{J}{\rho}-\frac{J_d}{\rho} \tag{58}$$

where $J_d=-(1-n)^{-1}\rho(Dn/Dt)$ is a virtual fluid source due to diagenetic pore collapse. This equation is equivalent to Eq. (20) for incompressible solid grains, isodensity fluid and no thermal expansion of the pores ($\alpha_{Tp}=0$). The material derivatives indicate that the equation applied to packets of sediment as they were advected through the system. Here, σ_t is defined as $(\sigma_{zz}+\sigma_{xx})/2$, or the mean of overburden and lateral tectonic stress. Shi and Wang treated permeability as a function of effective stress and, because they cast the analysis in terms of stress, had to specify effective bulk moduli, K_{eff}, for the sediments. K_{eff} values were computed from an Athy (1930)-type porosity relation (see *Porosity and stress gradients as indicators of long-term strain or effective deformation moduli*).

Shi and Wang distinguished a gradient in vertical stress σ_{zz} due to prism thickening and a gradient in horizontal "tectonic" stress σ_{xx} that was considered to increase linearly in the direction of accretion. The latter condition arose from their assumption that tectonic stress is limited by the strength of the sediment which, in turn, is controlled by the frictional coefficient for thrust faulting and the linear thickening of the complex. Vertical stress σ_{zz} was simply related to depth. Rates of advection along stress gradients were then equated to $D\sigma_t/Dt$ in Eq. (58) to compute pressures and flow. With this approach, Shi and Wang delineated what appears to be an intimate relation between deformation and the fluid regime in the Barbados complex. The use of reasonable permeabilities resulted in marked fluid overpressures that, as the authors noted, "will affect the tectonic processes in the prism." In other words, coupling in both directions is important (see the discussion of corresponding effects of fluid pressure on shearing and faulting in *Shearing, faulting, and seismicity*).

A somewhat more direct approach is to consider porosity gradients in an accretionary complex. By considering the conservation of sediment mass as it moves through the prism in tandem with a rule for the vertical porosity distribution, the rates of change of porosity (or volumetric strain rates) can be specified for any packet of sediment. This strategy has some parallels to that used in compacting sedimentary basins where porosity loss is a pre-specified function of vertical effective stress σ'_{zz}. Its application to accretionary complexes is less ambiguous, however, because strain in these systems is (or at least appears to be) more predictable than compaction in basins. Screaton et al. (1990), who also analyzed the Barbados accretionary complex, developed this approach.

Screaton et al. (1990) considered the conservation of both fluid and solid mass passing through the coordinate system. They used Eq. (14) without fluid sources, that is

$$\frac{\partial}{\partial t}(\rho n)+\nabla\cdot(\rho\boldsymbol{q}_{rel})=0 \tag{59}$$

referenced to the "fixed" coordinate system to describe fluid mass conservation. Because the sediment as well as fluid is in motion, the fluid flux $\boldsymbol{q}_{rel}$ in the fixed coordinate system is defined by $\boldsymbol{q}_{rel}=\boldsymbol{q}+n\,\mathbf{v}_s$ where $\boldsymbol{q}$ is the Darcy flux, or flux relative to the sediment, and $\mathbf{v}_s$ is the sediment velocity. A similar statement can be written for sediment mass conservation, namely

$$\frac{\partial}{\partial t}[\rho_s(1-n)]+\nabla\cdot[\rho_s(1-n)\mathbf{v}_s]=0 \tag{60}$$

If it is assumed that fluid density ρ and grain density ρ_s are constant, Eqs. (59) and (60) can be manipulated and combined (Screaton et al. 1990) to yield

$$\nabla\cdot q+\nabla\cdot\mathbf{v}_s=0 \tag{61}$$

or

$$\nabla\cdot\left[-\frac{k}{\mu}\nabla(p-\rho gz)\right]+\nabla\cdot\mathbf{v}_s=0 \tag{62}$$

Equation (62) amounts to a statement of steady-state fluid flow with a source term, in this case the divergence of sediment velocity, or $\nabla\cdot\mathbf{v}_s$. The divergence of sediment velocity is a virtual fluid source because it represents the gain or, in this case, the loss of pore volume per unit volume per time (dimension T^{-1}) occurring as the sediments pass through any part of the complex.

By fitting an Athy-type relation to available porosity data for the Barbados complex, Screaton et al. estimated porosity throughout the system. With porosity specified, it was possible to evaluate $\nabla\cdot\mathbf{v}_s$ numerically throughout the complex, as shown in Fig. 14b, allowing Eq. (62) to be solved. This analysis hinged on porosity estimates of uncertain accuracy, but the resulting errors were limited by continuity requirements for the sediment solids advected at a well-constrained rate. Screaton et al. assumed that fluid pressures would hydrofracture the sediments and increase permeability when they reached the lithostatic load. This allowed them to estimate the temporal mean permeability in the prism, décollement, and the underthrust sediments.

The soft, often clay-rich ocean floor sediments accumulating in prism complexes would seem to allow another approach to describing their hydromechanical behavior. Specifically, application of rheological models developed for geotechnical applications seem to offer obvious possibilities. Such a strategy was, in fact, used by

 DOI 10.1007/s10040-002-0230-8

Stauffer and Bekins (2001) to examine coupling between deformation and fluid pressure near the deformation front, or toe, of the Barbados accretionary complex.

Stauffer and Bekins chose to use the model developed by Borja (1984) and Borja and Kavazanjian (1985; see *Inelastic rheologies from a geotechnical perspective*) that incorporates modified Cam-clay behavior and viscoelasticity. The model is available in the coupled hydromechanics simulator SPIN 2D (Borja and Kavazanjian 1984). In addition to the constitutive relation describing visco-elastoplastic deformation [see Eq. (35)], the simulator uses the stress equilibrium relations and a statement of fluid conservation. Because the constitutive relations are in terms of time derivatives of stress and strain, force equilibrium [Eq. 4)] is also expressed in time derivative form, namely

$$\frac{\partial \dot{\sigma}_{ij}}{\partial x_j} = 0 \tag{63}$$

using indicial notation. It is also assumed that the fluid and sediment grains are much less compressible than the sediment porous matrix, and that there are no fluid sources. Under these circumstances, fluid density ρ can be considered constant and $\partial n/\partial t = \nabla \cdot \dot{\boldsymbol{u}}$. The equation of fluid mass conservation (14) can then be expressed as

$$\nabla \cdot \dot{\boldsymbol{u}} + \nabla \cdot \boldsymbol{q} = 0 \tag{64}$$

which, with Darcy's law, is used by SPIN 2D to describe fluid flow.

Stauffer and Bekins (2001) focused on the hydromechanical role of the décollement, or zone of shearing between underplating and accreting sediments. In seismic imaging, parts of the décollement appear to be underconsolidated and this may result from high fluid pressures within the complex that are intermittently propagated along the décollement. Stauffer and Bekins found that expulsion of fluid can affect the mechanical behavior of sediments as much as 3 km ahead of the deformation front. From a broader perspective, this study is noteworthy and perhaps unique in its application of a rather complex rheological model in a fully coupled hydromechanical analysis of tectonic deformation.

Barometric and moisture loading and earth tides

Earth's crust experiences a variety of high frequency, cyclical mechanical loadings. These include earth tides, barometric effects, and loading by moisture and snow. In the present context, "high frequency" refers to periods that range from diurnal to seasonal and thus are very short in a geologic sense. These loadings and the resulting fluid pressure changes are of interest for a number of reasons. Because they are repetitive and small in magnitude, they belong to the relatively exclusive class of crustal deformations that are very nearly linear-elastic; the changes in fluid pressure that they induce should be quite accurately described by linear poroelastic theory. In addition, the coupling can reveal a great deal about the causative mechanical loadings as well as the mechanical and hydraulic properties of the host media. In some cases it would be difficult to obtain this information any other way.

High frequency loadings typically cause little fluid advection because their periods are short compared to the time scales for "drainage" or hydraulic response to occur. This is particularly true for earth tides with periods measured in hours. In such cases, Eq. (23) with the flow term, thermal term, and fluid sources set to zero provides the relation between stress and fluid pressure changes, namely

$$p = \beta \sigma_t \tag{65}$$

We see that p and σ_t are linearly related through Skempton's coefficient β, or the three-dimensional loading efficiency defined in Eq. (22). Here, the physical meaning of β as the ratio of the change in fluid pressure to the change in mean total stress becomes clear. Because $0 \leq \beta \leq 1$, pressure changes of any magnitude between zero and σ_t are possible. The highest efficiencies, approaching unity, are associated with relatively compressible media such as clays.

Barometric and moisture or snow loading tend to be areally extensive and reasonably homogeneous at scales of tens to hundreds of kilometers. They represent yet another instance when strain can often be assumed to be purely vertical. Setting lateral strains to zero, Eqs. (36) for σ_{xx} and σ_{yy} can be combined with Eq. (65) and the definition of σ_t to yield, after some manipulation

$$p = \zeta \sigma_{zz} \tag{66}$$

where ζ, the one-dimensional loading efficiency defined following Eq. (45), is now seen to be the ratio of the change in fluid pressure to the change in vertical load under conditions of lateral confinement; like β, ζ takes on values between 0 and 1. The fluid pressure response thus depends on the quantities that comprise ζ, namely, the elastic moduli of the porous medium, porous medium solids, and fluid, and the Poisson's ratio and porosity of the porous medium. As van der Kamp and Gale (1983) noted, if the solids are taken to be incompressible, ζ reduces to a quantity known as Jacob's (1940) tidal loading efficiency, or

$$\zeta = \frac{1/K'}{1/K' + 1/K_f} \tag{67}$$

Here, "tidal" refers to loading by ocean tides rather than by earth tides.

The relation expressed by Eq. (66) offers the possibility of measuring load changes if ζ is known. Such a capability is potentially very useful for monitoring changes in soil moisture or snowpack and the technique has the helpful property of averaging load changes over increasingly large areas as the depth of the pressure measurement is increased. Unfortunately, there are difficulties in practice, including the confounding effects of fluid storage (known as compliance) in the pressure

 DOI 10.1007/s10040-002-0230-8

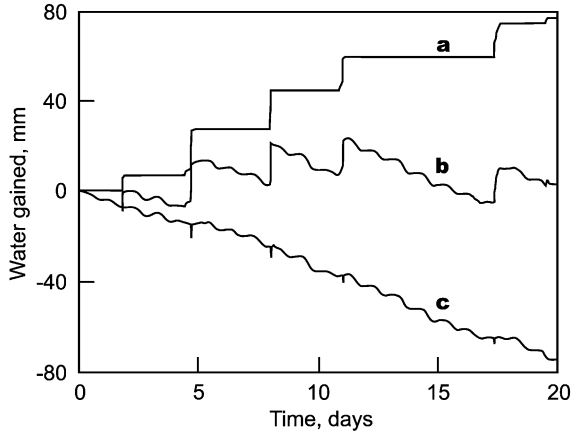

Fig. 15 Plot showing rainfall events and fluid pressure response to the resulting soil moisture loading as measured by van der Kamp and Schmidt (1997) in a specially constructed borehole piezometer. Trend *a* is cumulative rainfall, *b* is subsurface fluid pressure including the moisture-loading effects, and *c* is subsurface fluid pressure with loading effects subtracted, revealing a steady extraction of soil water by evapotranspiration. Plot modified from van der Kamp and Schmidt (1997)

measurement installation. The technique can be made to work, however, as van der Kamp and Schmidt (1997) demonstrated by monitoring changes in soil moisture using a borehole in low-permeability glacial till. Their pressure data revealed a delicate balance between rainfall and evapotranspiration (Fig. 15) that would have been difficult, if not impossible, to document using more conventional techniques.

Another form of cyclical loading, earth tides, results from passage of the tidal bulge around the Earth. The crust can be envisioned as a thin skin that is alternately stretched and contracted as the bulge passes. Changes in g itself and thus in vertical stress σ_{zz} are small enough to be ignored near the ground surface, which acts as a free surface. For earth tides, with wavelengths of many thousands of kilometers, the entire crust can be considered to be near the surface (Rojstaczer and Agnew 1989). With the crust merely "along for the ride," the magnitude of the stretching and contracting is controlled by the deformation properties of the whole Earth and is relatively predictable. This imposed lateral strain is

$$\varepsilon_T = \varepsilon_{xx} + \varepsilon_{yy} \tag{68}$$

In contrast, vertical tidal strain should be controlled by local formation properties. Because $\sigma_{zz} = 0$, and $p = \beta\sigma$, the vertical component of Eq, (7) is found to be given by

$$\varepsilon_{zz} = -\frac{1}{K}\left[\frac{\nu}{\beta(1-2\nu)} + \frac{\alpha}{3}\right]p \tag{69}$$

where α and ν are those of the local formation, and temperatures are constant. From Eq. (7) one can also deduce that volumetric tidal strain $\varepsilon_{kk} = \varepsilon_T + \varepsilon_{zz}$ is given by

$$\varepsilon_{kk} = -\frac{1}{K}\left(\frac{1}{\beta} - \alpha\right)p \tag{70}$$

Equations (69) and (70) yield the result that

$$p = 2G\zeta\varepsilon_T \tag{71}$$

(van der Kamp and Gale 1983). Thus, the fluctuations in fluid pressure in response to tidal strains depend on the formation shear modulus and loading efficiency, allowing these properties to be determined under certain conditions. Sometimes, too, flow into and out of open wells in response to tidal strains causes the observed response to lag the tidal forcing. The lag can be analyzed to estimate the hydraulic conductivity of the formation (Hsieh et al. 1987).

Creep and seismic slip along faults

Although faults often accomodate large displacements on geologic time scales, on human time scales displacement occurs as local seismic slips or aseismic creep on portions of faults. Slip and creep events alter nearby stress fields and fluid pressures essentially instantaneously. During the ensuing quiescent portion of the cycle, transient flow gradually dissipates the pressure perturbations. Since the strains, pressure perturbations, and subsequent fluid flow occur repeatedly through many earthquake cycles, one would expect that they can be quite accurately described using linear poroelastic theory. The flow transients of interest here should not be confused with those caused by permeability changes, sediment liquifaction, or other phenomena related to seismic shaking, which have been analyzed and discussed by Rojstaczer et al. (1995) and Roeloffs (1996, 1998), among others.

The pattern of stress and fluid pressure changes produced by a displacement can be predicted theoretically. This is usually done by treating the displacement as a dislocation in an elastic medium (e.g., Rudnicki 1985). Nearly 40 years ago, Press (1965) had shown that strains predicted using this approach were reasonably consistent with observed strains. Corresponding fluid pressure responses can be calculated with Eq. (65), that is, $p = \beta\sigma_t$. Conversely, observed coseismic fluid pressure changes should also be useful for determining volumetric strains. This is important because water level data are usually more readily available than strain data.

In practice, the interpretation of coseismic fluid pressure changes can be difficult. Following a small earthquake near Parkfield, California, Quilty and Roeloffs (1997) analyzed water-level changes in several wells near the epicenter and found that strains predicted by a dislocation model of the rupture were in good agreement with the changes in most, but not all, of the wells (Fig. 16a). Quilty and Roeloffs speculated that complicating effects, such as dynamic strains, affected some of the wells. Wang (1997) proposed that, rather than deforming poroelastically, rocks at the Parkfield site experienced some dilatation in response to increased deviatoric stress. This interpretation does not fit certain other observations (E. Roeloffs, US Geol. Survey, personal communication, 2002) but can explain the water level changes in the problematic wells (Fig. 16b). In

 DOI 10.1007/s10040-002-0230-8

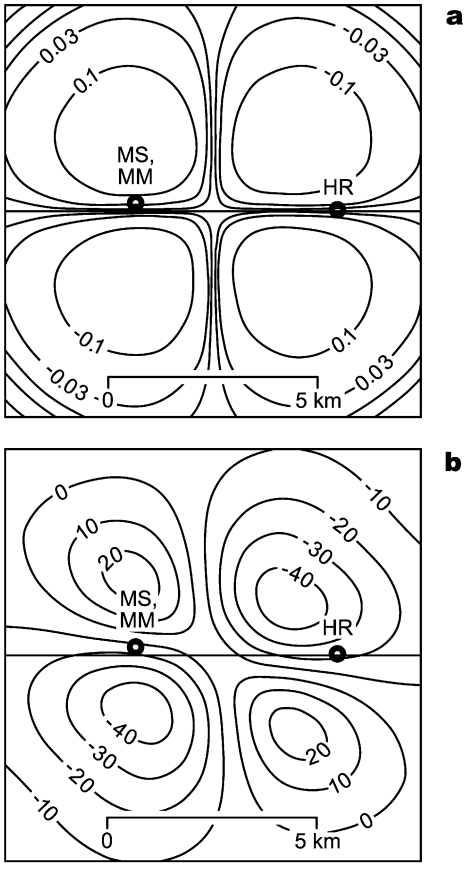

Fig. 16 Computed response patterns to an earthquake near Parkfield, California, USA, on December 20, 1994. **a** Predicted elastic dilatation adapted from Quilty and Roeloffs (1997) (contours in microstrains; expansion negative). **b** Predicted water-level changes adapted from Wang (1997) (contours in cm). Water-level changes were computed assuming that some dilatation is caused by increasing deviatoric stress. This causes the deformation pattern to be skewed, helping to explain observed water level declines in wells *MM*, *MS* and *HR*. In both plots the horizontal line is the trace of the San Andreas Fault

another instance, water-level changes accompanying an earthquake at Roermond in the Netherlands were analyzed by Grecksch et al. (1999). While the sense of the water-level changes (up or down) was largely in agreement with volume strains predicted by poroelastic theory, the magnitudes and duration of the changes were significantly larger than expected.

Instances of aseismic creep on faults have also been studied. Wesson (1981) was able to explain observed water-level changes in a well near the San Andreas fault by hypothesizing that a dislocation had migrated along the fault near the well and then stopped at a kink in the fault. Similarly, Lippincott et al. (1985) were able to explain spikes in water-level records in a well near the Garlock fault as resulting from several creep dislocations that migrated past the well. Transient creep events such as these may precede major earthquakes, and there is thus interest in fluid-pressure changes as possible earthquake precursors. To date, hydrologic precursors have proven difficult to interpret (e.g., Roeloffs 1988; King et al. 2000), but potential benefits are so great that they continue to be investigated.

Magmatic intrusions

Intrusions cause dramatic changes in surrounding rocks and sediments by supplying huge amounts of heat, giving off significant volumes of volatiles, and generating large displacements to accomodate the magma. The behavior of the intrusion and its surroundings after emplacement is highly complex because of the resulting large temperature changes and gradients and their effects on both the fluids and the solids. A number of couplings are significant, including thermomechanical and hydromechanical.

A number of studies (e.g., Cathles 1977; Norton 1982) have examined thermo-and hydromechanical effects of intrusion in an ad hoc fashion by considering the fluid pressure increases, resulting hydrofracturing and permeability increases, and fluid-flow regimes that are generated once an intrusion is in place. Permeability increases are believed to be pronounced near an intrusion because of rapid and large fluid pressure increases that cause hydrofracturing, and may set the stage for thermally driven convection that can transport a great deal of chemical mass and accelerate the cooling of the intrusion (e.g., Norton and Knight 1977; Norton 1982).

A fuller treatment would also consider the mechanical effects of intrusion, that is the displacements to accomodate the intrusion and the thermo-poroelastic response in the surrounding rock. To my knowledge, a full analysis rigorously incorporating these couplings has never been attempted. The hydromechanical effects of emplacement have, however, been studied by Elsworth and Voight (1991) for the case of an approximately cylindrical intrusion. This phenomenon is similar to the movement of a creep dislocation along a fault discussed above. Elsworth and Voight approximated the intrusion as a moving point dislocation within an infinite poroelastic medium, and developed predictions of the effect on fluid pressures; comparison with observed fluid pressure changes accompanying intrusive activity at Krafla, Iceland yielded reasonable agreement.

Effects of Fluid Pressure on Crustal Mechanics

The effects of the fluid regime on deformation and failure in the crust are no less conspicuous or important than the coupling in the opposite sense just discussed. As noted by Rudnicki (1985), they include dynamic phenomena, such as changes in wave velocity, as well as static. This section focuses on static deformation phenomena that reflect the mediation of fluid pressure and flow. In some instances, the same geologic phenomena considered in the preceding sections will be discussed from the viewpoint of coupling in the opposite direction.

 DOI 10.1007/s10040-002-0230-8

Arrested compaction

Compaction-generated fluid overpressures (see *Sediment compaction*) have a profound influence on the progress of compaction itself. Mechanically, compaction is analogous to consolidation in geotechnical problems, the phenomenon that inspired Terzaghi's concept of effective stress and his development of the pressure diffusion equation. In an idealized compacting system where lateral strains are zero ($\varepsilon_{xx} = \varepsilon_{yy} = 0$), Eqs. (7) indicate that vertical strain is given by

$$\varepsilon_{zz} = \frac{1}{K}(\sigma_t - \alpha p) \tag{72}$$

where σ_t is the mean normal stress. Simply stated, vertical strain is determined by the effective rather than the total stress. As seen in the sections, *Porosity and stress gradients as indicators of long-term strain or effective deformation moduli* and *Approximating deformation over short time steps as poroelastic*, although sediments generally do not deform poroelastically, Eq. (72) may be a useful description of compaction if it is imagined that K is a function of effective stress and perhaps time. In sediments with hydrostatic or so-called normal fluid pressures, this variation in K_{eff}, or the effective value of K, reveals itself through the more or less regular and approximately exponential porosity loss with depth that was first quantified by Athy (1930). This pattern is interrupted when fluid overpressures limit effective stress increases, leaving higher than expected porosities in parts of the sedimentary column. The dynamics of this process have been observed directly in areas where extraction of water or other fluids has led to land subsidence (e.g., Domenico and Schwartz 1998; Galloway et al. 1999; also Fig. 1). Various numerical basin simulators, including Basin2 (Bethke et al. 1999), BASIN3D2P (Tokunaga 1996), DYME-TOUGH2 (McPherson and Bredehoeft 2001), and RIFT2D (M. Person et al., Indiana University, in preparation, 2002) account for arrested compaction by tracking vertical effective stress and tying vertical deformation to it. Recognizing that compactional strain is mostly plastic, these simulators also compute decompaction with larger values of K_{eff} that are determined by a separate Athy-type relation [Eq. (55)] applicable when σ'_{zz} is less than the maximum. This mimics loading-unloading-reloading behavior in sediments (see Figs. 3a, 5b, and 8).

Arrested compaction is conspicuous in many areas of active deposition, such as the US Gulf Coast (Harrison and Summa 1991) and the continental slope off the US east coast (Dugan and Flemings 2000). Indeed, it has an important practical role as an indicator of fluid pressure because porosity is often routinely measured by borehole logging but fluid pressure is not (Fertl et al. 1994; Dugan and Flemings 2000). A classic analysis of arrested compaction is Magara's (1968) study of the mudstones of the Nagaoka Plain, Japan. Because of their low permeability, mudstones are especially troublesome for fluid-pressure measurement. However, Magara was able to generate vertical two-dimensional maps of inferred fluid pressure and flow in the mudstones using profiles of measured porosity (Fig. 17). Although useful, this technique demands caution because of potential inaccuracies. For example, Harrold et al. (1999) cite instances where vertical effective stress was an inconsistent proxy for mean total effective stress, leading to errors when fluid pressure patterns were estimated from porosity profiles.

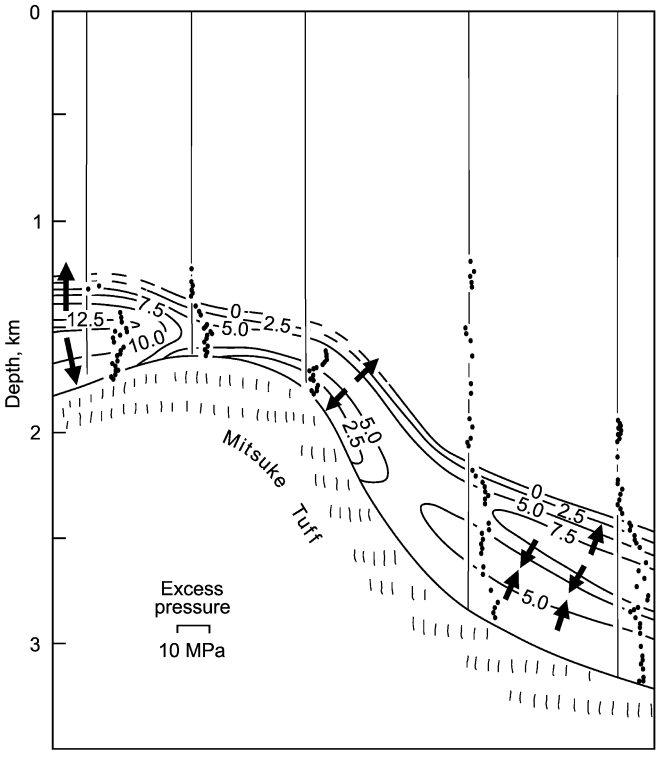

Fig. 17 Cross section through mudstones (*contoured region*) and underlying Mitsuke Tuff, Nagaoka Plain, Japan, showing inferred fluid overpressures (in MPa) and flow directions. Boreholes are shown as *vertical lines* and the horizontal scale is unspecified. *Data points* show overpressure inferred from sonic log determination of porosity (adapted from Magara 1968)

Compactional strain states may also contain information about fluid pressure history. If overpressures are generated after compaction, they have comparatively little effect on the porosity. Because of this, it should be possible to determine whether part or all of present-day fluid overpressures were generated after compaction. Hart et al. (1995) used this approach to analyze overpressures in the US Gulf Coast. Extrapolating a porosity-effective stress relation with depth predicted smaller fluid pressures than were found, leading Hart et al. to conclude that part of the overpressure was generated after compaction. A similar conclusion was reached by Harrison and Summa (1991).

Natural hydrofracturing

At meter scales and larger, as Secor (1965) notes, discontinuities are nearly ubiquitous in rock, and the vast majority are joints without significant displacement. This

 DOI 10.1007/s10040-002-0230-8

implies tensile Mode I type failure, or failure under forces tending to pull the rock apart normal to the joint plane. Stress states in the subsurface, however, are almost always compressive. It has been argued that horizontal stress in the crust can become tensile when erosion causes cooling and uplift follows the diverging radii of the Earth (Haxby and Turcotte 1976). However, compressive stress states in the crust remains an observational fact. In view of this, how can the ubiquity of tensile-style fractures be explained?

It is almost certain that fluids play a crucial role. By the 1930s the physical processes by which magma fractures and invades rock were beginning to be recognized (Anderson 1938), and by the late 1940s oil and gas wells were routinely "hydrofractured" with water under high pressure to enhance production. In the following decade Hubbert and Willis (1957) worked out the relation between hydrofracture orientation and the state of stress in the rock. However, it was Secor (1965) who explicitly linked natural jointing in rock to net tensile stresses created by high fluid pressures. In other words, tensile *effective* stresses in regimes of compressive total stress are probably responsible for most jointing.

The component of the effective stress law [Eq. (5)] in the direction of least principal stress can be written as

$$\sigma_3' = \sigma_3 - \alpha p \tag{73}$$

where subscript 3 indicates the least principal stress direction. If the differential stress $\sigma_d = \sigma_1 - \sigma_3$ is nonzero but not large enough to cause shear failure, Eq. (73) shows that increasing p sufficiently will lead to $\sigma_3' < 0$, that is, to a tensile effective stress. Depending on the stress regime, depth, and tensile strength of the rock, fluid overpressures, or pressures in excess of hydrostatic, appear to be required for natural hydrofracturing to occur (Secor 1965).

Superhydrostatic fluid pressures are found in a variety of environments and may themselves be a result of deformation, such as the overpressures caused by depositional compaction or tectonic squeezing effects that were discussed in the sections *Sediment compaction* and *Tectonic deformation*. They may also result from heating and diagenetic reactions, including oil and gas generation. As widespread and varied as high fluid pressure environments are, however, most of the upper crust, at least, does not appear to host overpressures. This is difficult to reconcile with the pervasiveness of jointing in the crust, which seems to imply a history of correspondingly pervasive fluid overpressures. Do high fluid pressures nearly always occur during certain phases of crustal development or are they more widespread in the crust than currently believed? Alternatively, are some joints generated without high fluid pressures?

The nucleation of Mode I fractures also poses interesting questions. It requires a fluid pressure p given by

$$p = \sigma_3' + \frac{K_{Ic}}{Y\sqrt{c}} \tag{74}$$

where σ_3' is the least principal effective stress, K_{Ic} is the fracture toughness, or critical stress intensity factor, at the fracture tip, Y is a flaw shape factor, and c is the radius of the flaw around which the fracture nucleates (Lawn and Wilshaw 1975). How does this condition give rise to numerous, relatively closely spaced fracture nucleations? Finite permeability throughout a rock mass effectively prevents meter-scale pressure excursions that, at first glance, might seem necessary for closely spaced fractures to nucleate and propagate. One explanation of the pore-scale mechanics of joint initiation has been proposed by Engelder (1993). As fluid pressure increases in flaws (which by definition are larger than the representative pore size), the stress holding the flaws closed increases by a smaller amount because some of the fluid pressure load is carried by the strength of the porous skeleton. This is the effect accounted for by α in Eq. (73). Ultimately, it is reasoned, the pressure in the flaw is sufficient to initiate a fracture.

Once a tensile fracture is initiated, its propagation must be controlled by fluid pressure. As a fracture opens, the fluid pressure in it decreases, causing flow into the fracture and locally depressing fluid pressure. More fluid must flow in to propagate the fracture and propagation is therefore partly controlled by permeability. At the same time, Eq. (74) shows that the fluid pressure needed to maintain or propagate a fracture decreases as the crack radius c increases (if a crack is considered to be an elliptical feature, c is the long axis). For most rocks, when c reaches about 1 m the necessary pressure has decreased nearly to σ_3' (Engelder 1993). A different process, subcritical fracture propagation, occurs where chemical reactions weaken the medium at the fracture tip. Subcritical propagation occurs at stress intensities less than the critical value needed for purely mechanical propagation.

Fracture propagation is more complex than the preceding paragraph suggests, and this is particularly true in layered and otherwise heterogeneous media. In addition, propagation actually involves interactions amongst multiple fractures in three dimensions. Nevertheless, insight can be gained from analysis of a single fracture. Because of the small strains and relatively short time scales involved, poroelasticity provides a useful framework for analysis. Renshaw and Harvey (1994) used poroelastic theory to analyze lateral propagation of a single vertical fracture under conditions of plane strain. The governing equations were the deformation equations in terms of stress (12) for isothermal conditions or, in indicial notation,

$$\nabla^2\sigma_{ij} + \frac{1}{1+\nu}\frac{\partial^2\sigma_{kk}}{\partial x_i \partial x_j} - \frac{1-2\nu}{1-\nu}\alpha\left[\frac{1-\nu}{1+\nu}\frac{\partial^2 p}{\partial x_i \partial x_j} + \delta_{ij}\nabla^2 p\right] = 0 \tag{75}$$

Equations (75) were coupled with an isothermal form of the flow equation (20), written as

 DOI 10.1007/s10040-002-0230-8

$$\nabla \cdot \kappa \nabla \frac{p}{\rho g} = \left[\left(\frac{1}{K} - \frac{1}{K_s} \right) + \left(\frac{n}{K_f} - \frac{n}{K_s} \right) \right] \frac{\partial p}{\partial t} - \left(\frac{1}{K} - \frac{1}{K_s} \right) \frac{\partial \sigma_t}{\partial t} \quad (76)$$

Renshaw and Harvey considered quasi-steady fracture propagation, meaning that the fluid pressure inside the fracture is always just sufficient for propagation, and the criterion expressed by Eq. (74) applies. They constrained the stress intensity at the fracture tip to be at the critical value (K_{Ic}) and required that the flux of fluid into the fracture be equal the rate of increase in fracture cross-sectional area, that is

$$-\frac{2\kappa}{\rho g} \int_{-a}^{a} \left. \frac{\partial p}{\partial x} \right|_{y=0+} dy = \frac{dA_f}{dt} \quad (77)$$

where A_f is the fracture cross-sectional area, y denotes the direction of fracture growth, and x denotes the direction normal to a fracture of length $2a$. Equation (77) merely equates the Darcy flux across both fracture walls to the volume increase in the fracture. For this problem, the remote stresses (those on the domain boundaries) were held constant. Solutions in dimensionless terms (Fig. 18) show that fracture extension is nearly proportional to dimensionless time, which is defined as $(\kappa t)/\left(S_{s3}\, a_0^2\right)$. Hydraulic diffusivity (κ/S_{s3}) thus controls the rate of propagation, as would be expected, because it controls the supply of fluid to the fracture. This suggests that the rate of fracture propagation under these conditions will readily vary by a factor of 10^6 or more for various lithologies, as κ/S_{s3} is observed to do. This is exactly what Renshaw and Harvey (1994) found; simulated quadrupling of the length of meter-long fractures took from several seconds to several tens of days for different rock types. Renshaw and Harvey (1994) also tried a partially coupled model that accounted for the effects of the stress field on fluid pressure, but not the effects of pressure on the stress field. Notably, the results from the partially coupled and fully coupled poroelastic analyses did not greatly differ.

The logical next step, consideration of interactions between multiple fractures and multiple sets of fractures in three dimensions, is proving difficult. Renshaw and Pollard (1994), among others, have simulated the growth of multiple fractures under plane strain conditions and have shown that their geometry is sensitive to the relation between rate of extension and stress concentration at the fracture tip. There are also complex interactions that govern whether propagating fractures cross or terminate at preexisting fractures (Renshaw 1996).

Mechanisms controlling the growth of interacting fractures have yet to be integrated into coupled hydromechanical models, but they are a crucial aspect of fluid-solid coupling because they ultimately control permeability. Fracture generation and propagation have little effect on the fluid flow regime until the percolation threshold, or fracture density necessary to form an interconnected network of fractures, is reached and the permeability of the rock increases dramatically. Thus, it might be expected that high fluid pressures generate and extend joints until the percolation threshold is reached, at which time the pressures bleed down via flow through the fracture network. Stated differently, one would expect the growth of fracture systems to be self-limiting through their effect on the fluid regime, which may in fact be the case. Renshaw (1996) estimated fracture densities from several published fracture maps and found that they appear to be close to the percolation threshold, and Gueguen et al. (1991) have suggested that the fractal nature of fracture systems is also evidence that they are near the percolation threshold.

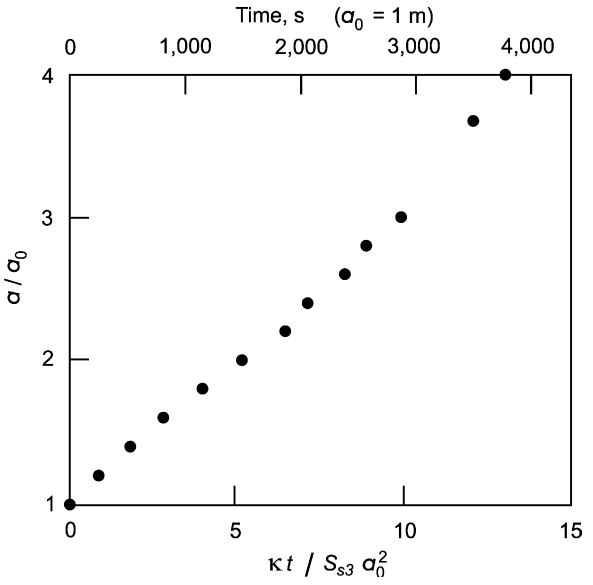

Fig. 18 Simulated normalized length (a/a_0) versus dimensionless time $\left(\kappa t/S_{s3}\, a_0^2\right)$ of a single fracture propagating in a quasi-static fashion in a poroelastic medium. The time scale along the top axis applies for an initial fracture half-length a_0 of 1 m and properties describing the Ruhr Sandstone. Plot adapted from Renshaw and Harvey (1994)

There are two ways that a system can be brought to the threshold of fluid release. First, fluid pressures may simply increase until hydrofracturing occurs under the prevailing stress regime. Second, rocks that are able to contain fluid overpressures may hydrofracture when the stress regime changes. Specifics of how this process might occur have been discussed by Sibson (2000).

Additional evidence for a close linkage between fluid pressures and fracturing can be sought in fluid regimes themselves. Because natural hydrofracturing occurs when fluid pressure exceeds the least principal effective stress plus a relatively small nucleation term [see Eq. (74)], fluid pressures should never significantly exceed the overburden load. With rare exceptions representing unusual conditions, this is observed to be the case worldwide (Fertl 1976; Fertl et al. 1994). Instances where horizontal stress is known to be less than overburden load are still more definitive. In such environments, fluid pressure should be limited to the least horizontal stress.

 DOI 10.1007/s10040-002-0230-8

This too appears to hold true. In part of the Gulf of Mexico Basin, fluid pressures consistently peak at about 85% of overburden, a value that seems to correspond to the least horizontal stress (Engelder 1993).

Hydrofracturing and fluid release can be a one-time event or, as seems more likely in many instances, can be reinitiated many times if fractures are able to close or reseal. Different lines of evidence in crystalline basement rocks (Nur and Walder 1990) and sedimentary sequences (Neuzil 1994) point to time-averaged permeabilities that are much higher than those measured, suggesting that relatively permeable fracture systems dominate at times, and the low permeability of the unfractured matrix dominates at others. On the basis of presumed plastic strain rates and permeabilities in crystalline rocks at depth, Nur and Walder (1990) argued that cycles of fluid pressure buildup and release occur with 10^3- to 10^5-year periods and that tens to tens of thousands of cycles occur during crustal dewatering. Brine plumes, pressure anomalies, and thermal anomalies in sediments of the US Gulf Coast are also thought to point to repeated episodes of fluid expulsion. Simulating the generation of observed brine plumes, for instance, Ranganathan (1992) found that they probably are created and dissipated rather rapidly. By implication, episodes of expulsion must recur. Roberts et al. (1996) simulated expulsion through compressible fractures with permeabilities that depend on fluid pressure. They found that observed pressure and heat anomalies are best explained by a series of expulsion events. Others (e.g., Dewers and Ortoleva 1994) have interpreted geochemical modeling results as indicating that fluid expulsion must be episodic.

Shearing, faulting, and seismicity

Differential stress is defined as the difference between the greatest and least principal stresses (see previous section, *Natural hydrofracturing*). Plastic yielding and shear failure limit the magnitude of differential stress that can be maintained by intact geologic media. Clays and other soft sediments generally deform plastically after yielding as described by Cam-clay and similar geotechnical models (see *Inelastic rheologies from a geotechnical perspective*). At high pressures and temperatures, rocks too yield plastically. Under more moderate conditions or high strain rates, however, rocks experience brittle failure. The initiation of shear failure in compacted sediments and rocks in the upper crust seems to be reasonably well described by Coulomb's law, which gives the shear stress τ at failure as

$$\tau = \tau_0 + \mu^* \sigma_n \qquad (78)$$

where τ_0 is the cohesion of the medium, σ_n is the stress normal to the shear plane, and μ^* is a coefficient representing the strength of the medium. Once rock has failed, the threshold shear stress for slippage along preexisting discontinuities is still usually well-described by Eq. (78). After failure, however, μ^* represents the so-called coefficient of static friction and τ_0 is typically close to zero. In either case, Eq. (78) indicates that shear stress must overcome both cohesion and a resistance to shear displacement that is proportional to the stress normal to the plane of displacement.

Mohr diagrams are a useful tool for considering the relation between differential stress, shear stress, and shear failure or shear slippage in two dimensions (e.g., Ingebritsen and Sanford 1999). With shear stress on the vertical axis and normal stress on the horizontal, the Mohr circle (Fig. 19) shows the combinations of shear and normal stress on planes oriented at angle θ to σ_1, the greatest principal stress. Representative envelopes for shear failure and shear slippage, which are medium-dependent, are also plotted in Fig. 19. If changes in the stress state cause the Mohr circle to touch the failure envelope, the indicated type of failure is expected to occur. Fig. 19 shows that failure can be brought on by either increasing σ_1 or decreasing σ_3 (recall that a two-dimensional system is being considered).

The crucial role played by hydromechanical coupling arises from the fact that the operative stresses are *effective* stresses, such that σ_n in Eq. (78) should be replaced by $\sigma_n - \alpha p$. The effect of fluid pressure can be visualized on the Mohr diagram as a simple leftward translation of the Mohr circle by an amount equal to the pressure (Fig. 19). Note that simple hydrofracture generation and propagation, discussed in the previous section, is represented by Mohr circles that plot below the indicated fracture limit; fracturing is initiated when fluid pressures increase, the Mohr circle translates leftward, and σ_3 becomes sufficiently tensile to generate fractures.

Most geologic media seem to become fractured early in their history (Secor 1965) so shear slippage typically occurs on preexisting discontinuities. Shear displacement along discontinuities can be either continuous in time or, as is common in geologic systems, of the stick-slip type (see *Creep and seismic slip along faults*). In the latter, shear stress builds until shear slippage occurs and relieves the stress, causing the slippage to cease and initiating another cycle of stress buildup (Rojstaczer and Bredehoeft 1988). This implies that hydromechanical coupling has a role in initiating earthquakes. Although there are few data on fluid pressures at depths where most earthquakes occur, there have been numerous instances when seismic activity could be tied directly to anthropogenic fluid pressure changes and many more where such a connection appears to be likely (e.g., Nicholson and Wesson 1990). Because of their potential utility for understanding natural seismicity, it is worth examining two representative cases of induced seismicity.

Nearly 40 years ago, swarms of small earthquakes were observed to be correlated in time with injection of liquid waste into basement rock beneath the Denver Basin, central USA (Fig. 20a). Using the injection history, Hsieh and Bredehoeft (1981) were able to demonstrate that the seismicity could be explained by the generation and diffusion of a fluid pressure increase. Specifically, seismicity apparently was triggered when fluid pressures exceeded undisturbed values by a particular (and rela-

 DOI 10.1007/s10040-002-0230-8

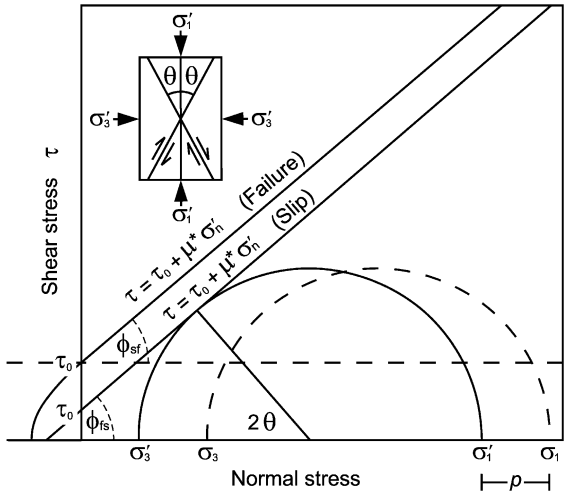

Fig. 19 Mohr circle diagram showing failure envelopes for shear failure [Eq. (78) with $\mu^* = \tan \Phi_{sf}$] and frictional slip [Eq. (78) with $\mu^* = \tan \Phi_{fs}$] where Φ_{sf} and Φ_{fs} are the internal friction angles for shear failure and frictional slip, respectively. The *region below the straight dashed line* is where hydrofracture initiation and propagation occur. Fluid pressure p translates the *circle to the left*; in the instance shown, the initial, stable, stress state at $p = 0$ (*dashed circle*) is brought to shear slip (*solid circle*) in this manner

tively small) amount. Some years later, an attempt was made at Rangely, Colorado, to induce earthquakes by injecting fluids (Raleigh et al. 1976). That experiment underscored the importance of effective stress in Eq. (78) because it showed both *increased* seismicity near the injection point and *decreased* seismicity where water was extracted and fluid pressures decreased. Thus both decreases and increases in effective stress were shown to have the anticipated effects on fault strength. In a more recent experiment, researchers induced seismicity at 9.1 km depth in the German KTB (Kontinentales Tiefbohrprogramm der Bundesrepublik Deutschland) borehole (Zoback and Harjes 1997; Fig. 20b). Like the Denver earthquakes, the KTB earthquakes apparently were triggered by relatively small pressure perturbations. This suggests that differential stresses at both sites are mediated by fluid pressure.

A curious style of fluid pressure-induced seismicity has been analyzed by Segall (1989, 1992) and Segall et al. (1994). In a number of locations, including the Wilmington Oil Field, California, and the Laq Gas Field, France, seismicity appears to have been triggered by fluid withdrawals and the resulting *decreases* in fluid pressure. Segall (1989) analyzed this seemingly counterintuitive phenomenon as a fully coupled poroelastic problem. His approach was somewhat unusual in that it considered changes of fluid mass per volume rather than changes in fluid pressure or head. This was done to accomodate the causative process in terms of the known fluid withdrawal. The displacement form of the governing equations for deformation (10) had to be cast in terms of fluid mass, yielding

$$G\nabla^2 u_i + \frac{G}{1-2\nu}\,\frac{\partial^2 u_j}{\partial x_i \partial x_j} = \frac{1}{\rho_0}\,\frac{\beta K}{1-\alpha\beta}\,\frac{\partial}{\partial x_i}(\rho n) \qquad (79)$$

(Wang 2000, p. 75). Segall considered only the effects of changes in the fluid regime so that the elevation term in flow equation (20) could be ignored. Substituting the compatibility relation (13) into (20) and manipulating (see Rice and Cleary 1976), he then obtained a statement of fluid conservation that is also in terms of fluid mass per volume, that is

$$D_h \nabla^2(\rho n) = \frac{\partial}{\partial t}(\rho n) \qquad (80)$$

where D_h is a coefficient of complex form (see Rice and Cleary 1976, Eq. 17) that can be interpreted as a hydraulic diffusivity. Coupling and analytically solving Eqs. (79) and (80) for a representative fluid extraction regime, Segall (1989) found pressure decreases did, as expected, strengthen faults *within* the fluid reservoir. However, the mechanical coupling between the reservoir and surrounding less permeable rock perturbed the stress field in the latter as well. It is apparently these stress changes where the system was "undrained" because of its low permeability that caused seismicity. Segall's poroelastic predictions of deformations and styles of faulting agreed well with those observed, supporting this interpretation.

Slip on a fault is often preceded or succeeded by additional seismic events on the same or a nearby fault. These events are clearly interrelated mechanically, but because they take place over hours to months, some mechanism must cause the mechanical interactions to evolve over time. Nur and Booker (1972) were among the first to suggest that the delays are related to fluid flow. Although slip events alter the local total stress field nearly instantaneously, effective stresses evolve for some time after that as transient flow allows fluid pressures to re-equilibrate after the disturbance (see *Creep and seismic slip along faults*). Thus, another Coulomb failure may occur some time after the stress field has been modified by a prior event. Nur and Booker proposed this as an explanation for aftershocks. An analogous process may explain certain fault interactions. In 1987, large earthquakes occurred about 11 h apart on two nearly orthogonal strike-slip faults in southern California. Hudnut et al. (1989) hypothesized that slip on one fault decreased σ_n on part of the second. The weakening effect of the decrease was offset by a decrease in fluid pressure (which lessened the effective stress decrease), and the second large earthquake was triggered after fluid flow increased the pressure. Cocco and Rice (2002) note that, depending on the hydraulic diffusivity, the time scales of these interactions can range from minutes to years. In rocks of particularly low permeability, the delays could conceivably be much longer.

In addition to initiating slippage on faults, fluid pressure may mediate the slippage itself. As discussed in the sections *Deformation in crustal processes* and *Inelastic rheologies from a geotechnical perspective*,

 DOI 10.1007/s10040-002-0230-8

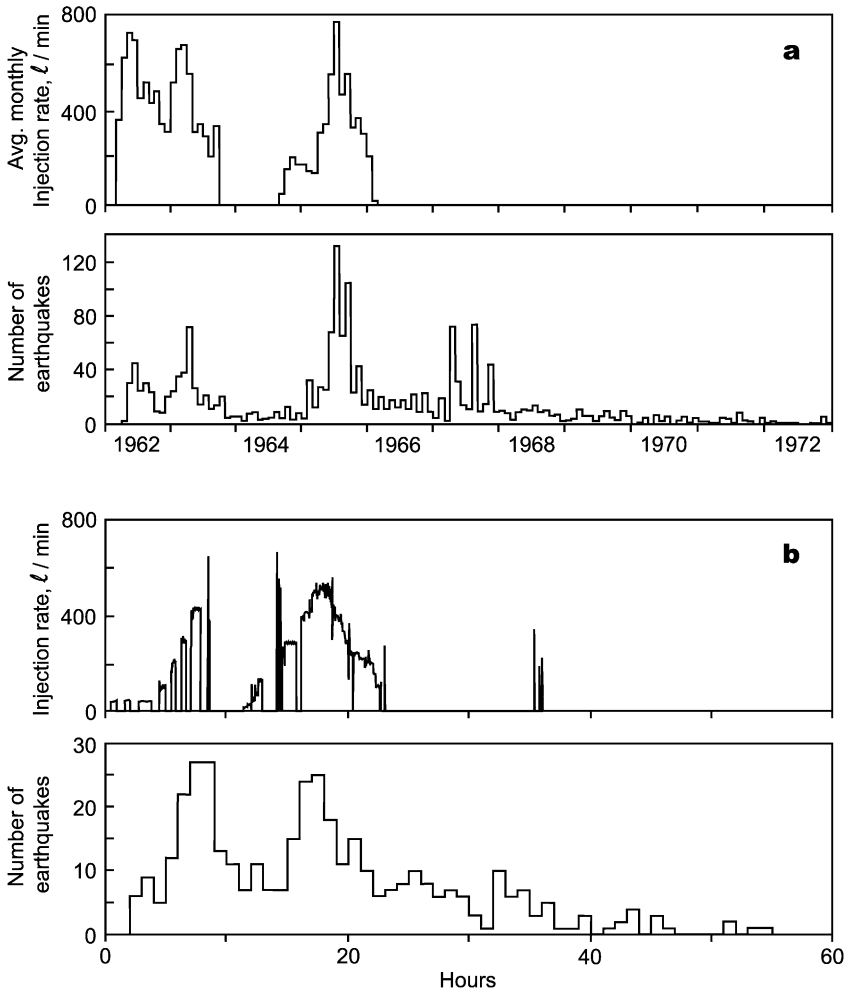

Fig. 20 Fluid injection rates and number of earthquakes through time in two instances of induced seismicity. **a** Injection at 3.7 km depth near Denver, Colorado, USA (adapted from Hsieh and Bredehoeft 1981). **b** Injection at 9.1 km depth at KTB site near Windischeschenbach, Germany (adapted from Zoback and Harjes 1997). Note the different time scales of the plots

volumetric strain can accompany shearing. Based on experiments by Marone et al. (1990), Segall and Rice (1995) developed a model for volumetric strain, or dilatancy, in fault gouge that is experiencing shear. Using a constitutive relation wherein porosity evolves to a steady state value that depends on slip velocity, they were able to explain porosity changes observed in the Marone et al. (1990) experiments. In simulations of slip behavior, this constitutive model suggested a number of complex behaviors are possible. For example, dilation during shearing may decrease fluid pressure and strengthen the fault, limiting the amount of slip. Subsequently, as flow relieves the lowered pressures, the fault may then weaken, initiating further slippage. As Segall and Rice (1995) note, this "may explain the apparent occurrence of aftershocks within zones of substantial mainshock slip." Their results also indicate that the stress drop in slip events can decrease with decreasing hydraulic diffusivity, as a result of the dilatancy strengthening.

Many fundamental questions related to fluids and seismicity revolve around the nature of fluid regimes at seismogenic depths and physicochemical effects of fluids on fault strength, in addition to the hydromechanical coupling per se (Hickman et al. 1994). Clearly, it would be very useful to know whether overpressures are present, whether cyclic pressure changes occur, and what pressure-mediating processes are involved. An interesting observation related to the San Andreas Fault in California is pertinent to these questions. The so-called heat-flow anomaly there is an unexpected absence of frictionally generated warming along the fault (Zoback and Lachenbruch 1992). The absence of elevated heat-flow values along the fault could be due to heat dispersal by topographically driven groundwater flow (Williams and Narasimhan 1989) or low friction along the fault, which presumably would indicate the presence of high fluid pressures (Ingebritsen and Sanford 1999). Segall and Rice (1995) argue against the latter. Their analysis of fault gouge dilation suggests that high fluid pressures can make earthquake nucleation difficult, instead favoring stable sliding.

The earliest quantitative discussion of the role of fluid pressures in faulting was concerned not with seismicity, but with explaining thrust fault displacement. That work, by M. King Hubbert and W.W. Rubey (Hubbert and Rubey 1959; Rubey and Hubbert 1959) is now considered classic. Hubbert and Rubey were concerned with the observation that thrust sheets up to hundreds of kilometers

 DOI 10.1007/s10040-002-0230-8

long have moved large distances. The frictional resistance to sliding, $\mu^*\sigma_n$ in Eq. (78), should be too great to permit pushing so large a sheet, which would fail inelastically rather than slide. The great insight of Hubbert and Rubey was the recognition that the frictional resistance to sliding is actually $\mu^*(\sigma_n - \alpha p)$; if fluid pressures are sufficiently high, relatively small lateral forces can displace a large sheet while leaving it more or less intact.

Accretionary complexes are a tectonic environment where thrust fault movement, accompanied by seismicity, is known to be occurring. As discussed earlier, ongoing deformation of sediments in accretionary complexes tends to decrease porosity and increase fluid pressures (see Fig. 14b). Seismic studies (Bangs and Westbrook 1991; Cochrane et al. 1994) have revealed apparent high porosities in décollements, presumably an indication that they host fluid overpressures. There seems to be little doubt that overpressures enable thrusting along décollements as well as within the complexes themselves. Similar processes probably occur in other settings. For example, Unruh et al. (1992) have described evidence for high fluid pressures in western California, another setting where active thrusting is occurring. These seem to be examples of high fluid pressures "caught in the act" of facilitating thrusting.

There is a satisfying bit of additional evidence for the important mechanical role of fluid pressure in accretionary complexes. The taper angle of accretionary prisms is thought to be controlled by the balance between internal frictional forces and gravity forces. In other words, sediments throughout the prism are on the verge of Coulomb failure. If so, fluid pressures would be expected to control the taper angle because of their weakening effect on shear surfaces. High fluid pressures should, in turn, be favored by high convergence rates and low prism permeabilities. Simulations by Saffer and Bekins (2002) of several accretionary prisms have demonstrated that the expected relationship does, in fact, appear to exist. Using permeabilities estimated from sediment characteristics in the Mexico, Cascadia, Nankai, and Barbados complexes, Saffer and Bekins found that their predictions of stable taper angles matched prism geometries.

As Saffer and Bekins (2002) note, coupling in both directions is important. Specifically, thrusting itself contributes to the high fluid pressures required for continued displacement, and this complicated their analysis. As discussed in *Tectonic deformation*, Shi and Wang (1988) envisioned overpressures as resulting from both lateral loading and thickening. Such processes are not unique to accretionary complexes. Ge and Garven (1994) studied their role in foreland basin thrust faulting by specifying elastoplastic behavior in special "slip elements" defining the thrust zone. The initiation of plastic deformation was described with a Mohr-Coulomb criterion of the form of Eq. (78). Ge and Garven (1994) found significant fluid overpressuring was generated in the vicinity of the fault after the start of thrusting and low permeabilities in the region of the fault tended to maintain high pressures and presumably shorten the interval between thrust events. Stated differently, it appears that in many cases movement along thrust faults creates conditions favorable to further thrusting and the process may often be, to some degree at least, self perpetuating.

Concluding Remarks

The Importance of Hydromechanical Coupling

Efforts to better understand hydromechanical coupling are driven by many considerations. Most fundamentally, Earth's crust is a fluid-filled porous medium and its behavior and evolution cannot be fully understood except in the context of hydromechanical coupling. Rather than viewing this as a burden that complicates analysis, mechanical coupling between fluids and solids in the crust can be seen as a rich source of additional information about and constraints upon crustal processes, a result of the fact that geologic processes leave their imprint on the fluid regime and vice versa. In many cases these sources of information have not been exploited.

A couple of examples will serve to illustrate the potential utility of hydromechanical coupling in a wide range of problems. Monitoring of fluid pressures in oceanic basement on the flank of the Juan de Fuca Ridge revealed changes that coincided with nearby seismic activity. Davis et al. (2001) analyzed the pressure changes and concluded that they and the seismicity were both caused by an episode of seafloor spreading. The spreading event would otherwise have been undetected. A rather different form of crustal dynamism was detected using anomalous fluid pressures in the North Sea basin. Comparing the patterns of fluid pressure with the basin stress regime, Grollimund and Zoback (2000) deduced that crustal flexure is occurring, probably in response to glacial unloading. Many similar examples could be cited.

Hydromechanical coupling also has immediate relevance to a number of societal problems and needs. Among the most conspicuous is its role in seismicity and potential utility in earthquake prediction. It is likely that fluid pressures frequently determine earthquake size and recurrence interval through their control of effective stress and fault strength. There are a number of other areas of immediate importance to society, of which only a few examples will be cited. Anomalous pressures, most of which appear to result from some form of hydromechanical coupling, pose severe risks during drilling operations; they influence much of the exploration for and extraction of hydrocarbon fuels. Natural hydrofracturing, a completely different manifestation of hydromechanical coupling, controls the availability and quality of groundwater in many regions. Hydromechanics is also a crucial aspect of geologic isolation of toxic materials, such as high level radioactive waste (National Research Council 1996). To summarize, discovery and extraction of geologic resources, management of geologic risks, and a working understanding of crustal processes can all be enhanced by an understanding of hydromechanical coupling.

 DOI 10.1007/s10040-002-0230-8

How Hydromechanical Coupling in Geology Is Understood and Analyzed

Revolutions in understanding hydromechanical phenomena were catalyzed by two events, the development of poroelastic theory in the 1940s and the advent of digital computing in the 1960s. The first provided a theoretical framework for describing the coupling and the second provided the means of applying that description, and numerous derivatives of it, to realistic geologic problems. Other developments were influential as well. Among the most important were the analyses of thrust faulting by Hubbert and Rubey (1959), of rock jointing by Secor (1965), and of compaction-generated anomalous fluid pressures by Bredehoeft and Hanshaw (1968). Together, these studies probably did more than any other published works to raise awareness of hydromechanical coupling in geology.

Judiciously applied, poroelasticity and the more general fully coupled theories appear to provide usable descriptions of hydromechanical phenomena in geologic systems, at least over the short periods of time that can be observed. Studies demonstrating this include an analysis by Lewis and Schrefler (1987), who showed that fully coupled poro-viscoelasticity could describe compaction in soft sediments at Baglan Moors, England, and the work by Segall et al. (1994) showing that stress changes and seismicity in the Lacq Gas Field, France, were accurately described by a fully coupled poroelastic model combined with Coulomb failure criteria.

When the same rigorous approaches are applied to longer-term and larger-scale geologic phenomena the outcomes are less clear. The reason is familiar to Earth scientists; in most of the subsurface, one is ignorant of the details of how different media are arranged in three dimensions (the geologic architecture), how geologic systems and external forces acting on them have evolved through time, and how mechanical, hydraulic, and chemical properties are distributed now and in the past. Permeability is an extreme example of the latter, ranging over at least 17 orders of magnitude in different geologic media, changing by orders of magnitude as a result of strain, and appearing to vary significantly depending on the scale of measurement.

The difficulties are well illustrated by the study of Schiffman et al. (1969), who compared coupled and uncoupled consolidation under loading (see *Sediment compaction*). They applied one-dimensional (purely vertical strain and flow) and coupled two-dimensional (two-dimensional flow and plane strain) analyses to the instantaneous application of a finite-length load on an infinite half-plane. This, as noted earlier, is analogous to spatially varying sedimentary deposition. Schiffman et al. found, among other differences, that dissipation of fluid overpressure took roughly ten times longer in the one-dimensional analysis than in the coupled analysis. Although this difference would certainly be significant in engineering practice, it is comparable to or perhaps even smaller than the error typically expected in geologic analyses, where order-of-magnitude resolution of permeability, for example, is considered good.

Symptomatic of the limitations imposed by geologic uncertainty is the number of analytical shortcuts and tricks that have been developed to approximate full coupling, rather than to fully describe it. Certain details are lost by using these techniques, but resulting inaccuracies are on a par with those arising from inaccuracies in the description of the systems themselves. The two biggest successes of hydromechanics in geology may be what has been learned about accretionary complexes and compacting sedimentary basins, both of which have been analyzed largely without using fully coupled descriptions.

In view of this, are rigorous approaches that fully invoke two- and three-dimensional coupling worthwhile? The answer is problem-dependent. Rigorous prediction or retrodiction of hydromechanical behavior in geologic systems is usually unrealistic. With that said, rigorous models of hydromechanical coupling certainly have an important role in conceptual development and testing. If one is concerned with examining the viability of different conceptual models, and the mechanics of various processes and how they may interact, then poroelasticity and its more general successors are not only very useful, but also quite necessary. Full hydromechanical coupling allows the physical precepts of continuum mechanics to be incorporated into analyses and, if the results are more uncertain than one would like, they can still reveal a great deal. In the case of the system analyzed by Schiffman et al. (1969) (described in the preceding section), the evolution of lateral stresses, the Mandel-Cryer effect, and certain other behaviors can only be analyzed or, for that matter understood through full hydromechanical coupling. Analyses of tectonic deformation and fracture propagation are notable instances where accounting for full coupling has provided insight and understanding of geologic processes that is not otherwise obtainable.

Many quite capable theoretical approaches and numerical tools are already available for analyzing full hydromechanical coupling in two and three dimensions. In particular, geotechnical researchers have successfully incorporated complicated modes of deformation in fully coupled models; their approaches are a largely untapped resource for studying hydromechanical processes in geology. For some problems, however, such as those involving both hydromechanical and thermomechanical processes, fully coupled analyses still await development of the appropriate numerical tools.

An important component of future advances in hydromechanical coupling in geology will be the collection of data in critical settings. Steps in this direction are exemplified by the SAFOD (San Andreas Fault Observatory at Depth) effort, a 4-km-deep borehole to be drilled into the San Andreas Fault at Parkfield, California. Instrumented with strainmeters, seismometers, fluid pressure transducers, and other sensors, this effort should provide critical data on hydromechanical processes in seismogenesis. Complementary efforts to investigate the seismogenic portion of a décollement by deep ocean

 DOI 10.1007/s10040-002-0230-8

drilling are in the planning stages. These relatively risky and costly efforts are part of a range of investigations that are needed to better constrain hydromechanical models of crustal processes.

Acknowledgements Evelyn Roeloffs, Mike Ryan, Alden Provost, Eyal Stanislavsky, and two anonymous reviewers provided helpful comments on this manuscript, although responsibility for any errors remains with me. This work was made possible by the National Research Program of the US Geological Survey.

Appendix

Notation

a compaction factor of Terzaghi equivalent to one-dimensional specific storage (S_S) [L^{-1}]. Also half-length of a fracture [L].

c flaw radius in porous medium [L].

e void ratio [dimensionless].

$e_{\sigma\ max}$ void ratio corresponding to $\sigma'_{t\ max}$[dimensionless].

g gravitational acceleration [L/T^2].

h hydraulic head [L].

h' $= p/(\rho g)-(l_s - z)$; excess hydraulic head [L].

$\boldsymbol{k}$ or k_{ij} second-order permeability tensor [L^2].

k permeability scalar [L^2].

l measure of the size of a geologic domain representing the shortest distance from the domain center to a boundary [L].

l_s elevation of land surface [L].

m mass of pore fluid per volume of porous medium [M/L^3].

n porosity [dimensionless].

n_{ir} "irreducible" porosity [dimensionless].

n_{min} minimum porosity [dimensionless].

n_s porosity at ground surface [dimensionless].

p fluid pressure [M/T^2L] (*depending on context, may be either a difference or an absolute quantity*).

p' fluid pressure in excess of hydrostatic [M/T^2L] (*depending on context, may be either a difference or an absolute quantity*).

$\boldsymbol{q}$ pore fluid specific flux vector [L/T].

$\boldsymbol{q}_n$ component of $\boldsymbol{q}$ normal to a domain boundary [L/T].

$\boldsymbol{q}_{rel}$ $= \boldsymbol{q}+n\mathbf{v}_s$; specific flux vector relative to a fixed coordinate system [L/T].

t *time [T].*

$\boldsymbol{t}$ traction, or force vector per unit area on a domain boundary [M/T^2L].

u, v, w displacements in the x, y, $z$coordinate directions [L].

$\boldsymbol{u}$ $= (u, v, w)$ displacement vector [L].

$\mathbf{v}_s$ sediment velocity vector [L/T].

x, y, z distance in coordinate direction (horizontal, horizontal, vertical; $z$positive upward) [L].

A_f fracture cross-sectional area [L^2].

C^{c1}_{ijkl} fourth-order elastic coefficient tensor for Kelvin body [M/T^2L].

C^{c2}_{ijkl} fourth-order viscous coefficient tensor for Kelvin body [M/TL].

C^{e}_{ijkl} fourth-order elastic coefficient tensor [M/T^2L].

C^{ep}_{ijkl} fourth-order elastoplastic coefficient tensor [M/T^2L].

C^{vep}_{ijkl} fourth-order visco-elastoplastic coefficient tensor [M/T^2L].

D_h hydraulic diffusivity [L^2/T].

G shear modulus of porous medium [M/T^2L].

G_T geothermal gradient [degrees/L].

J strength of fluid source [M/TL^3].

J_d $=-(1-n)^{-1}\rho(Dn/Dt)$; virtual fluid source due to diagenetic pore collapse [M/TL^3].

K drained bulk modulus of the porous medium [M/T^2L].

K_{eff} effective drained bulk modulus of the porous medium [M/T^2L].

K' drained confined (vertical) modulus of porous medium [M/T^2L].

K'_{eff} effective drained confined (vertical) modulus of porous medium [M/T^2L].

K_f bulk modulus of pore fluid [M/T^2L].

K_s bulk modulus of solids in the porous medium [M/T^2L].

K_{Ic} fracture tip critical stress intensity factor [$M/T^2L^{1/2}$].

M slope of critical state plane in Cam-clay model [dimensionless].

S_s one-dimensional specific storage [Eq. (40)] [L^{-1}].

S_{s3} three-dimensional specific storage [Eq. (21)] [L^{-1}].

S'_{s3} modified three-dimensional specific storage [Eq. (25)] [L^{-1}].

T temperature [degrees].

Y porous medium flaw shape factor [dimensionless].

α $=1-K/K_s$ [dimensionless].

α_T linear thermal expansivity of porous medium [$degrees^{-1}$].

$\hat{\alpha}_T$ bulk thermal expansivity of porous medium [$degrees^{-1}$].

α_{Tf} bulk thermal expansivity of pore fluid [$degrees^{-1}$].

α_{Tp} bulk thermal expansivity of pores [$degrees^{-1}$].

β three-dimensional loading efficiency (Skempton's coefficient) [Eq. (22)] [dimensionless].

$\gamma, \gamma_1, \gamma_2$ Athy porosity-loss coefficients for compaction [T^2L/M].

γ_d Athy porosity-gain coefficient for decompaction [T^2L/M].

δ_{ij} Kronecker delta, equal to zero when $i \neq j$ and equal to one when $i=j$ [dimensionless].

ε general designation of strain [dimensionless].

ε_{ij} second-order strain tensor, positive for contraction; $i= j$ indicates contractional/extensional component; $ij=xx$, yy indicates horizontal strain, $ij=zz$ indicates vertical strain; $i \neq j$ indicates shear component [dimensionless].

 DOI 10.1007/s10040-002-0230-8

ε_{kl}^{c1} second-order elastic strain tensor for Kelvin body [dimensionless].

$\dot{\varepsilon}_{kl}^{c2}$ second-order rate of viscous strain tensor for Kelvin body [T^{-1}].

ε_{kl}^{d} second-order diagenetic strain tensor [dimensionless].

ε_{kl}^{e} second-order elastic strain tensor [dimensionless].

ε_{kl}^{ep} second-order elastoplastic strain tensor [dimensionless].

ε_{kl}^{p} second-order plastic strain tensor [dimensionless].

ε_{kl}^{v} second-order viscous strain tensor [dimensionless].

$\dot{\varepsilon}_{kl}^{vep}$ second-order rate of visco-elastoplastic strain tensor [T^{-1}].

ε_{kk} $=\varepsilon_{xx}+\varepsilon_{yy}+\varepsilon_{zz}$; volumetric strain (positive for contraction) [dimensionless].

ε_{kk}^{p} plastic component of volumetric strain (positive for contraction) [dimensionless].

$\dot{\varepsilon}_{kk}$ rate of volumetric strain [T^{-1}].

ε_{shear}^{p} plastic component of shear strain [dimensionless].

ε_T sum of lateral strains due to earth tides [dimensionless].

ζ $=[\beta(1+\nu)]/[3(1-\nu)-2\alpha\beta(1-2\nu)]$; one-dimensional loading efficiency [dimensionless].

κ hydraulic conductivity [L/T].

$\boldsymbol{\kappa}$ hydraulic conductivity tensor [L/T].

κ_{cc} virgin compression parameter in Cam-clay model [dimensionless].

λ $=2\alpha(1-2\nu)/3(1-\nu)$ [dimensionless].

λ_{cc} swelling-recompression parameter in Cam-clay model [dimensionless].

μ dynamic viscosity of pore fluid [M/LT].

μ^* coefficient of strength or coefficient of static friction of the porous medium [dimensionless].

μ_{ref} reference value of dynamic viscosity of pore fluid [M/LT].

μ_{rel} $=\mu_{ref}/\mu$[dimensionless].

ν Poisson's ratio [dimensionless].

ξ dilatancy factor [dimensionless].

ρ density of pore fluid [M/L^3].

ρ' $=\rho/\rho_{ref}$ [dimensionless].

ρ_{ref} reference value of density of pore fluid [M/L^3].

ρ_{rel} $=(\rho-\rho_{ref})/\rho_{ref}$ [dimensionless].

ρ_s density of solid grains in porous medium [M/L^3].

σ general designation of stress [M/T^2L].

σ_d $=\sigma_1-\sigma_3$; differential stress [M/T^2L].

σ'_d $=\sigma'_1-\sigma'_3$; differential effective stress [M/T^2L].

σ_{ij} second order stress tensor, positive for compression; $i=j$ indicates normal stress, $ij=xx$, yy indicates horizontal stress, $ij=zz$ indicates vertical stress; $i\neq j$ indicates shear stress [M/T^2L] (*depending on context, may be either a difference or an absolute quantity*).

σ_{kk} $=\sigma_{xx}+\sigma_{yy}+\sigma_{zz}$ sum of normal stresses or volumetric stress (positive for compression) [M/T^2L] (*depending on context, may be either a difference or an absolute quantity*).

σ_n stress normal to a shear plane [M/T^2L].

σ_t $=(\sigma_{xx}+\sigma_{yy}+\sigma_{zz})/3$, mean total stress; positive for compression [M/T^2L] *(depending on context, may be either a difference or an absolute quantity).*

σ'_t $=\left(\sigma'_1+\sigma'_2+\sigma'_2\right)/3$, mean total of principal effective stress [M/T^2L] (*depending on context, may be either a difference or an absolute quantity*).

$\sigma'_{t\ \max}$ maximum previous value of σ'_t experienced by a porous medium [M/T^2L].

σ'_{ij} second order effective stress tensor; positive for compression; $ij=xx$, yy indicates horizontal effective stress, $ij=zz$ indicates vertical effective stress [M/T^2L] (*depending on context, may be either a difference or an absolute quantity*).

σ''_{ij} $=\sigma'_{ij}-\{[2G\alpha_T(1+\nu)]/(1-2\nu)\}T\delta_{ij}$; second-order thermally compensated effective stress tensor, positive for compression; $ij=xx$, yy indicates horizontal compensated effective stress, $ij=zz$ indicates vertical compensated effective stress [M/T^2L] (*depending on context, may be either a difference or an absolute quantity*).

$\sigma'_{zz\ (\max)}$ maximum vertical effective stress the formation has experienced [M/T^2L].

σ'_{kk} $=\sigma'_{xx}+\sigma'_{yy}+\sigma'_{zz}\left[M/T^2L\right]$ (*depending on context, may be either a difference or an absolute quantity*).

σ_1, σ_3 greatest and least principal stresses [M/T^2L].

σ'_1, σ'_3 greatest and least effective principal stresses [M/T^2L].

$\dot{\sigma}'_{ij}$ rate of change of the effective stress tensor [M/T^3L].

$\dot{\sigma}'^{r}_{ij}$ effective stress relaxation rate tensor [M/T^3L].

τ component of shear stress on an arbitrarily oriented plane [M/T^2L] (*depending on context, may be either a difference or an absolute quantity*).

ω creep deformation coefficient for porous medium [TL/M].

Λ $=\alpha_{Tf}-\alpha_{Tp}$; thermal response coefficient of fluid-saturated porous medium [degrees^{-1}].

Λ' $=\alpha_{Tf}+(\lambda/n)\hat{\alpha}_T-\alpha_{Tp}$; modified thermal response coefficient of fluid-saturated porous medium [degrees^{-1}].

Operators

$$\nabla \frac{\partial}{\partial x}, \frac{\partial}{\partial y}, \frac{\partial}{\partial z}$$

$$\nabla \cdot \frac{\partial}{\partial x}+\frac{\partial}{\partial y}+\frac{\partial}{\partial z}$$

$$\nabla^2 \frac{\partial^2}{\partial x^2}+\frac{\partial^2}{\partial y^2}+\frac{\partial^2}{\partial z^2}$$

$\dot{(\ )}$ time derivative of ( ).

 DOI 10.1007/s10040-002-0230-8

References

Anderson EM (1938) The dynamics of sheet intrusion. Proc R Soc Edinb 58:242–251

Angevine CL, Turcotte DL (1983) Porosity reduction by pressure solution: a theoretical model for quartz arenites. Geol Soc Am Bull 94(10):1129–1134

Athy, LF (1930) Density, porosity, and compaction of sedimentary rocks. Bull Am Assoc Petrol Geol 14(1):1–24

Bangs NLB,Westbrook, GK (1991) Seismic modeling of the decollement zone at the base of the Barbados Ridge accretionary complex. J Geophys Res 96(B3):3853–3866

Barbour SL, Fredlund DG (1989) Mechanisms of osmotic flow and volume change in clay soils. Can Geotech J 26(4): 551–562

Batu V (1998) Aquifer hydraulics, Wiley, New York

Bekele EB, Person MA, Rostron BJ (2000) Anomalous pressure generation within the Alberta Basin: Implications for oil charge to the Viking Formation. J Geochem Explor 69–70:601–605

Bennett PC, Hibert FK, Rogers JR (2000) Microbial control of mineral-groundwater equilibria: macroscale to microscale. Hydrogeol J 8(1):47–62

Berry FAF (1973) High fluid potentials in California coast ranges and their tectonic significance. Am Assoc Petrol Geol Bull 57(7):1219–1249

Bethke CM (1989) Modeling subsurface flow in sedimentary basins. Geol Rundsch 78(1):129–154

Bethke CM, Corbet TF (1988) Linear and nonlinear solutions for one-dimensional compaction flow in sedimentary basins. Water Resour Res 24(3):461–467

Bethke CM, Lee M-K, Park J (1999) Basin modeling with Basin 2, Release 4. University of Illinois, Urbana, Illinois

Biot MA (1941) General theory of three-dimensional consolidation. J Appl Phys 12(2):155–164

Biot MA (1955) Theory of elasticity and consolidation for a porous anisotropic solid. J Appl Phys 26(2):182–185

Biot MA (1956a) Theory of deformation of a porous viscoelastic anisotropic solid. J Appl Phys 27(5):459–467

Biot MA (1956b) Theory of propagation of elastic waves in a fluid-saturated porous solid. I. Low frequency range. J Acoust Soc Am 28(2):168–178

Biot MA (1956c) Theory of propagation of elastic waves in a fluid-saturated porous solid: II. Higher frequency range. J Acoust Soc Am 28(2):179–191

Biot MA (1972) Theory of finite deformations of porous solids. Ind Univ Math J 21(7):597–620

Biot MA (1973) Nonlinear and semilinear rheology of porous solids. J Geophys Res 78(23): 4924–4937

Biot MA, Willis DG (1957) The elastic coefficients of the theory of consolidation. J Appl Mech 24:594–601

Bitzer K (1997) BASIN: A finite element model for simulation of consolidation, fluid flow, solute transport and heat flow in sedimentary basins. In: Pavlowsky-Glahn V (ed) Proc IAMG 97, CIMNE, UPC, Barcelona, pp 444–449

Bitzer K, Salas J, Ayora C (2000) Fluid pressures, flow velocities and transport processes in a consolidating sedimentary column with transient hydraulic properties. J Geochem Explor 69–70:127–131

Boley BA, Weiner JH (1960) Theory of thermal stresses. Wiley, New York

Borja RI (1984) Finite element analysis of the time-dependent behavior of soft clays. PhD Thesis, Stanford University, Stanford, California

Borja RI, Kavazanjian E Jr. (1984) Finite element analysis of the time-dependent behavior of soft clays. Geotech Eng Rep No GT1, Dept Civ Eng, Stanford University, Stanford, California (Available from the first author)

Borja RI, Kavazanjian, E Jr. (1985) A constitutive model for the stress-strain-time behaviour of 'wet' clays. Géotechnique 35(3):283–298

Brace WF, Paulding B, Scholz CH (1966) Dilatancy in the fracture of crystalline rocks. J Geophys Res 71(16):3939–3954

Bredehoeft JD, Hanshaw BB (1968) On the maintenance of anomalous fluid pressures. I. Thick sedimentary sequences. Geol Soc Am Bull 79(9):1097–1106

Bredehoeft JD, Wesley JB, Fouch TD (1994) Simulation of the origin of fluid pressure, fracture generation, and the movement of fluids in the Uinta Basin, Utah. Am Assoc Petrol Geol Bull 78(11):1729–1747

Britto AM, Gunn MJ (1987) Critical state soil mechanics via finite elements. Wiley, New York

Cartwright JA, Lonergan L (1996) Volumetric contraction of mudrocks: a mechanism for the development of regional-scale polygonal fault systems. Basin Res 8(2):183–193

Cathles LM (1977) An analysis of the cooling of intrusives by ground-water convection which includes boiling. Econ Geol 72(5):804–826

Cocco M, Rice JR (2002) Pore pressure and poroelasticity effects in Coulomb stress analysis of earthquake interactions. J Geophys Res 107(B2):ESE 2.1 1–17

Cochrane GR, Moore JC, MacKay ME, Moore GF (1994) Velocity and inferred porosity model of the Oregon accretionary prism from multichannel seismic reflection data: implications on sediment dewatering and overpressure. J Geophys Res 99(B4):7033–7043

Connolly JAD, Podladchikov YY (2000) Temperature-dependent viscoelastic compaction and compartmentalization in sedimentary basins. Tectonophysics 324(3):137–168

Cooley RL (1975) A review and synthesis of the Biot and Jacob-Cooper theories of ground- water motion. Hydro and Water Resources Publ No 25, Center for Water Resources Research, Desert Research Institute, University of Nevada

Corbet TF, Bethke CM (1992) Disequilibrium fluid pressures and groundwater flow in the Western Canada Sedimentary Basin. J Geophys Res 97(B5):7203–7217

Curtis GP (2002) Comparison of approaches for simulating reactive solute transport involving organic degradation reactions by multiple terminal electron acceptors. Comput Geosci (in press)

Davis EE, Wang K, Thomson RE, Becker K, Cassidy JF (2001) An episode of seafloor spreading and associated plate deformation inferred from crustal fluid pressure transients. J Geophys Res 106(B10):21953–21963

Dewars T, Ortoleva P (1994) Nonlinear dynamical aspects of deep basin hydrology: Fluid compartment formation and episodic fluid release. Am J Sci 294(6):713–755

Detournay E, Cheng AH-D (1993) Fundamental of poroelasticity: In: Hudson JA (ed) Comprehensive rock engineering: principles, practice & projects, vol 2. Pergamon Press, Oxford

Domenico PA, Palciauskas VV (1979) Thermal expansion of fluids and fracture initiation in compacting sediments. Geol Soc Am Bull Part 2 90(6):953–979

Domenico PA, Schwartz FW (1998) Physical and Chemical Hydrogeology, 2nd edn. Wiley, New York

Dugan B, Flemings PB (2000) Overpressure and fluid flow in the New Jersey continental slope: implications for slope failure and cold seeps. Science 289(5477):288–291

Elsworth D, Voight B (1991) Poroelastic response around an intrusion. In: Wittke W (ed) Proc 7th Int Congr on Rock Mech, Aachen, vol 1, Int Soc for Rock Mech, pp 455–461

Engelder T (1993) Stress regimes in the lithosphere. Princeton University Press, Princeton, New Jersey

Fertl WH (1976) Abnormal formation pressures. Elsevier, Amsterdam

Fertl WH, Chapman RE, Hotz RF (eds) (1994) Studies in abnormal pressures. Elsevier, Amsterdam

Freeze RA, Cherry JA (1979) Groundwater. Prentice-Hall, Englewood Cliffs, New Jersey

Galloway DL, Jones DR, Ingebritsen SE (1999) Land subsidence in the United States. US Geological Survey Circular 1182

Gambolati G (1974) Second-order theory of flow in three-dimensional deforming media. Water Resour Res 10(6):1217–1228

 DOI 10.1007/s10040-002-0230-8

Garven G (1989) A hydrogeologic model for the formation of giant oil sands deposits of the Western Canada sedimentary basin. Am J Sci 289(2):105–166
Ge S, Garven G (1989) Tectonically induced transient groundwater flow in foreland basin. In: Price RA (ed) Geophys Monograph No 3, International Union of Geodesy and Geophysics, pp 145–158
Ge S, Garven G (1992) Hydromechanical modeling of tectonically driven groundwater flow with application to the Arkoma foreland basin. J Geophys Res 97(B6):9119–9144
Ge S, Garven G (1994) A theoretical model for thrust-induced deep groundwater expulsion with application to the Canadian Rocky Mountains. J Geophys Res 99(B7):13851–13868
Geertsma J (1966) Problems of rock mechanics in petroleum production engineering. In: Proc of the 1st Int Congr of the Int Soc of Rock Mech, vol I, pp 585–594
Gibson RE (1958) The progress of consolidation in a clay layer increasing in thickness with time. Géotechnique 8(4):171–182
Gibson RE, Lo KY (1961) A theory of consolidation for soils exhibiting secondary compression. Publ 41, Nor Geotech Inst, Oslo, Norway
Giles M (1997) Diagenesis: a quantitative perspective. Kluwer, Dordrecht
Gordon DS, Flemings PB (1999) Two-dimensional modeling of groundwater flow in an evolving deltaic environment. In: Harbaugh JW, Watney WL, Rankey EC, Slingerland R, Goldstein RH, Franseen EK (eds) Numerical experiments in stratigraphy: recent advances in stratigraphic and sedimentologic computer simulations. Soc for Sediment Geol (SEPM), Spec Pub No 62
Grecksch G, Roth F, Kümpel H-J (1999) Coseismic well-level changes due to the 1992 Roermond earthquake compared to static deformation of half-space solutions. Geophys J Int 138(2):470–478
Grollimund B, Zoback MD (2000) Post glacial flexure and induced stresses and pore pressure changes in the northern North Sea. Tectonophysics 327(1–2):61–81
Grün G-U, Wallner H, Neugebauer HJ (1989) Porous rock deformation and fluid flow – numerical FE-simulation of the coupled system. Geol Rundsch 78(1):171–182
Gueguen Y, David C, Gavrilenko P (1991) Percolation networks and fluid transport in the crust. Geophys Res Lett 18(5):931–934
Gunn MJ, Britto AM (1981) CRISP – User's and Programmer's Manual. Eng Dept, Cambridge University, Cambridge
Gwo JP, D'Azevedo EF, Frenzel H, Mayes M, Yeh G, Jardin PM, Salvage KM, Hoffman FM (2001) HBGC123D: a high-performance computer model of hydrogeologic and biogeochemical processes. Comput Geosci 27(10):1231–1242
Harrison WJ, Summa LL (1991) Paleohydrology of the Gulf of Mexico Basin. Am J Sci 291(2):109–176
Harrold TWD, Swarbrick RE, Goulty NR (1999) Pore pressure estimation from mudrock porosities in Tertiary basins, Southeast Asia. Am Assoc Petrol Geol Bull 83(7):1057–1067
Hart BS, Flemings PB, Deshpande A (1995) Porosity and Pressure: Role of compaction disequilibrium in the development of geopressures in a Gulf Coast Pleistocene basin. Geology 23(1):45–48
Haxby WF, Turcotte DL (1976) Stresses induced by the addition and removal of overburden and associated thermal effects. Geology 4(3):181–184
Hickman S, Sibson R, Bruhn R (eds) (1994) Proc of Workshop LXIII, The Mechanical Involvement of Fluids in Faulting, US Geological Survey Open-File Report 94–228
Hibbitt, Karlsson, and Sorenson, Inc (1998) ABAQUS, Standard User's manual, Version 5.8, vols. I-III. Pawtucket, Rhode Island
Hsieh PA (1994) Guide to BIOT2: a finite element model to simulate axisymmetric/plane-strain solid deformation and fluid flow in a linearly elastic porous medium. US Geological Survey
Hsieh PA, Bredehoeft JD (1981) A reservoir analysis of the Denver earthquakes: a case of induced seismicity. J Geophys Res 86 (B2):903–920
Hsieh PA, Bredehoeft JD, Farr JM (1987) Determination of aquifer transmissivity from earth tide analysis. Water Resour Res 23(10):1824–1832
Hubbert MK, Willis DG (1957) Mechanics of hydraulic fracturing. Petroleum Trans Am Inst Mining Eng 210:153–166
Hubbert MK, Rubey WW (1959) Role of fluid pressure in mechanics of overthrust faulting: I. Mechanics of fluid-filled porous solids and its application to overthrust faulting. Geol Soc Am Bull 70(2):115–166
Hudnut KW, Seeber L, Pacheco J (1989) Cross-fault triggering in the November 1987 Superstition Hills earthquake sequence, southern California. Geophys Res Lett 16(2):199–202
Humbert P (ed) (1988) Manuel théorique de CESAR-LCPC [Theoretical Handbook of CESAR-LCPC]. Laboratoire Central des Ponts et Chaussées, Paris
Ingebritsen SE, Sanford WE (1999) Groundwater in geologic processes. Cambridge University Press, Cambridge
Jacob CE (1940) On the flow of water in an elastic artesian aquifer. Am Geophys Union Trans 21:574–586
Jaeger JC, Cook NGW (1969) Fundamentals of rock mechanics. Methuen & Co, London
Jayko AS (1996) Late Cenozoic strain rates across the La Honda Basin. In: Jayko AS, Lewis SD (eds) Toward assessing the seismic risk associated with blind faults, San Francisco Bay Region, California. US Geolological Survey Open-File Report 96-0267:74-80
Karig DE (1985) The framework of deformation in the Nankai Trough, Initial Report of the Deep Sea Drill Project 87, pp 927–940
Karig DE, Hou G (1992) High-stress consolidation experiments and their geologic implications. J Geophys Res 97(B1):289–300
Keith LA, Rimstidt JD (1985) A numerical compaction model of overpressuring in shales. J Int Assoc Math Geol 17(2):115–135
King C-Y, Azuma S, Ohno M, Asai Y, He P, Kitagawa Y, Igarashi G, Wakita H (2000) In search of earthquake precursors in the water-level data of 16 closely clustered wells at Tono, Japan. Geophys J Int 143(2):469–477
King FH (1892) Fluctuations in the level and rate of movement of ground-water on the Wisconsin Agricultural Experiment Station Farm at Whitewater, Wisconsin. US Dept of Agriculture Bulletin 5
Kruseman GP, De Ridder NA (1970) Analysis and evaluation of pumping test data. Bulletin 11, Int Inst for Land Reclam and Improv, Wageningen, Netherlands
Kümpel H-J (1991) Poroelasticity: parameters reviewed. Geophys J Int 105(3):783–799
Lai WM, Rubin D, Krempl E (1978) Introduction to continuum mechanics (reviseded in SI/metric units). Pergamon Press, Oxford
Lawn BR, Wilshaw TR (1975) Fracture of brittle solids. Cambridge University Press, Cambridge
Lewis RW, Schrefler BA (1987) The finite element method in the deformation and consolidation of porous media. Wiley, New York
Lippincott DK, Bredehoeft JD, Moyle WR Jr. (1985) Recent movement on the Garlock Fault as suggested by water level fluctuations in a well in Fremont Valley, California. J Geophys Res 90(B2):1911–1924
Lohman SW (1979) Ground-water hydraulics. US Geological Survey, Professional Paper 708
Luo X, Vasseur G (1995) Modelling of pore pressure evolution associated with sedimentation and uplift in sedimentary basins. Basin Res 7(1):35–52
Luo X, Vasseur G (1996) Geopressuring mechanism of organic matter cracking: numerical modeling. Am Assoc Petrol Geol Bull 80(6):856–874
Luo X, Vasseur G, Pouya A, Lamoureux-Var V, Poliakov A (1998) Elastoplastic deformation of porous media applied to the

 DOI 10.1007/s10040-002-0230-8

modelling of compaction at basin scale. Mar Petrol Geol 15(2):145–162
Magara K (1968) Subsurface fluid pressure profile, Nagaoka Plain, Japan. Bull Jpn Petrol Inst 10:1–7
Makurat A, Barton N, Rad NS, Bandis S (1990) Joint conductivity variation due to normal and shear deformation, in rock joints. In: Barton N, Stephansson O (eds) Proc of the Int Symp on Rock Joints, Loen, Norway, pp 535–540
Marone C, Raleigh CB, Scholz CH (1990) Frictional behavior and constitutive modeling of simulated fault gouge. J Geophys Res 95(B5): 7007–7025
McMahon PB, Chapelle FH, Falls WF, Bradley PM (1992) Role of microbial processes in linking sandstone diagenesis with organic-rich clays. J Sediment Petrol 62(1):1–10
McPherson BJOL, Bredehoeft JD (2001) Overpressures in the Uinta Basin, Utah: analysis using a three-dimensional basin evolution model. Water Resour Res 37(4):857–871
McPherson BJOL, Garven G (1999) Hydrodynamics and overpressure mechanisms in the Sacramento Basin, California. Am J Sci 299(6):429–466
McTigue DF (1986) Thermoelastic response of fluid-saturated porous rock. J Geophys Res 91(B9):9533–9542
Meinzer OE (1928) Compressibility and elasticity of artesian aquifers. Econ Geol 23(3):263–291
Muskat M (1937) The flow of homogeneous fluids through porous media. McGraw-Hill, New York
National Research Council (1996) Rock fractures and fluid flow. National Academy Press, Washington, DC
Neuzil CE (1986) Groundwater flow in low-permeability environments. Water Resour Res 22(8):1163–1195
Neuzil CE (1993) Low fluid pressure within the Pierre Shale: a transient response to erosion. Water Resour Res 29(7):2007–2020
Neuzil CE (1994) How permeable are clays and shales? Water Resour Res 30(2):145–150
Neuzil CE (1995) Abnormal pressures as hydrodynamic phenomena. Am J Sci 295(6):742–786
Nicholson C, Wesson RL (1990) Earthquake hazard associated with deep well injection. Report to the US Environmental Protection Agency, US Geological Survey Bulletin 1951
Noorishad J, Tsang CF, Witherspoon PA (1984) Coupled thermal-hydraulic-mechanical phenomena in saturated fractured porous rocks: numerical approach. J Geophys Res 89(B12):10365–10373
Norton D (1982) Fluid and heat transport phenomena typical of copper-bearing pluton environments, southeastern Arizona. In: Titley SR (ed) Advances in geology of porphyry copper deposits, southwestern North America, pp 59–72
Norton D, Knight J (1977) Transport phenomena in hydrothermal systems cooling plutons. Am Jour of Sci 277(8):937–981
Nur A, Booker JR (1972) Aftershocks caused by pore fluid flow? Science 175(4024):885–887
Nur A, Byerlee JD (1971) An exact effective stress law for elastic deformation of rock with fluids. J Geophys Res 76(26):6414–6419
Nur A, Walder J (1990) Time-dependent hydraulics of the Earth's crust. In: The role of fluids in crustal processes. National Academy Press, Washington, DC
Oliver J (1986) Fluids expelled tectonically from orogenic belts: their role in hydrocarbon migration and other geological phenomena. Geology 14(2):99–102
Ortoleva P, Al-Shaieb Z, Puckette J (1995) Genesis and dynamics of basin compartments and seals. Am J Sci 295(4):345–427
Palciauskas VV, Domenico PA (1989) Fluid pressures in deforming porous rocks. Water Resour Res 25(2):203–213
Palciauskas VV, Domenico PA (1982) Characterization of drained and undrained response of thermally loaded repository rocks. Water Resour Res 18(2):281–290
Pfiffner OA, Ramsay JG (1982) Constraints on geological strain rates: Arguments from finite strain states of naturally deformed rocks. J Geophys Res 87(B1):311–321
Picarelli L, Urciuoli G (1993) Effeti dell'erosione in argilliti di alta plasticità [Consequences of erosion in highly plastic clay shales]. Riv Ital Geotec 27(1):29–47
Potdevin JL, Chen W, Park A, Chen Y, Ortoleva P (1992) CIRF; a general reaction-transport code; mineralization fronts due to the infiltration of reactive fluids. In: Kharaka YJ, Maest AS (eds) Proc 7th Int Symp on Rock-Water Interaction, pp 1047–1050
Press F (1965) Displacements, strains, and tilts at teleseismic distances. J Geophys Res 70(10):2395–2412
Quilty EG, Roeloffs EA (1997) Water-level changes in response to the 20 December 1994 earthquake near Parkfield, California. Bull Seis Soc Am 87(2):310–317
Raleigh CB, Healy JH, Bredehoeft JD (1976) An experiment in earthquake control at Rangely, Colorado. Science 191(4233): 1230–1236
Ranganathan V (1992) Basin dewatering near salt domes and formation of brine plumes. J Geophys Res 97(B4):4667–4683
Rendulic L (1936) Porenziffer und Porenwasserdruck in Tonen [Void ratio and pore water pressure in clays]. Der Bauingenieur 17:559–564
Renshaw CE (1996) Influence of subcritical fracture growth on the connectivity of fracture networks. Water Resour Res 32(6):1519–1530
Renshaw CE, Harvey CF (1994) Propagation velocity of a natural hydraulic fracture in a poroelastic medium. J Geophys Res 99(B11):21667–21677
Renshaw CE, Pollard DD (1994) Numerical simulation of fracture set formation: a fracture mechanics model consistent with experimental observations. J Geophys Res 99(B5):9359–9372
Revil A (1999) Pervasive pressure-solution transfer: a poro-visco-plastic model. Geophys Res Lett 26(2):255–258
Reynolds O (1886) Experiments showing dilatancy, a property of granular materials. Proc of the R Inst, vol 11, pp 354–363
Rice JR, Cleary MP (1976) Some basic stress diffusion solutions for fluid-saturated elastic porous media with compressible constituents. Rev Geophys Space Phys 14(2):227–241
Rieke HH III, Chilingarian GV (1974) Compaction of argillaceous sediments. Developments in sedimentology, no 16. Elsevier, Amsterdam
Roberts SJ, Nunn JA, Cathles L, Cipriani F-D (1996) Expulsion of abnormally pressured fluids along faults. J Geophys Res 101(B12):28231–28252
Roeloffs E (1988) Hydrologic precursors to earthquakes: a review. Pure Appl Geophys 126(2–4):177–209
Roeloffs E (1996) Poroelastic techniques in the study of earthquake-related hydrologic phenomena. In: Dmowska R, Saltzman B (eds) Advances in Geophysics 37, pp 135–195
Roeloffs E (1998) Persistent water level changes in a well near Parkfield, California, due to local and distant earthquakes. J Geophys Res 103(B1):869–889
Rojstaczer S, Agnew DC (1989) The influence of formation material properties on the response of water levels in wells to earth tides and atmospheric loading. J Geophys Res 94(B9):12403–12411
Rojstaczer SA, Bredehoeft JD (1988) Ground water and fault strength. In: Back WJ, Rosenshein S, Seaber PR (eds) The geology of North America, vol O-2. Hydrogeology. Geol Soc Am, pp 447–460
Rojstaczer S, Wolf S, Michel R (1995) Permeability enhancement in the shallow crust as a cause of earthquake-induced hydrological changes. Nature 373(6511):237–239
Roscoe KH, Burland JB (1968) On the generalized stress-strain behavior of "wet" clay. In: Heyman J, Leckie FA (eds) Engineering plasticity, pp 535–609
Roscoe KH, Schofield AN, Thurairajah A (1963) Yielding of clays in states wetter than critical. Géotechnique 13(3):211–240
Rubey WW, Hubbert MK (1959) Role of fluid pressure in mechanics of overthrust faulting: II. Overthrust belt in geosynclinal area of western Wyoming in light of fluid-pressure hypothesis. Geol Soc Am Bull 70(2):167–206

 DOI 10.1007/s10040-002-0230-8

Rudnicki JW (1985) Effect of pore fluid diffusion on deformation and failure of rock. In: Bazant ZP (ed) Mechanics of geomaterials; rocks, concretes, soils, vol 15, pp 315–347
Rutqvist J, Börgesson L, Chijimatsu M, Kobayashi A, Jing L, Nguyen TS, Noorishad J, Tsang C- F (2001) hermohydromechanics of partially saturated geologic media: governing equations and formulation of four finite element models. Int J Rock Mech Miner Sci 38(1):105–127
Saffer DM, Bekins BA (2002) Hydrologic controls on the morphology and mechanics of accretionary wedges. Geology 30(3):271–274
Schiffman RL, Chen, AT-F, Jordan JC (1969) An analysis of consolidation theories. Proc Am Soc Civil Eng 95(SM1):285–312
Schneider F, Potdevin JL, Wolf S, Faille I (1996) Mechanical and chemical compaction model for sedimentary basin simulators. Tectonophysics 263(1–4):307–317
Schofield AN, Wroth CPW (1968) Critical state soil mechanics. McGraw-Hill, New York
Screaton EJ, Wuthrich DR, Dreiss SJ (1990) Permeabilities, fluid pressures, and flow rates in the Barbados Ridge complex. J Geophys Res 95(B6):8997–9007
Secor DT Jr (1965) Role of fluid pressure in jointing. Am J Sci 263(8):633–646
Segall P (1989) Earthquakes triggered by fluid extraction. Geology 17(10):942–946
Segall P (1992) Induced stresses due to fluid extraction from axisymmetric reservoirs. Pure Appl Geophys 139(3/4):535–560
Segall P, Grasso J-R, Mossop A (1994) Poroelastic stressing and induced seismicity near the Lacq gas field, southwestern France. J Geophys Res 99(B8):15423–15438
Segall P, Rice JR (1995) Dilatancy, compaction, and fault instability of a fluid-infiltrated fault. J Geophys Res 100(B11): 22155–22171
Shames IH (1964) Mechanics of deformable solids. Prentice-Hall, Englewood Cliffs, New Jersey
Sherwood JD (1993) Biot poroelasticity of a chemically active shale. Proc R Soc Lond A 440:365–377
Shi Y, Wang C-Y (1986) Pore pressure generation in sedimentary basins: overloading versus aquathermal. J Geophys Res 91(B2):2,153–2,162
Shi Y, Wang C-Y (1988) Generation of high pore pressures in accretionary prisms: Inferences from the Barbados subduction complex. J Geophys Res 93(B8):8893–8910
Sibson RH (2000) Tectonic controls on maximum sustainable overpressure: fluid redistribution from stress transitions. J Geochem Explor 69–70:471–475
Simila GW (1998) Comparison of the seismicity and associated stress systems to the GPS strain rates for the Ventura Basin and Northridge regions (abstr). Am Assoc Petrol Geol Bull 82(5A):858
Skempton AW (1954) The pore pressure coefficients A and B. Géotechnique 4(4):143–147
Smith MB, Patillo PD (1983) A material model for inelastic rock deformation with spatial variation of pore pressure. Int J Numer Anal Meth Geomech 7(4):457–468
Stauffer P, Bekins BA (2001) Modeling consolidation and dewatering near the toe of the northern Barbados accretionary complex. J Geophys Res 106(B4):6369–6383
Šuklje L (1969) Rheological aspects of soil mechanics. Wiley-Interscience, London
Swenson JB, Person M (2000) The role of basin-scale transgression and sediment compaction in stratiform copper mineralization: Implications from White Pine, Michigan, USA. J Geochem Explor 69-70:239–243
Terzaghi K (1923) Die Berechnung der Durchlässigkeitziffer des Tones aus dem Verlauf der hydrodymanischen Spannungserscheinungen [The computation of permeability of clays from the progress of hydrodynamic strain]. Akad der Wissenschaften in Wien, Sitzungsberichte, Mathematisch-naturwissenschaftliche Klasse, Part IIa, 132(3/4), pp 125–138
Theis CV (1935) The relation between the lowering of the piezometric surface and the rate and duration of discharge of a well using ground-water storage. Am Geophys Union Trans 16:519–524
Timoshenko SP, Goodier JN (1987) Theory of elasticity, 3rd edn. McGraw-Hill, New York
Tokunaga T (1996) Development of a Three-Dimensional Basin Simulator and its Application to an Actual Sedimentary Basin [in Japanese]. PhD Thesis, Univ of Tokyo, Tokyo, Japan
Tóth J, Almási I (2001) Interpretation of observed fluid potential patterns in a deep sedimentary basin under tectonic compression: Hungarian Great Plain, Pannonian Basin. Geofluids 1(1):11–36
Tullis TE, Tullis J (1986) Experimental rock deformation techniques, in Mineral and Rock Deformation: Laboratory Studies. In: Hobbs BE, Heard HC (eds) The Paterson Volume. Am Geophys Union Geophys Monogr 36:297–324
Turcotte DL, Schubert G (1982) Geodynamics. Wiley, New York
Unruh JR, Davisson ML, Criss RE, Moores EM (1992) Implications of perennial saline springs for abnormally high fluid pressures and active thrusting in western California. Geology 20(15):431–434
van der Kamp G, Gale JE (1983) Theory of earth tide and barometric effects in porous formations with compressible grains. Water Resour Res 19(2):538–544
van der Kamp G, Schmidt R (1997) Monitoring of total soil moisture on a scale of hectares using groundwater piezometers. Geophys Res Lett 24(6):719–722
Verruijt A(1969) Elastic storage of aquifers. In: De Wiest RJM (ed) Flow through porous media, pp 331–336
Vinard PH (1998) Generation and Evolution of Hydraulic Underpressures in a Marl-Shale Aquitard at Wellenberg, central Switzerland. Thèse de D Sc, Univ. de Neuchâtel, Switzerland
Vinard P, Blumling P, McCord JP, Aristorenas G (1993) Evaluation of hydraulic underpressures at Wellenberg, Switzerland. Int J Rock Mech Mining Sci 30(7):1143–1150
Vrolijk P, Fisher A, Gieskes J (1991) Geochemical and geothermal evidence for fluid migration in the Barbados accretionary prism, ODP Leg 110. Geophys Res Lett 18(5):947–950
Wang HF (1997) Effects of deviatoric stress on undrained pore pressure response to fault slip. J Geophys Res 102(B8):17943–17950
Wang HF (2000) Theory of linear poroelasticity. Princeton University Press, Princeton, New Jersey
Ward SN (1998) On the consistency of earthquake moment release and space geodetic strain rates: Europe. Geophys J Int 135(3):1011–1018
Wesson RL (1981) Interpretation of changes in water level accompanying fault creep and implications for earthquake prediction. J Geophys Res 86(B10):9259–9267
Williams CF, Narasimhan TN (1989) Hydrogeologic constraints on heat flow along the San Andreas fault: a testing of hypotheses. Earth Planet Sci Lett 92(2):131–143
Wilson AM, Garven G, Boles JR (1999) Paleohydrology of the San Joaquin basin, California. Geol Soc Amr Bull 111(3):432–449
Zimmerman RW (2000) Coupling poroelasticity and thermoelasticity. Int J Rock Mech Mining Sci 37(1–2):79–87
Zoback MD, Harjes H-P (1997) Injection-induced earthquakes and crustal stress at 9 km depth at the KTB deep drilling site, Germany. J Geophys Res 102(B8):18477–18491
Zoback MD, Lachenbruch AH (1992) Introduction to special section on Cajon Pass scientific drilling project. J Geophys Res 97(4):4991–4994

 DOI 10.1007/s10040-002-0230-8